AN INVESTIGATION OF TRANSITION AND TURBULENCE IN OSCILLATORY STOKES LAYERS

by

Rayhaneh Akhavan-Alizadeh

B.S., California Institute of Technology (1980)
S.M., Massachusetts Institute of Technology (1982)

Submitted to the Department of Mechanical Engineering
in Partial Fulfillment of the Requirements
for the Degree of

DOCTOR OF PHILOSOPHY

at the

MASSACHUSETTS INSTITUTE OF TECHNOLOGY
JUNE, 1987

Signature of Author _____
Department of Mechanical Engineering
May 1987

Certified by _____
Professor Roger D. Kamm
Thesis Supervisor

Certified by _____
Professor Ascher H. Shapiro
Thesis Supervisor

Accepted by _____
Professor Ain A. Sonin
Chairman, Department Committee on Graduate Studies

AN INVESTIGATION OF TRANSITION AND TURBULENCE IN OSCILLATORY STOKES LAYERS

by

Rayhaneh Akhavan

Submitted to the Department of Mechanical Engineering in May, 1987 in partial fulfillment of the requirements for the Degree of Doctor of Philosophy in Mechanical Engineering

ABSTRACT

Transition to turbulence in bounded oscillatory Stokes layers is investigated experimentally by LDV measurements for flow in a pipe, and numerically by direct simulations of the Navier-Stokes equations for flow in a channel. The experiments indicate a transitional Reynolds number based on Stokes boundary layer thickness of Re~500. The resulting turbulent flow is characterized by the sudden appearance of turbulence with the start of the deceleration phase of the cycle, and reversion to "laminar" flow during the acceleration phase. It is proposed that generation of turbulence in this flow is due to turbulent "bursts" similar in nature to those that occur for steady wall-bounded shear flows. Furthermore relaminarization of the flow during the acceleration phase is attributed to cessation of "bursting" because of the favorable pressure gradients that are present during this period.

Investigation of the stability of oscillatory channel flow to various infinitesimal and finite-amplitude two- and three-dimensional disturbances reveals that; (a) An infinitesimal perturbation introduced in the boundary layer would, over the course of a few cycles migrate to the center of the channel where it would decay with viscous time scales as predicted by a Floquet analysis. However, as long as the disturbance is still localized within the boundary layer, it would amplify with inviscid growth rates as predicted by quasi-steady theories. (b) No finite-amplitude two-dimensional equilibrium states were found; however, quasi-equilibria (with viscous decay rates) were observed at transitional Reynolds numbers. (c) The secondary instability of these two-dimensional finite-amplitude quasi-equilibrium states to infinitesimal three-dimensional perturbations can successfully explain the critical Reynolds numbers and turbulent flow structures that were observed in experiments.

Thesis Supervisors: Prof. R.D. KAMM
Prof. A.H. SHAPIRO
Thesis Committee : Prof. D.J. BENNEY
Prof. C.F. DEWEY
Prof. A.T. PATERA

ACKNOWLEDGMENTS

I would like to extend my sincere gratitude to my thesis supervisors Professors Roger Kamm and Ascher Shapiro for their guidance , patience and support throughout the period of my stay at MIT. I have always felt that no other group could have given me as much opportunity for independent growth as was provided by them. I would also like to acknowledge the invaluable help of Professor Tony Patera without whom the computational aspects of his work would not have been possible. Thanks also to Professor Steve Orszag for helpful discussions in the earlier stages of this work.

The friendship and assistance of all the members of the Fluid Mechanics Lab. has provided a wonderful environment to work in. In particular, I would like to thank Dick Fenner for all his help in constructing the experimental apparatus.

Finally, the love and support of my family and my good friend, Martin made this all possible.

TABLE OF CONTENTS

I. INTRODUCTION

The flow induced in a semi-infinite body of fluid by a plate undergoing sinusoidal oscillations in its own plane was originally investigated by Stokes [1851]. If the plate moves with velocity $U_p\cos\omega t$, then the unidirectional flow, parallel to the plate, in the surrounding fluid is given by $u(z,t) = U_p\exp(-z/\delta)\cos(\omega t - z/\delta)$, where $\delta=\sqrt{2\nu/\omega}$ is a measure of boundary layer thickness. The Stokes layer is the representative boundary layer in a large class of problems involving periodic flows within or around rigid boundaries. Our concern is with the stability and turbulent motion of the bounded oscillatory Stokes layer.

Previous work on transition in purely oscillatory flows is rather scarce. Here we make the distinction between "purely" oscillatory flows (about a zero mean) and flows modulated about some non-zero mean. The two problems are quite different, as the instability of flows modulated about a non-zero mean is usually associated with the (steady) mean flow. In this case, the modulations can usually be accounted for by perturbation methods about the mean flow. This contrasts with the situation for purely oscillatory flows where the basic flow is unsteady.

A number of experiments have been reported in literature on the problem of transition in purely oscillatory flows. As these experiments are generally performed in bounded geometries (such as in pipes or in channels), a new parameter describing the ratio of the physical dimensions of the flow (for example, pipe radius or channel half-width) to the Stokes boundary layer thickness is introduced in the problem; $\Lambda=d/2\sqrt{\omega/2\nu}$. Alternatively, Λ can be thought of as the ratio of the diffusive time scale of the flow to the period of oscillation. Note also that Λ is related to the parameter known as Womersley number, $\kappa=d/2\sqrt{\omega/\nu}$, by the relation $\Lambda=\kappa/\sqrt{2}$. All investigators agree that for sufficiently large Λ ($2\lesssim\Lambda$) transition is governed by a Reynolds number that is based on the Stokes boundary layer thickness. Furthermore, a value of Re^{δ} on the order of 500-550 is more often cited as the transitional Reynolds number. Here, $Re^{\delta}=U_o\delta/\nu$, where U_o is the amplitude of cross-sectional mean velocity and $\delta=\sqrt{2\nu/\omega}$ is the Stokes boundary layer thickness. For example, for flow in a straight pipe Sergeev [1966] found the transitional Reynolds number to be $Re^{\delta}\sim500$ for the range of $2.8<\Lambda<28$; while Hino, et al. [1976] and Ohmi, et al. [1982] each found the transitional Reynolds number to be $Re^{\delta}\sim550$ for the range of $2<\Lambda<6$ (Hino, et al.) and $2<\Lambda<29$ (Ohmi, et al.), respectively. In a different geometry, Li [1954] observed turbulence for $Re^{\delta}>565$ for flow in a channel with an oscillating bottom. The value of 500 for the transitional Reynolds number, however, is not

universal; for example, Merkli and Thomann [1975] observed that the flow in a resonant pipe became turbulent at a Re^{δ} of 280 ($30<\Lambda<50$); while Vincent [1957] and Collins [1963] found the flow due to periodic gravity waves on a smooth plate to become turbulent at Reynolds numbers of 110 and 160, respectively.

Of the various experimental studies, the works of Hino and coworkers are the most detailed. They distinguish four classes of flows in their experiments: (I) laminar flows, (II) distorted laminar or weakly turbulent flows, which are characterized by the appearance of small amplitude perturbations in the early stages of the acceleration phase, (III) turbulent flows, which are characterized by the explosive appearance of turbulence with the start of the deceleration phase and which recover to "laminar" flow during the acceleration phase, (IV) turbulent flows that remain turbulent throughout the cycle. Flow regime (IV) has not been observed by any of the investigators, although Ohmi, et al. observed that as Re^{δ} was increased, turbulent bursts occurred in the later stages of the acceleration phase as well as in the deceleration phase.

In the experiments of Hino, et al. and Ohmi, et al., the transitional Reynolds number of 550 marked the onset of flow regime (III) independent of Λ. Flow regime (II) was observed by Hino and coworkers over a range of Reynolds

numbers $Re^{\delta}_{min} < Re^{\delta} < 550$, where the value of Re^{δ}_{min} was dependent on Λ; for example, for $\Lambda=6.2$ flow regime (II) was observed for $70 < Re^{\delta} < 550$ while for $\Lambda=1.9$ the same flow regime was observed for $460 < Re^{\delta} < 550$. Ohmi, et al. on the other hand, found that onset of flow regime (II) in their experiments agreed well with the critical Reynolds number of $Re^{\delta} \sim 280$ which was proposed by Merkli and Thomann. In other words, flow regime (II) was observed by Ohmi, et al. for $280 < Re^{\delta} < 550$ independent of the value of Λ. Merkli and Thomann [1975] themselves do not make any distinction between flows of type (II) and (III), and therefore it is not possible to determine in giving the value of 280 for the transitional Reynolds number which type of flow they were referring to.

In general, when reference is made to turbulent oscillatory flows, the regime (III) described above is intended. The details of the flow structure in this regime was studied by Hino and coworkers [1983] for flow in a rectangular duct at $Re^{\delta}=876$ and $\Lambda=12.8$. The profiles of mean velocity, the turbulence intensities, the Reynolds stresses and the turbulent energy production rate were found to be completely different between the accelerating and decelerating phases, and in either case quite different from turbulence in flows which are steady in the mean. Nevertheless, they concluded that the basic processes such as ejection, sweep and interaction towards and away from the wall are the same as those of 'steady' wall turbulence.

Theoretical investigation of the stability of Stokes layers is also relatively new. The mathematics of the problem, even for the 'linearized' case is quite complicated. The complexity arises because in the presence of a time-periodic basic flow, the linearized equations for the disturbances have coefficients that are periodic functions of time; consequently, the time dependence of the perturbation is not separable and the method of normal modes is no more (formally) applicable. Two classes of solutions have been suggested in the literature for this problem; analysis by Floquet theory and solution based on the assumption of quasi-steadiness. Von Kerczek and Davis [1974] noted that since the linearized equations have coefficients that are periodic functions of time, the results of Floquet theory [Coddington and Levinson (1955), Yih (1968)] can be employed to predict that in the periodic steady state the disturbance stream function should be of the form $\phi(x,z,\tau)=e^{i\alpha x+\lambda\tau}\psi(z,\tau)$+complex conjugate. Here, $\tau=\omega t$ is the time normalized to the period of oscillation of the basic flow, α is the streamwise wavenumber (with x normalized to the Stokes layer thickness), λ is the Floquet exponent and represents the net growth (and phase change) of the disturbance field from one cycle to the next, and ψ is a periodic function of time with the same period as the basic flow and represents the variation of the disturbance field within each cycle. The disturbances experience a net growth from one cycle to the next if $\text{Real}(\lambda)>0$. Von Kerczek and

Davis used a Galerkin technique to numerically integrate the resulting system of equations for the geometry consisting of an oscillating plate with a second stationary plate placed a distance of eight boundary layer thicknesses away. For the range of wavenumbers $0.3<\alpha<1.3$ and Reynolds numbers $0<Re^{\delta}<800$, they found λ to be real and in all cases negative, indicating a net decay of disturbances from one cycle to the next. The periodic part of the stream function, $\psi(z,\tau)$, was also found to experience no considerable growth within a cycle; thereby ruling out the possibility that within a cycle the disturbances may grow to such an extent that the flow might become nonlinearly unstable. Therefore von Kerczek and Davis concluded that the Stokes layer is absolutely stable to infinitesimal disturbances for the range of parameters investigated and possibly for all Reynolds numbers.

As a corollary to their work, von Kerczek and Davis point out that since the principal Floquet exponent λ found in their numerical results was in all cases O(1), one must conclude that the time scale for the growth or decay of linear disturbances is of the same order of magnitude as the time scale of oscillation of the basic flow. This would serve as a warning against the use of quasi-steady theories; as the quasi-steady assumption would be valid only if the disturbances varied much faster than $1/\omega$.

Hall [1978] investigated the linear stability of the infinite Stokes layer using Floquet theory, and found this flow to be also stable for all Reynolds numbers investigated ($0<Re^{\delta}<300$). In addition to a discrete set of eigenvalues, the Orr-Sommerfeld equation for the infinite Stokes layer was found to also have a continuous spectrum of eigenvalues for all Reynolds numbers. The most dangerous modes were associated with this continuous spectrum. Hall also considered the effect of introducing a second boundary a long way from the Stokes layer, as was done in the problem addressed by von Kerczek and Davis. For the latter problem only a discrete set of eigenvalues exists. Hall showed that the least stable disturbance of the 'finite' Stokes layer was not the same as the least stable <u>discrete</u> eigenvalue of the infinite Stokes layer; rather the eigenmodes of the 'finite' Stokes layer were found to 'merge' into the continuous spectrum of the infinite Stokes layer as the separation between the two plates tended to infinity. Thus he concluded that the disturbances given by von Kerczek and Davis have no connection with those of the infinite Stokes layer.

Despite the objections raised by von Kerczek and Davis against the use of quasi-steady theories in studying the stability of Stokes layers, one can show that quasi-steadiness is a fair assumption if one is considering the inflectional instabilities of the Stokes layer. First, note

that at all time during the cycle the Stokes layer has an infinite number of inflection points, each satisfying Fjortoft's criterion for instability. For example, for a flat plate oscillating with velocity $U_p \cos\omega t$ there is an inflection point on the plate ($y/\delta=0$) at $\omega t=0$ (as well as other ones at $y/\delta=n\pi$) which move away from the wall as time progresses within a cycle. At asymptotically large Reynolds numbers, these inflection points may become inviscidly unstable. Since the time scale for the growth or decay of inflectional instabilities (δ/U_p) is much shorter than the period of oscillation ($1/\omega$); $(\delta/U_p)\sim 1/Re^{\delta}(1/\omega)$, one can neglect the time dependence of the base flow and study the stability of the flow by solving the (inviscid) Rayleigh equation for a succession of quasi-steady velocity profiles for different times during the cycle. This approach has been adopted by Cowley [1985] and by Monkewitz and Bunster [1985]. One problem with this type of analysis is that the normal modes, which are associated with the inflection points, completely change character from one cycle to the next as they move away from the wall. This makes it difficult to compare these results to those of the Floquet theory (which assumes the flow has reached a periodic steady state). Monkewitz and Bunster suggest a scenario where a mode associated with an inflection point moving away from the wall would pass its energy to a mode associated with an inflection point closer to the wall, before it gets damped out in the free stream where inflection points are exponentially weak.

Cowley [1985] carried out an inviscid quasi-steady analysis of the stability of the Stokes layer for asymptotically large Reynolds numbers where the effects of interaction between different modes was included in the analysis. His results showed that disturbances with wavelengths comparable to δ can grow. The most significant growth rates were observed between $\pi/4$ and $\pi/2$; i.e, just before the start of the acceleration phase of the cycle. None of these modes were found to evolve in such a way as to return to their original state (multiplied by a constant factor) after one cycle, as would be required by Floquet theory. Therefore, although these results are not necessarily incompatible with the results of the Floquet theory, no direct comparison between the two theories is possible either.

In short, the present status of knowledge with regards to the stability of flat Stokes layers can be summarized as follows. On the one hand, experimental results show that the flow undergoes violent transition to turbulence with the start of the deceleration phase of the cycle at Reynolds numbers on the order of 500. Theoretical studies, on the other hand, have so far been restricted to <u>infinitesimal</u> disturbances and either predict the flow to be absolutely stable in the periodic steady state (Floquet theory), or consist of analyses which are valid for <u>asymptotically</u> large Reynolds numbers and predict transient instability but at

phases during the cycle opposite to where turbulence is observed in experiments (inviscid quasi-steady theories). In either case no critical Reynolds number can be identified for comparison to the experimental value for the transitional Reynolds number. Clearly a large gap exists between theory and experiment in the problem of stability of flat Stokes layers.

In the present work we have tried to bridge some of this gap by performing simultaneous experimental and numerical studies of bounded oscillatory Stokes flows at transitional and turbulent Reynolds numbers. The experiments were performed in circular pipes. We felt these experiments were necessary; because even though a number of experiments have been reported in literature on the stability of oscillatory Stokes layers, the only detailed work is that of Hino and coworkers [1983] which is restricted to a single flow condition, $Re^{\delta}=876$, $\Lambda=12.8$. As we shall see, our experimental results are for the most part in agreement with, and serve as a confirmation of the earlier work of Hino and coworkers. We believe this confirmation by itself is quite important. Furthermore, comparisons between the two sets of experiments has allowed us to draw conclusions upon key features common to both sets that were neglected (or may have been rejected as noise) by Hino and coworkers.

To identify the nature of disturbances that could explain the experimentally observed values of transitional Reynolds numbers, and to gain an understanding of the physics of the transition back and forth between the laminar and turbulent states that is observed in experiments at values of Reynolds number above $Re_{trans.}$; we have performed direct numerical simulations of the full, time-dependent three-dimensional Navier-Stokes equation for oscillatory flow in a channel. The channel geometry was chosen for the ease of computation and in light of the close agreement between our experimental results for flow in a pipe, and the experiments of Hino, et al. which were performed in a channel. The channel flow is subjected to initial conditions that consist of various combinations of two- and three-dimensional infinitesimal and finite-amplitude disturbances and the time evolution of the disturbances are followed. The disturbances that most closely reproduce the experimentally observed features are identified, and the dynamics and mechanisms of transition is discussed.

II. EXPERIMENTS

2.1 Experimental Methods

The experiments were performed in a quartz circular pipe, 2 cm in inner diameter and 8 meters long using the experimental setup shown schematically in Figure 1. The length of the quartz pipe was chosen such that under all flow conditions the tube length was at least three times the stroke length of the flow in the quartz pipe; thereby ensuring that the flow in the middle section of the pipe was not suffering from any end effects. A tube geometry was chosen for the experiments over a two-dimensional channel or an oscillating plate, because of the great care required to ensure two-dimensionality in a channel and the complex flow systems that would be required for an oscillating plate. The choice of a particular geometry does not seem to be too critical, as earlier experimental studies show a close correspondence between the structure of the turbulent oscillatory flows in all three geometries.

The sinusoidal flow rate into the quartz pipe was generated by a piston whose motion was controlled by an electrohydraulic servovalve (MOOG model 76-102) with feedback control on the velocity. The sinusoidal output of a function generator served as the input command for the control circuitry. The quality of the sinusoidal flow rate

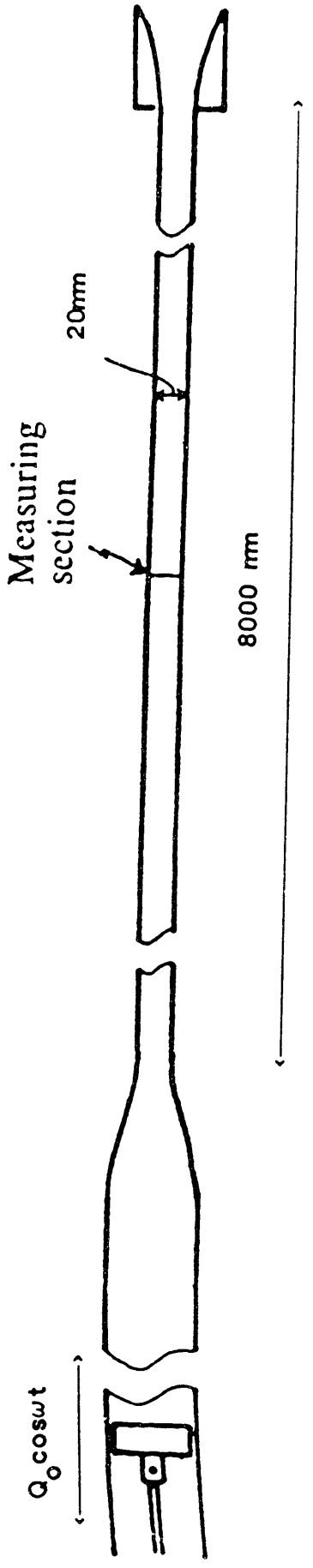

Figure 1. Schematic of the apparatus.

generated by this flow system was checked by monitoring the motion of the piston with a velocity transducer (LVDT, Schaevitz model 6L3-VTZ) and also by computing the flow rates based on LDA measurements of the velocity profiles. In each case an FFT fit was performed on the output. The results of these two measurements for the flow rate of poorest sinusoidal quality is shown in Figures 2a and 2b. As seen in these figures, the maximum deviation from a pure sinusoid occurs near the point of zero flow. At this point because of some backlash in the O-ring seals on the piston, the motion of the piston could not follow the input command. Despite considerable effort on our part to overcome this backlash, the problem was not eliminated. There was no mean flow.

Velocity measurements were obtained using a DISA two color laser doppler anemometer in which the blue (488 nm) and green (514 nm) lines of an Argon laser were used to measure simultaneously the axial and radial velocity components. The LDA was equipped with a Bragg cell and was operated in the backscatter mode. Counters were used for signal processing. The probe volume had dimensions of 20x20x100 microns and fringes were 2 microns apart. The front lense in the LDA system was mounted on a two-axis linear translation stage with micrometer control of position to within .0001". This traversing mechanism was used to position the probe volume at selected points along a diameter within the quartz pipe.

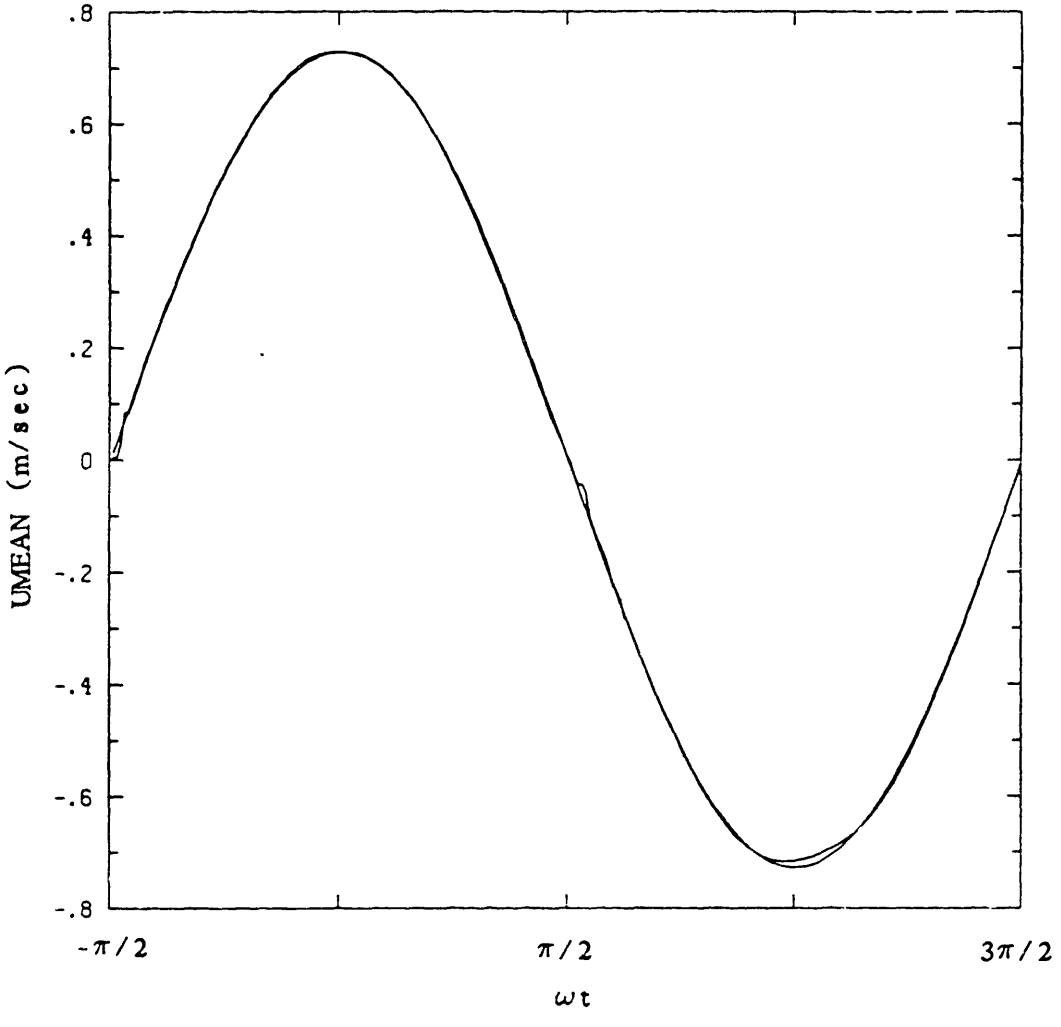

Figure 2a. Cross-sectional mean velocity calculated from the output of the LVDT that was used to measure the velocity of the piston.

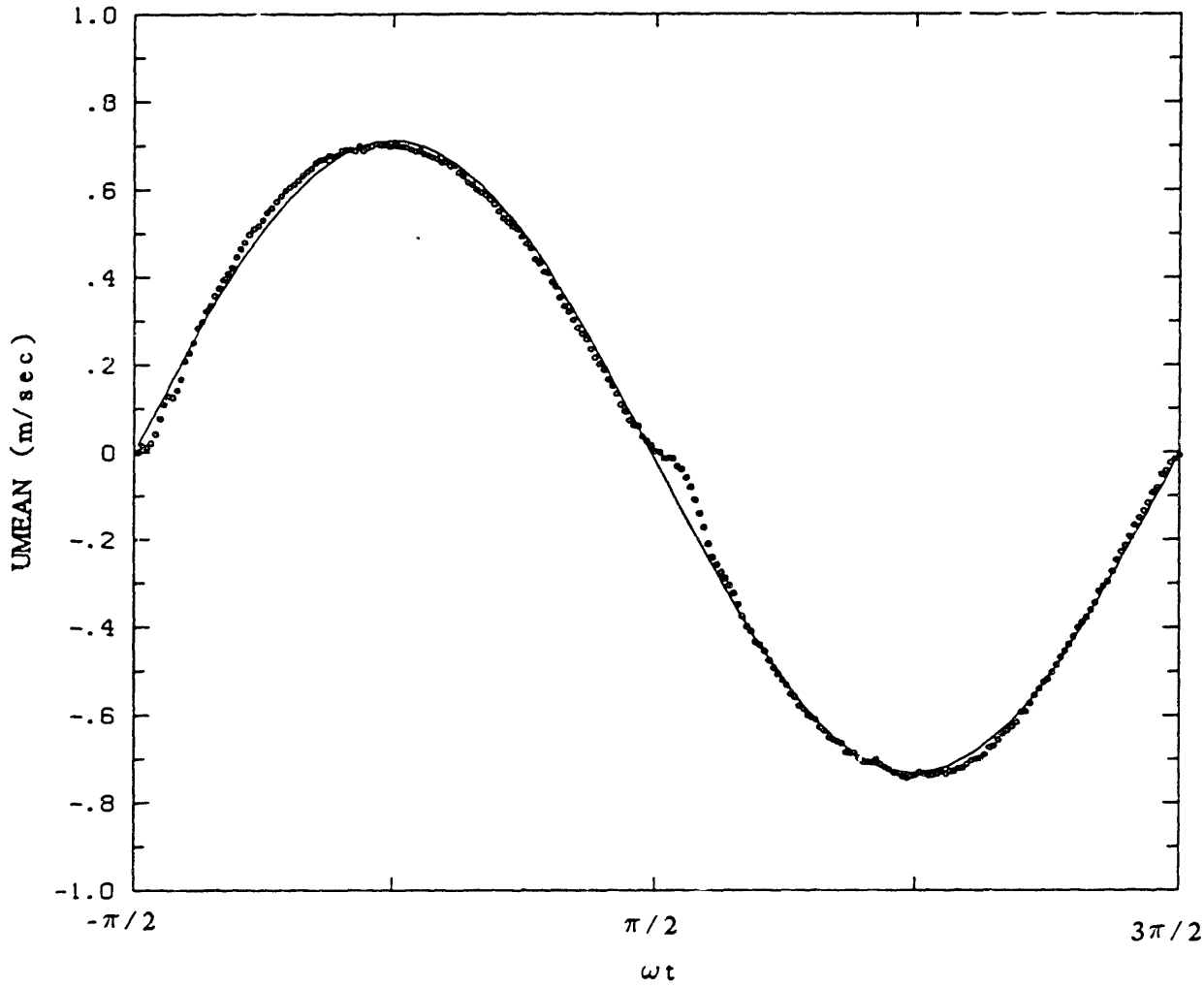

Figure 2b. Cross-sectional mean velocity calculated by integrating the velocity profiles that were obtained by the LDA system.

Because the basic flow was unsteady, the time of arrival of each doppler burst in relation to the periodic motion of the basic flow had to be determined. This was accomplished by a MINC PDP11/23 data acquisition computer. The computer was equipped with an internal clock, a DMA parallel interface board (DRV11-J), and A/D converters. In every cycle, at a point corresponding to (positive-going) zero flow rate into the system, the computer clock was triggered to start counting. The trigger point was determined from the output of the velocity transducer that monitored the motion of the driving piston. For the first few cycles, the time between successive triggers was measured to evaluate the precise period of the basic flow. This period was then used to set the clock so that every 1/240th of a cycle it would overflow and increment a register within the computer. This register would then indicate time in fractions of 1/240th of the cycle period. The register was reset at the beginning of each cycle. The data acquisition protocol can then be summarized as follows. Once both LDA counters had verified a doppler burst (within 15 μsec of each other), the computer would be interrupted via the parallel interface board. The time in increments of 1/240th of the period of the cycle would be read from the appropriate register, and the doppler information consisting of the doppler frequencies, the number of fringes associated with each doppler burst and the time would be stored in the computer for later processing. In addition to the above

information, the instantaneous pressure drop through the quartz pipe (measured with a Microswitch pressure transducer) and the flow rate through the system (as measured by the velocity transducer attached to the piston) were sampled through the A/D converters 240 times per cycle and stored.

Typically on the order of 2000 doppler bursts per sec were processed in this manner. The rate limiting factor was the amount of seeding that could be used before the flow became opaque.

The optical distortion of the quartz pipe was eliminated by index-matching the working fluid to that of quartz (n_d = 1.458) using an aqueous solution of ammonium thiocyanate. The solution was mixed until the correct index of refraction was achieved (approximately equal weights of ammonium thiocyanate salt and distilled water).A hand held refractometer (Extech, model K502192) with 0-90% sucrose range (n_d=1.333-1.512) and ±0.2% accuracy was used to measure the index of refraction of the solution. Otherwise, the solution had properties very close to water (ρ=1.1 g/cm^3 , ν=1.32 centistokes) . At the measurement site the quartz pipe was immersed in a rectangular chamber with quartz windows which was filled with the same index-matched fluid.

A variety of seeding particles including alumina, latex, silicon carbide and titanium dioxde were examined. Titanium dioxide (with particles of diameter from .5 to 1 microns) was chosen over the others because of its good signal to noise ratio and ability to follow the smaller scales of turbulence.

2.2 *Experimental Results*

2.2.1 *Calibration Run*

To check the reliability of our experimental methods, the velocity profiles for an example of laminar flow (Re^{δ}=233, Λ=3.6) were measured. In the laminar regime, the equations of motion have a closed form solution as given by Womersley [1955] and Uchida [1956], and provide a direct check on the experimental results. For a sinusoidal flow rate, $Q=Q_o\cos\omega t$, the instantaneous velocity profiles are given by,

$$\frac{u(r,\omega t)}{U_o} = \frac{B\cos(\omega t+\delta) + (1-A)\sin(\omega t+\delta)}{\sqrt{(1-C/\kappa)^2 + (D/\kappa)^2}} \qquad (1)$$

where, $\kappa = \Lambda/\sqrt{2}$ (note that $\kappa \equiv$ Womersley number)

$$A = \frac{ber(\kappa)\,ber(r\sqrt{\omega/\nu}) + bei(\kappa)\,bei(r\sqrt{\omega/\nu})}{ber^2(\kappa) + bei^2(\kappa)}$$

$$B = \frac{bei(\kappa)\,ber(r\sqrt{\omega/\nu}) - ber(\kappa)\,bei(r\sqrt{\omega/\nu})}{ber^2(\kappa) + bei^2(\kappa)}$$

$$C = \frac{ber(\kappa)\,bei'(\kappa) - bei(\kappa)\,ber'(\kappa)}{ber^2(\kappa) + bei^2(\kappa)}$$

$$D = \frac{ber(\kappa)\,ber'(\kappa) + bei(\kappa)\,bei'(\kappa)}{ber^2(\kappa) + bei^2(\kappa)}$$

$$\delta = \tan^{-1}\left\{\frac{1-C/\kappa}{D/\kappa}\right\}$$

The comparison between experiments and the theoretical solution of Uchida is shown in Figures 3 and 4. Figure 3 shows the time evolution of axial velocity at various radial locations. The theoretical solution predicts sinusoidal variation at each location, however the points in the boundary layer have a phase lead with respect to the core. In Figure 4, the experimental velocity profiles for various phases during the cycle are compared to the theoretical curve. The agreement between theory and experiment is in general very good. The maximum deviation from theory occurs at $\omega t=\pi/2$, which corresponds to 'turnaround' in the motion of the driving piston. At this phase because of some backlash in the O-ring seals, the motion of the piston deviated from a pure sinusoid as already discussed in section 2.1 .

2.2.2 Turbulent Flow Regime

Hino et al. [1976] have fairly extensively investigated the transitional regime in an oscillatory pipe flow. As already discussed in detail in the introduction, they observed two classes of non-laminar flows in their experiments. One class can be identified as "distorted laminar" or "weakly turbulent" and is characterized by the appearance of small amplitude disturbances that are superimposed on the laminar profile during the acceleration

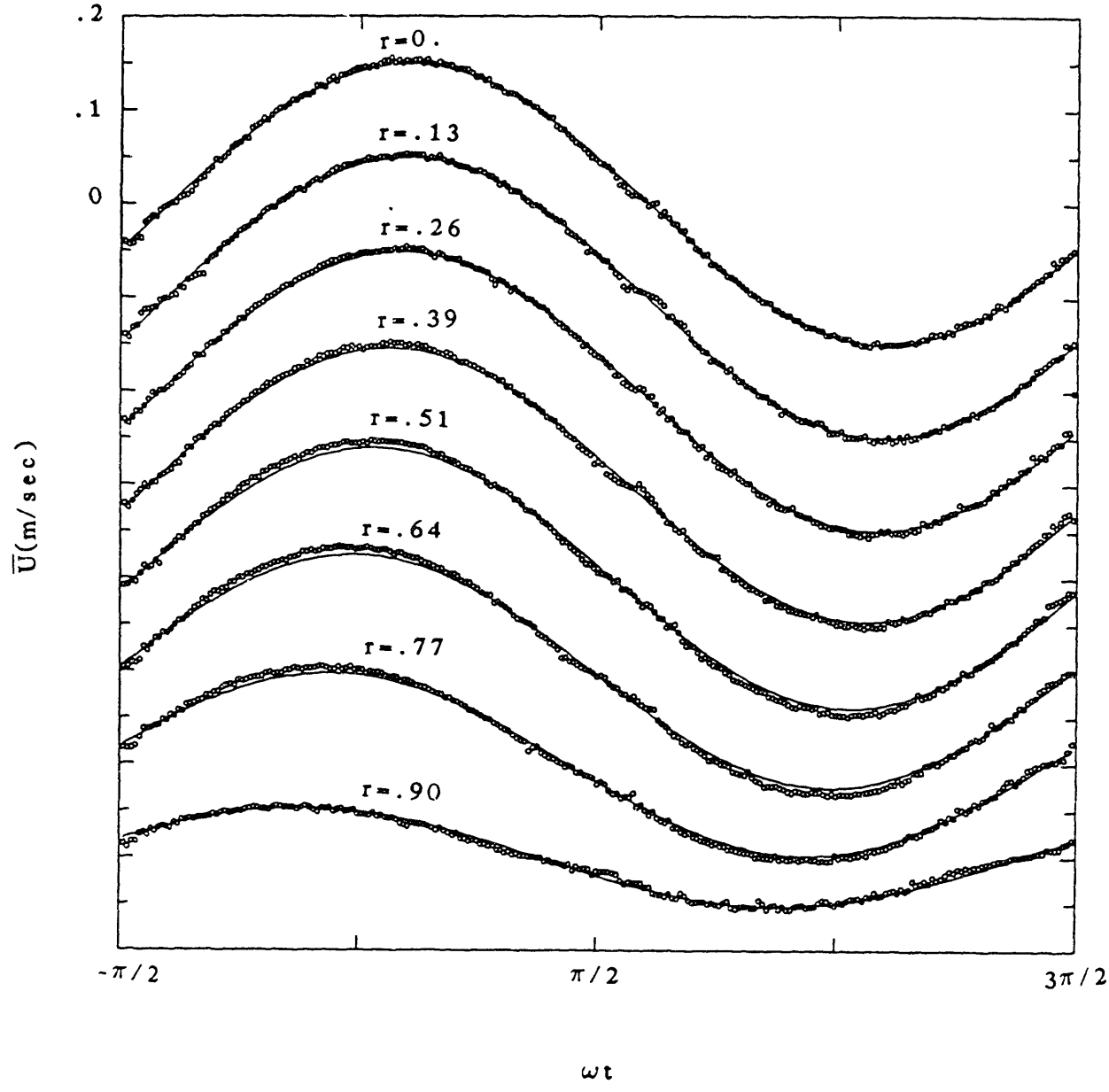

Figure 3. Phase variation of axial velocity at fixed radial locations compared to theory in the laminar flow regime. (Re^{δ}=233, Λ=3.6)

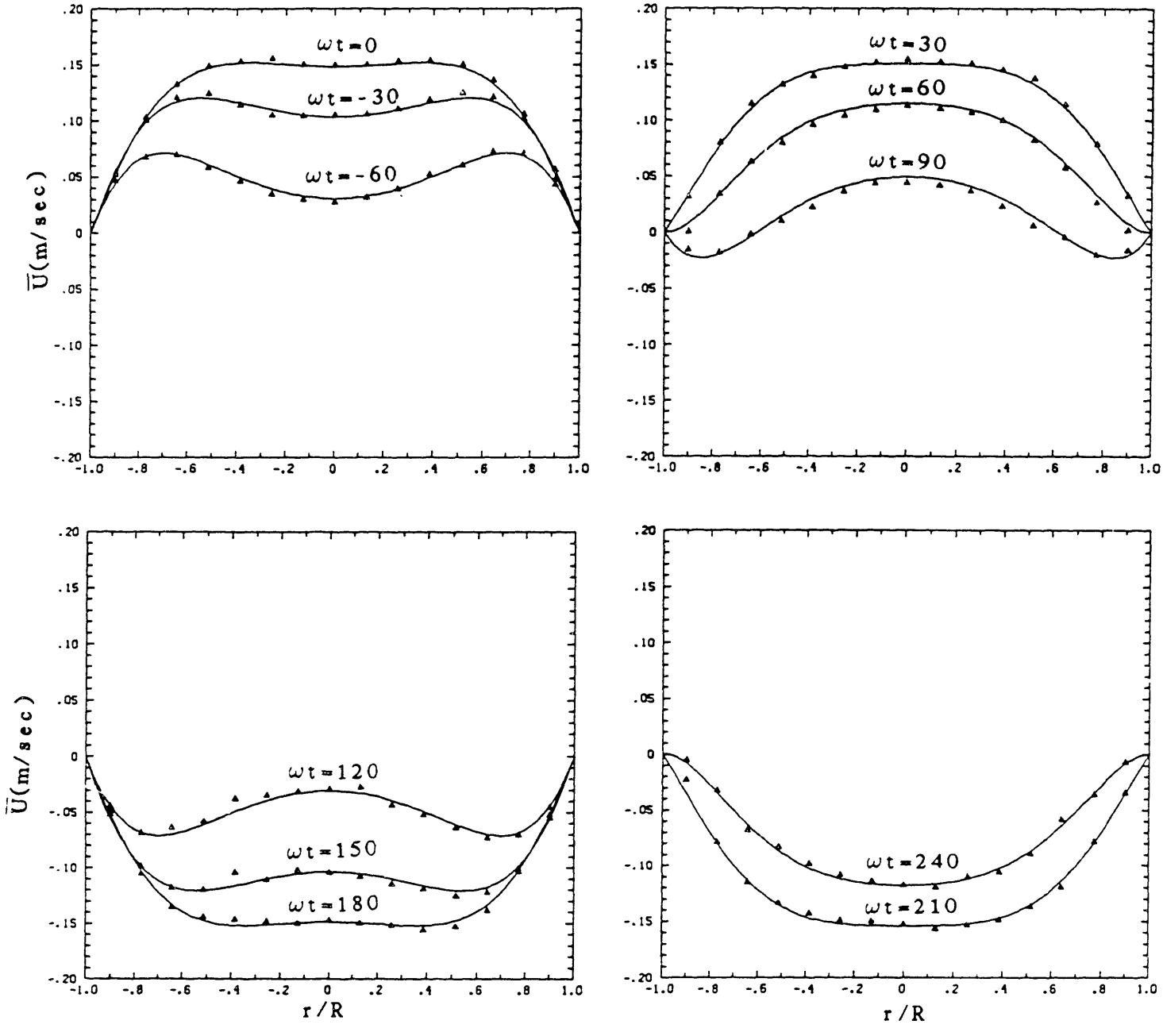

Figure 4. Experimental velocity profiles at various phases compared to theory for laminar flow. (Re^{δ}=233, Λ=3.6)

phase of the cycle. The other type of flow is what is generally considered "turbulent" and is characterized by the sudden explosive appearance of turbulent bursts with the start of the deceleration phase and recovers to laminar flow during the acceleration phase. Our main concern in this work is with the characterization of the latter "turbulent" type of flow.

The stability boundary for "turbulent" flows (of the second kind described above) is very well defined in our, as well as other investigators experiments. In particular, these flows were observed in our experiments for $Re^{\delta} \geq 500$ ($3 < \Lambda < 10$) consistent with observations of earlier investigators.

In contrast, the region of dominance of "distorted laminar" flows seems to be strongly dependent on the specific experimental apparatus. For example, Hino, et al. observed these flows for $70 < Re^{\delta} < 550$ at a Λ of 6.2, and for $460 < Re^{\delta} < 550$ at a Λ of 1.9; while the same flow regime was observed by Ohmi, et al. for $280 < Re^{\delta} < 550$ independent of the value of Λ. We have not made any attempt to identify these flows in our experiments.

In the turbulent regime we have made detailed measurements of the flow field for four flow conditions; Λ=10.6 Re^{δ}=530, 1080, 1720; and Λ=5.7 Re^{δ}=957. The

characteristics of the resulting turbulent flow will first be discussed in detail for the flow condition corresponding to Re^{δ}=1080, Λ=10.6 . Most of the features demonstrated by this flow are common to all the flow conditions studied, and as such this data point may be considered as a prototype flow. The effect of different values for Re^{δ} and Λ will then be discussed.

Figure 5 shows the phase variation of the ensemble averaged axial velocity at different radial positions. The ensemble-averaged velocity is defined as,

$$\bar{u}(r,\omega t) = \frac{1}{N}\sum_{j=1}^{N} u_j(r,\omega t \pm \Delta t) \qquad (2)$$

where N is typically on the order of 100, and phase of the cycle is resolved to within $2\Delta t$=1/240th of the period of oscillation. The averages are corrected for the bias errors associated with the finite transit time of the seeding particles through the probe volume [Buchave, 1979]. The solid lines are the theoretical laminar curve, and are given for reference.

The most striking feature of these velocity traces is the explosive appearance of turbulence with the start of the deceleration phase of the cycle, which transfers the momentum of the high speed fluid towards the wall and the momentum of the low speed fluid towards the center. This momentum exchange appears in the velocity traces of Figure

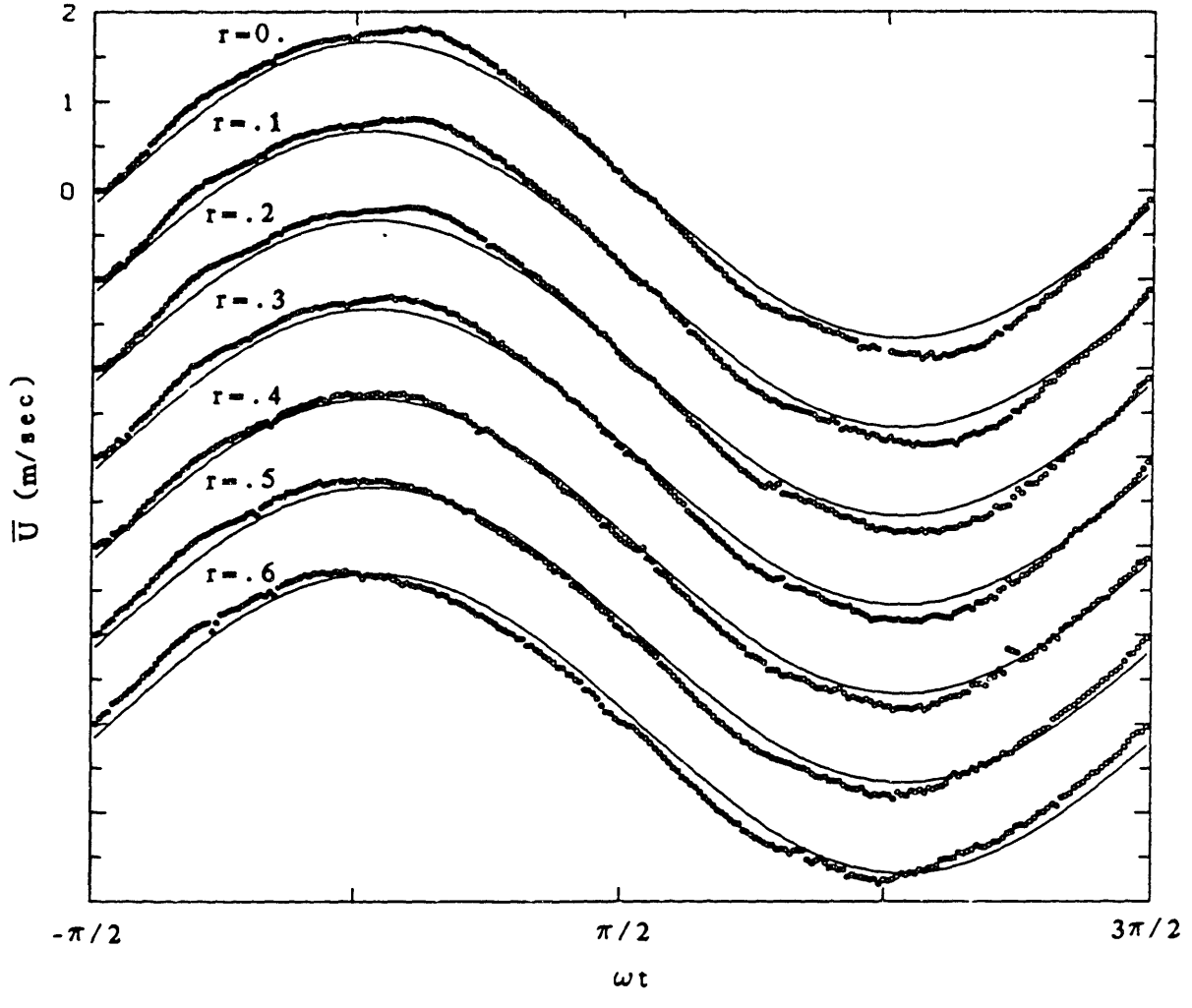

Figure 5a. For caption see Figure 5c.

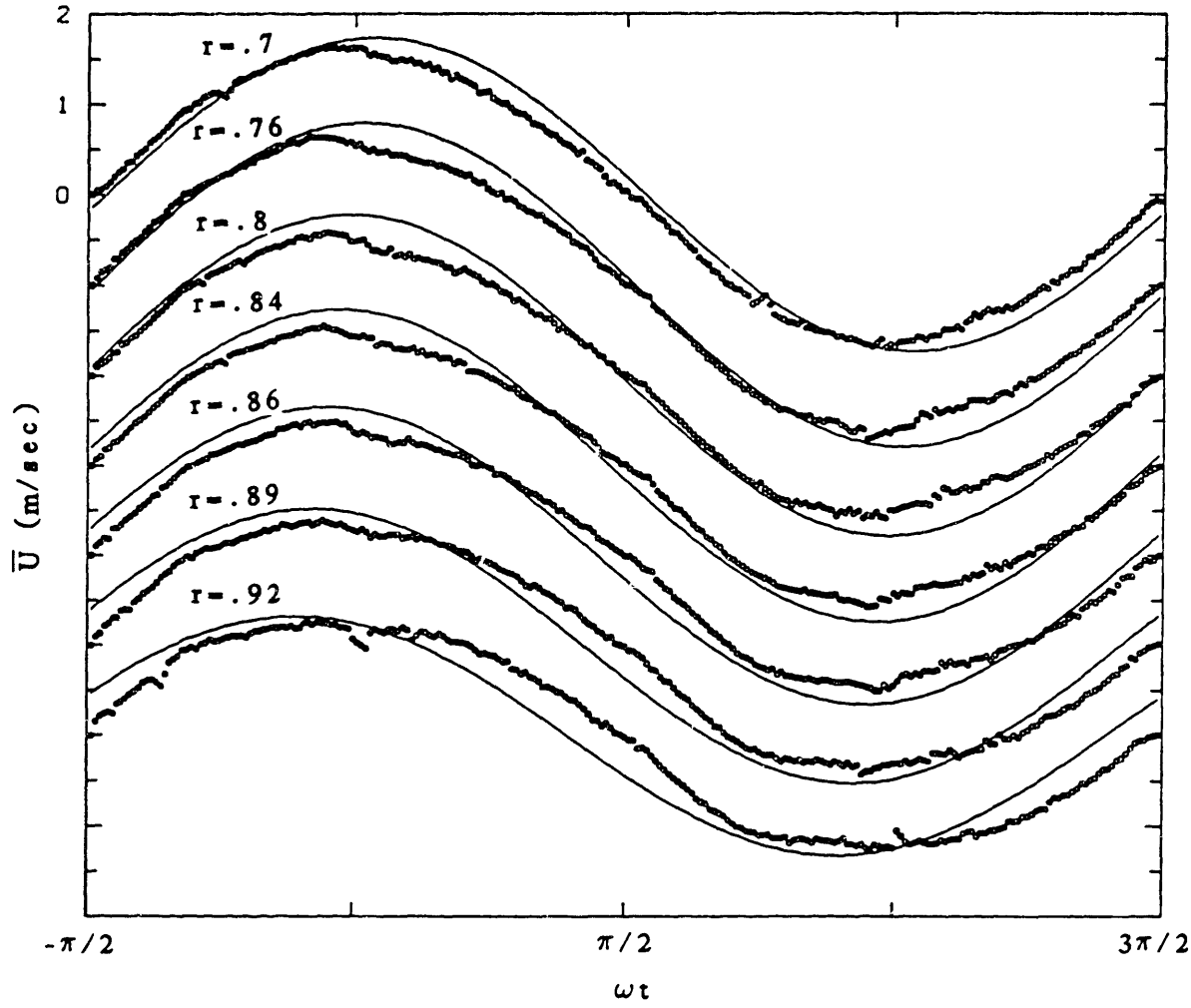

Figure 5b. For caption see Figure 5c.

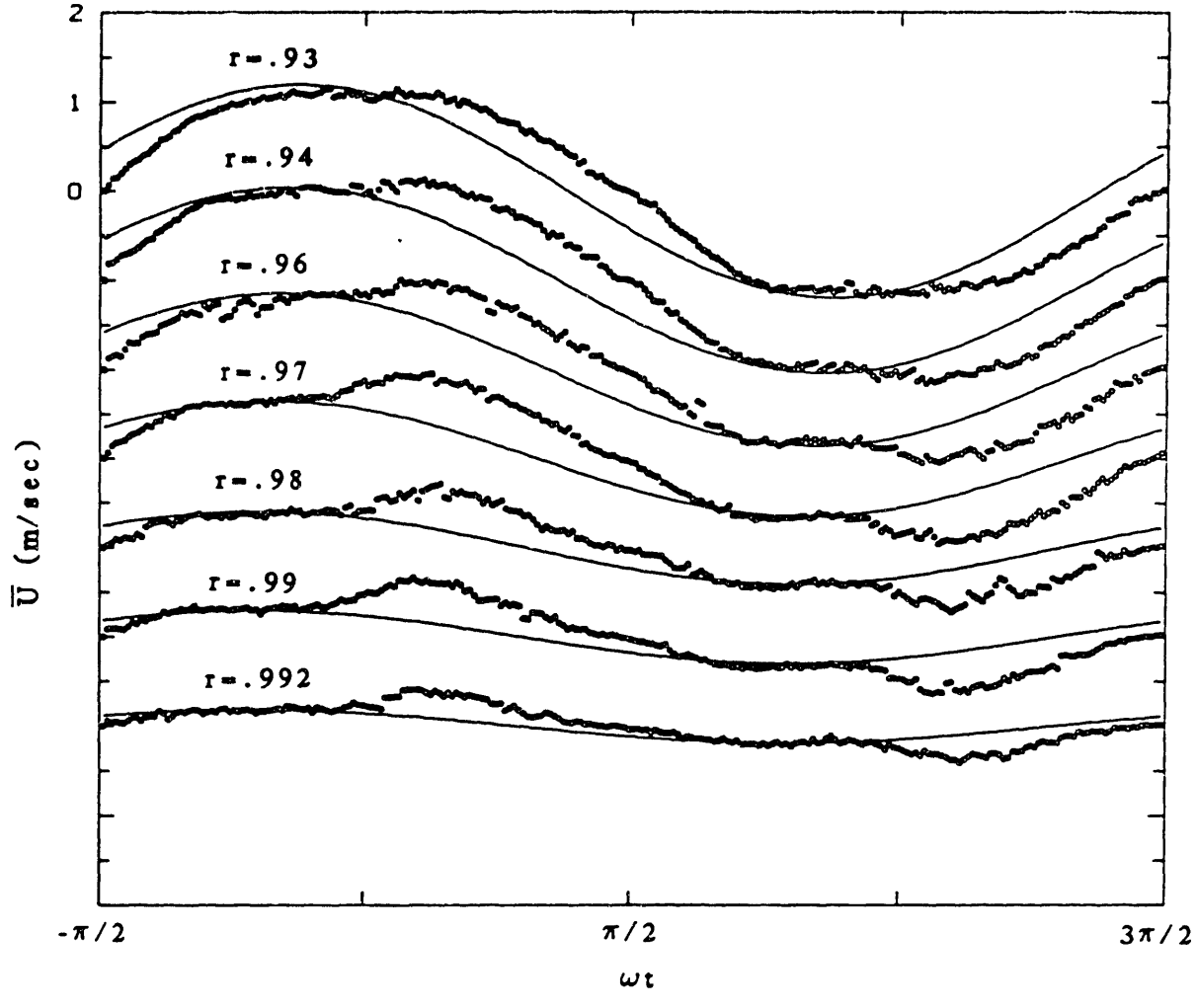

Figure 5c. Phase variation of the ensemble averaged turbulent axial velocity compared to the laminar theoretical curve for various radial positions. (Re^{δ}=1080, Λ=10.6)

5, as a dip at $\omega t=0$ for $0.7<r<0.9$ and a simultaneous hump in the velocity trace for $0.9<r<1.0$.

A direct consequence of this enhanced momentum exchange is that the phase difference in the motion between the boundary layer and the core is significantly reduced by the end of the deceleration phase. This point is best seen in plots of instantaneous average velocity profiles (Figure 6). Once again the solid line represents the laminar solution. Note, for example, that at the time $\omega t=\pi/2$ (corresponding to zero flow rate) there is practically no phase difference between the boundary layer and the core.

In general, the ensemble-averaged velocity profiles during the acceleration phase of the cycle ($-\pi/2<\omega t<0$, $\pi/2<\omega t<\pi$) are similar to the laminar profiles that would result in an oscillating pipe flow, starting from initial conditions $u(r,0)=0$. These profiles, however, are different from Uchida's solution because the flow has not yet reached a periodic steady state. As confirmation of this point, note that the thickness of the boundary layer in the acceleration phase grows approximately in proportion to $\sqrt{\nu t}$, as in Stokes' first problem.

During the deceleration phase of the cycle, ($0<\omega t<\pi/2$, $\pi<\omega t<3\pi/2$) the average velocity profiles are inflexional just outside the boundary layers. The shape of these

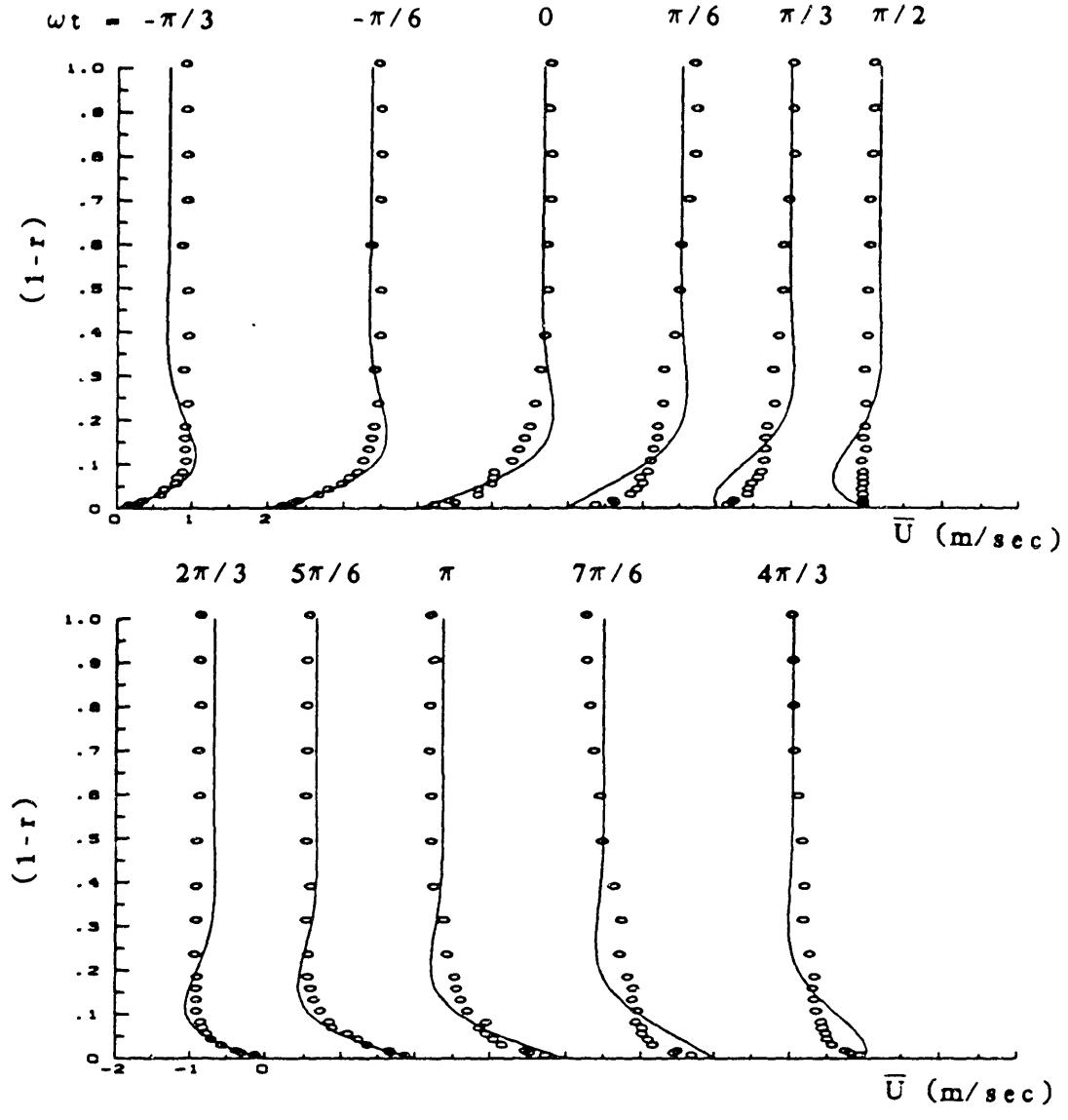

Figure 6. Instantaneous ensemble averaged velocity profiles in the turbulent flow regime compared to the laminar theoretical curve. (Re^{δ}=1080, Λ=10.6)

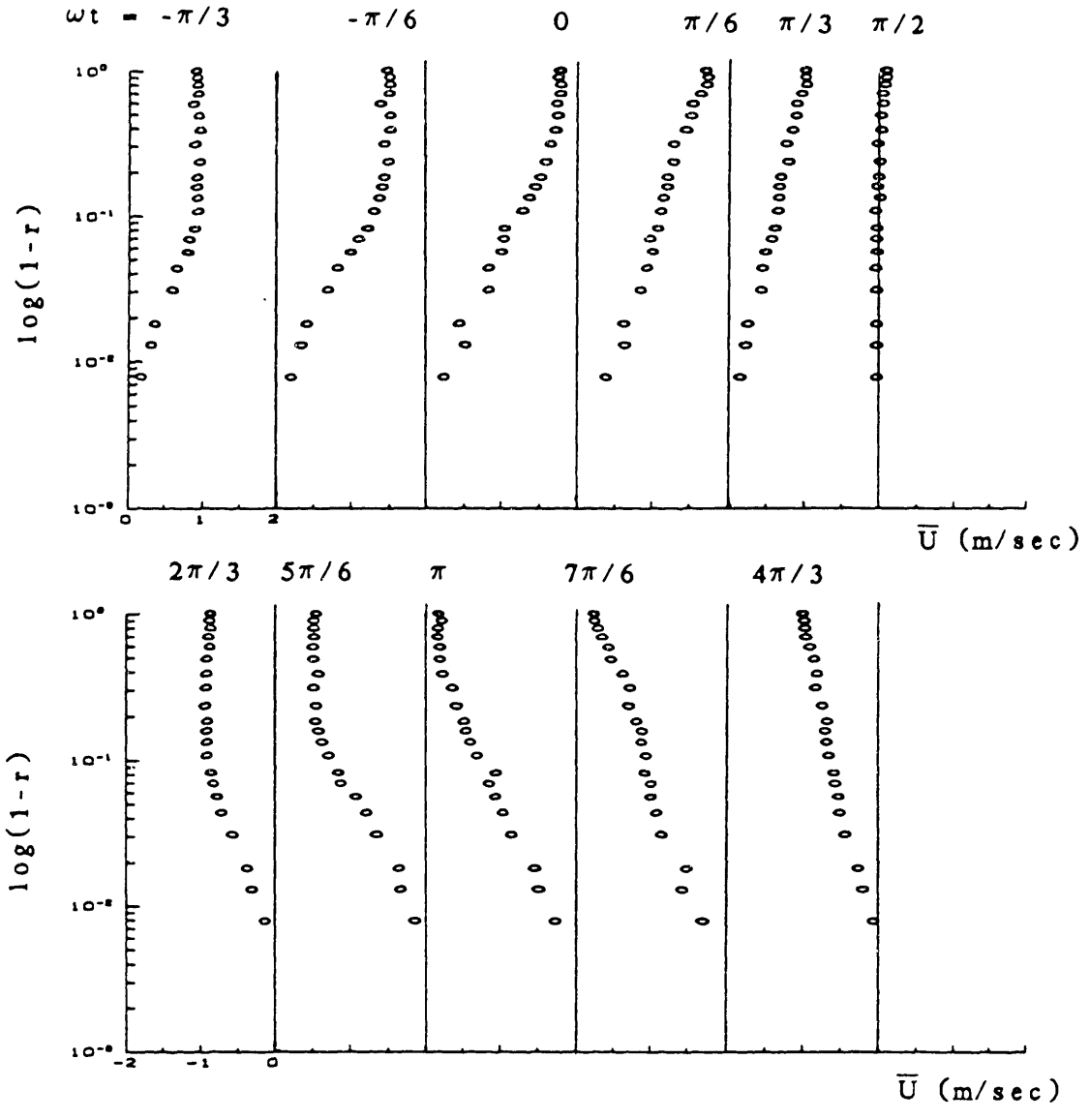

Figure 7. Semi-logarithmic plots of ensemble averaged axial velocity in the turbulent flow regime. (Re^{δ}=1080, Λ=10.6)

profiles is very similar to instantaneous profiles that obtain in steady wall flows during the ejection phase of a turbulent burst, and suggests that the fundamental process of generation of turbulence in oscillatory pipe flow may be the same as that of steady wall flows. This point will be discussed in more detail later.

The contrast between the velocity profiles during the acceleration phase and those for the deceleration phase is best shown in Figure 7, where these profiles are plotted on semi-logarithmic scale. As seen in this figure, during the acceleration phase the regions dominated by the semi-logarithmic law are very narrow, while for the deceleration phase the semi-logarithmic region extends across a much larger portion of the tube.

Instantaneous turbulent velocities are defined as the difference between the instantaneous and the ensemble-averaged velocities,

$$u'(r,\omega t) = u(r,\omega t) - \bar{u}(r,\omega t) \qquad (3)$$

$$v'(r,\omega t) = v(r,\omega t) - \bar{v}(r,\omega t) \qquad (4)$$

The turbulent intensities ($\langle u'^2 \rangle$ and $\langle v'^2 \rangle$) and the Reynolds stress ($\langle u'v' \rangle$) can then be defined as,

$$\langle u'^2 (r,\omega t) \rangle = \frac{1}{N} \sum_{j=1}^{N} u_j'^2(r,\omega t \pm \Delta t) \qquad (5)$$

$$\langle v'^2 (r,\omega t)\rangle = \frac{1}{N} \sum_{j=1}^{N} v_j'^2(r,\omega t \pm \Delta t) \qquad (6)$$

$$\langle u'v'(r,\omega t)\rangle = \frac{1}{N} \sum_{j=1}^{N} u_j'(r,\omega t \pm \Delta t)\ v_j'(r,\omega t \pm \Delta t) \qquad (7)$$

The phase variation of axial and radial turbulence intensities ($\langle u'^2\rangle$, $\langle v'^2\rangle$) at various radial locations is shown in Figures 8 and 10. Throughout the pipe, turbulence intensities remain at a very low level during the acceleration portion of the cycle. However, with the start of deceleration, turbulence appears abruptly in the boundary layer ($0.93 < r < 0.99$) and propagates towards the center. The abrupt generation of turbulence during the deceleration phase seems to first occur at $r \simeq 0.94$ $\omega t \simeq -\pi/8$. Thereafter turbulence levels rapidly intensify throughout the boundary layer; with the axial turbulence intensity reaching its peak value around $r \simeq 0.98$, $\omega t \simeq \pi/10$. During the later stages of the deceleration phase turbulence intensities gradually drop to low levels.

Spatially, axial turbulence intensities are substantially reduced as the center of the pipe is approached. The distribution of axial turbulence intensity across the pipe at different phases during the cycle is shown in Figure 9, and confirms the above arguments.

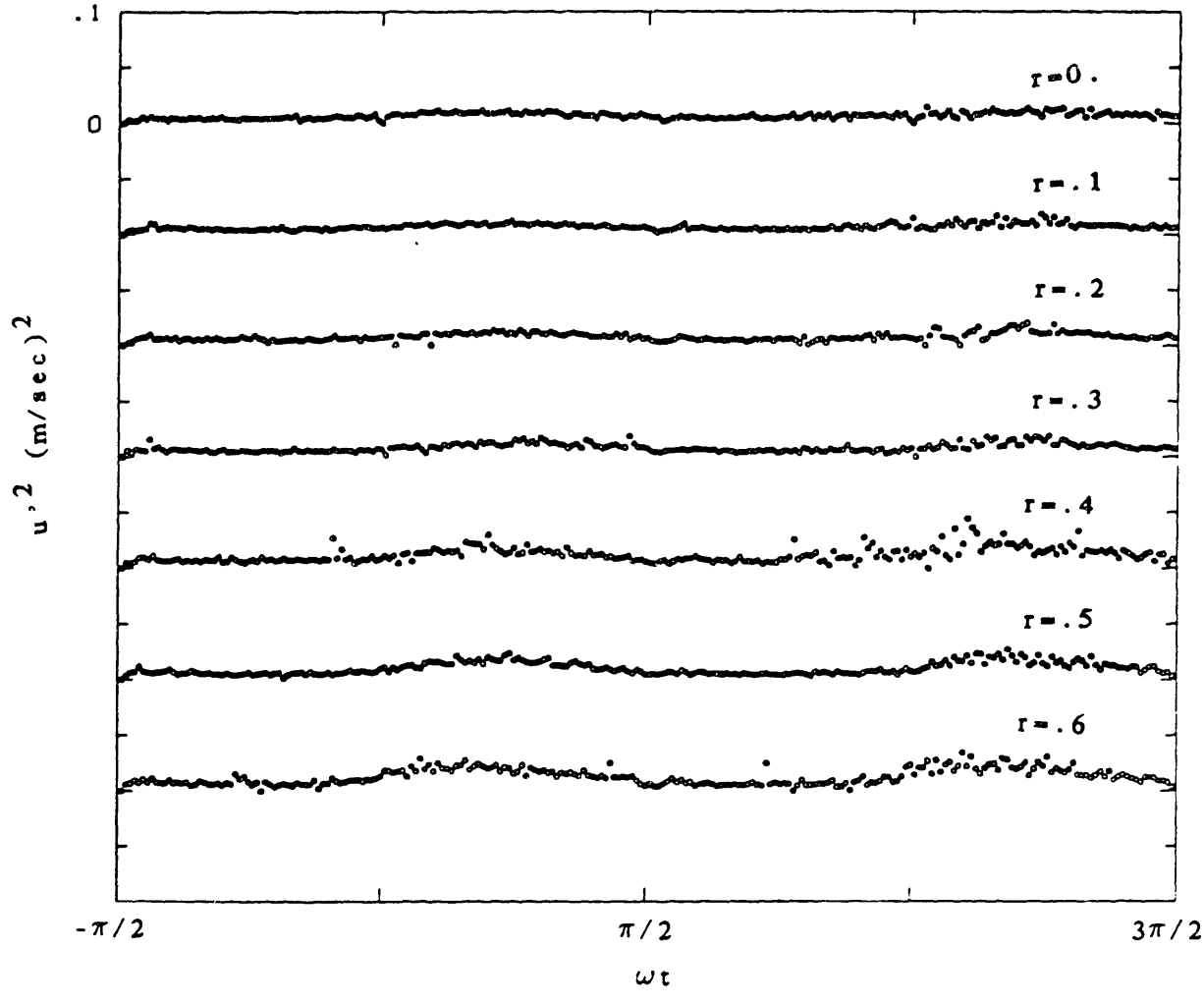

Figure 8a. For caption see Figure 8c.

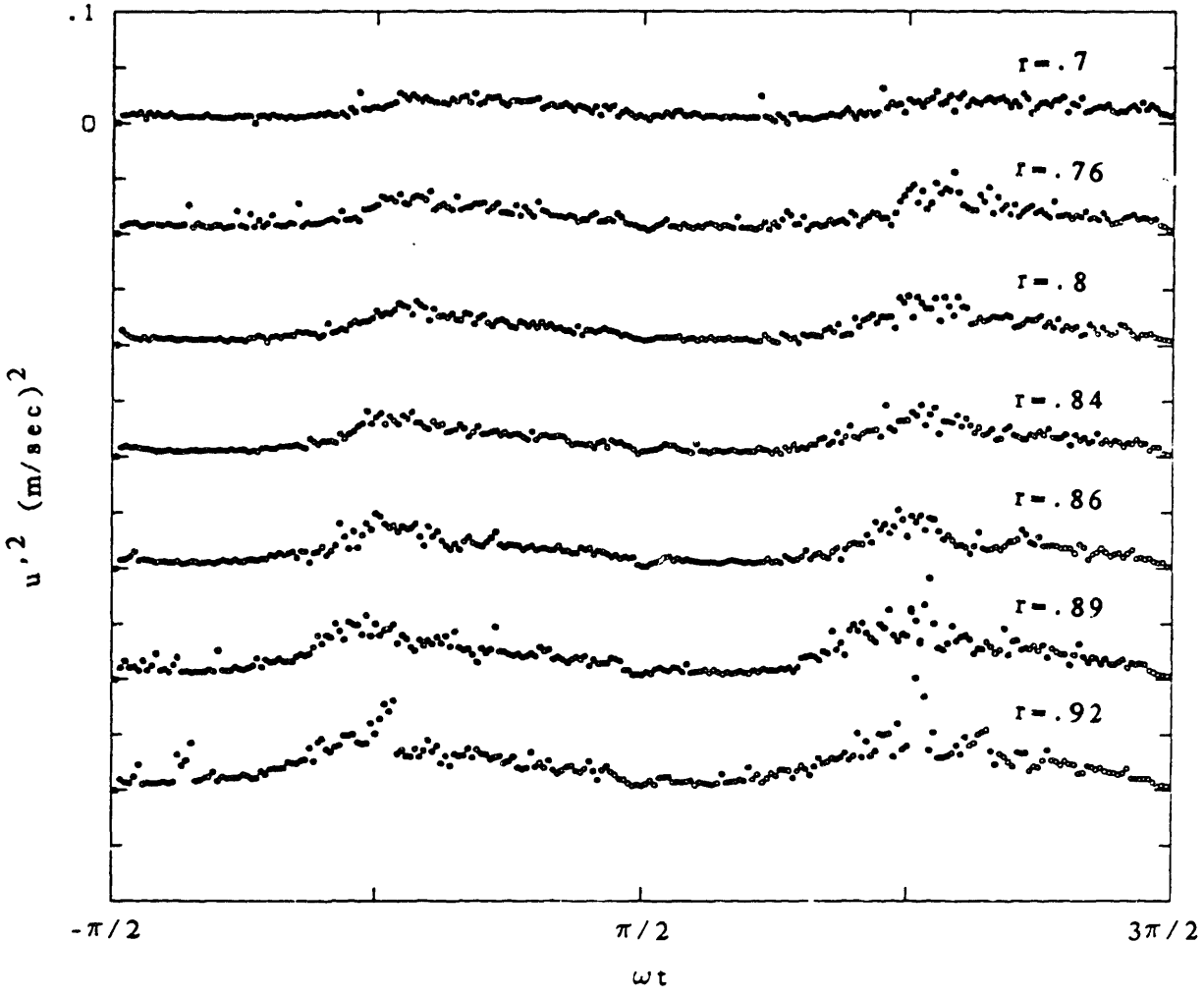

Figure 8b. For caption see Figure 8c.

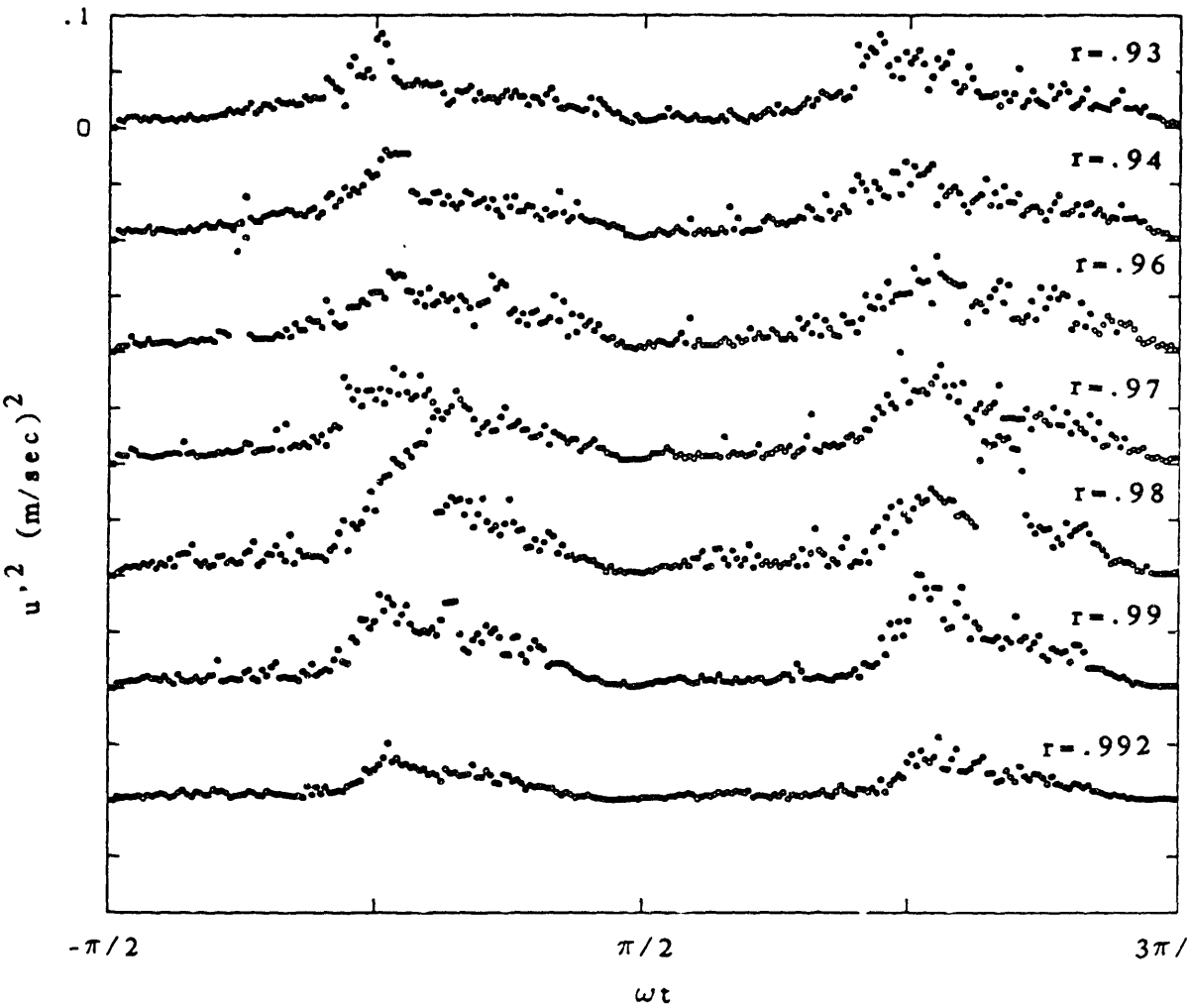

Figure 8c. Phase variation of axial turbulence intensities at various radial positions. (Re^{δ}=1080, Λ=10.6)

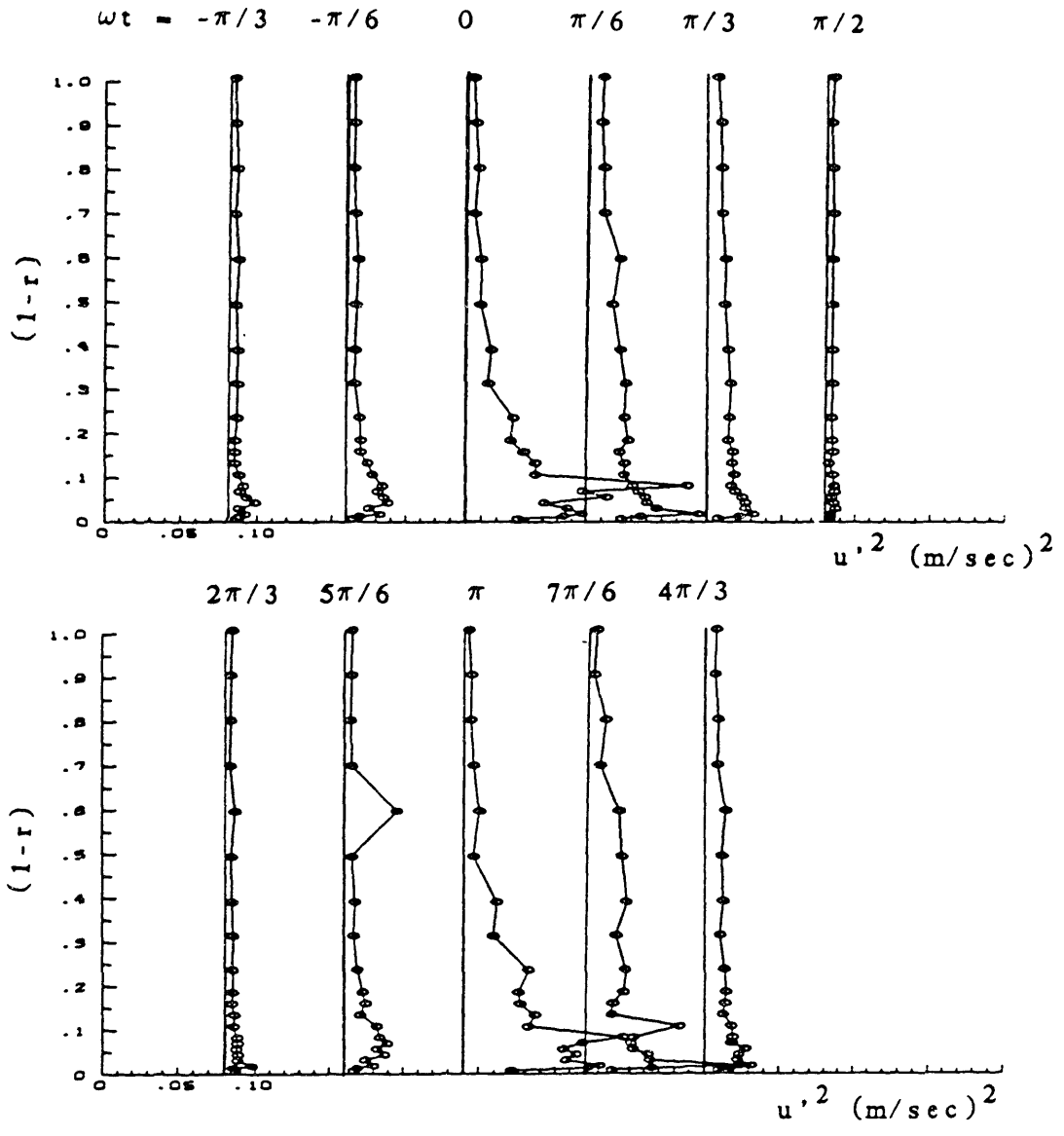

Figure 9. Distribution of axial turbulence intensity across the pipe radius for various phases. (Re^{δ}=1080, Λ=10.6)

Radial turbulence intensities ($\langle v'^2 \rangle$), in general have magnitudes on the order of 1/5th of $\langle u'^2 \rangle$ (see Figures 10 and 11). In addition, the distribution of $\langle v'^2 \rangle$ across the pipe is more uniform at a given phase (Figure 11). Notwithstanding these differences, the phase variation of $\langle v'^2 \rangle$ is very similar to that of $\langle u'^2 \rangle$.

The radial distribution of Reynolds stresses ($\langle u'v' \rangle$) is shown in Figure 12 for selected phases during the cycle. The Reynolds stress is almost negligible over the whole cross-section throughout the acceleration phase of the cycle, but with the start of the deceleration phase it gradually begin to grow within the boundary layer and spreads upwards towards the center as time progresses within the cycle. By the end of the deceleration phase the Reynolds stresses once again reduce to very low levels.

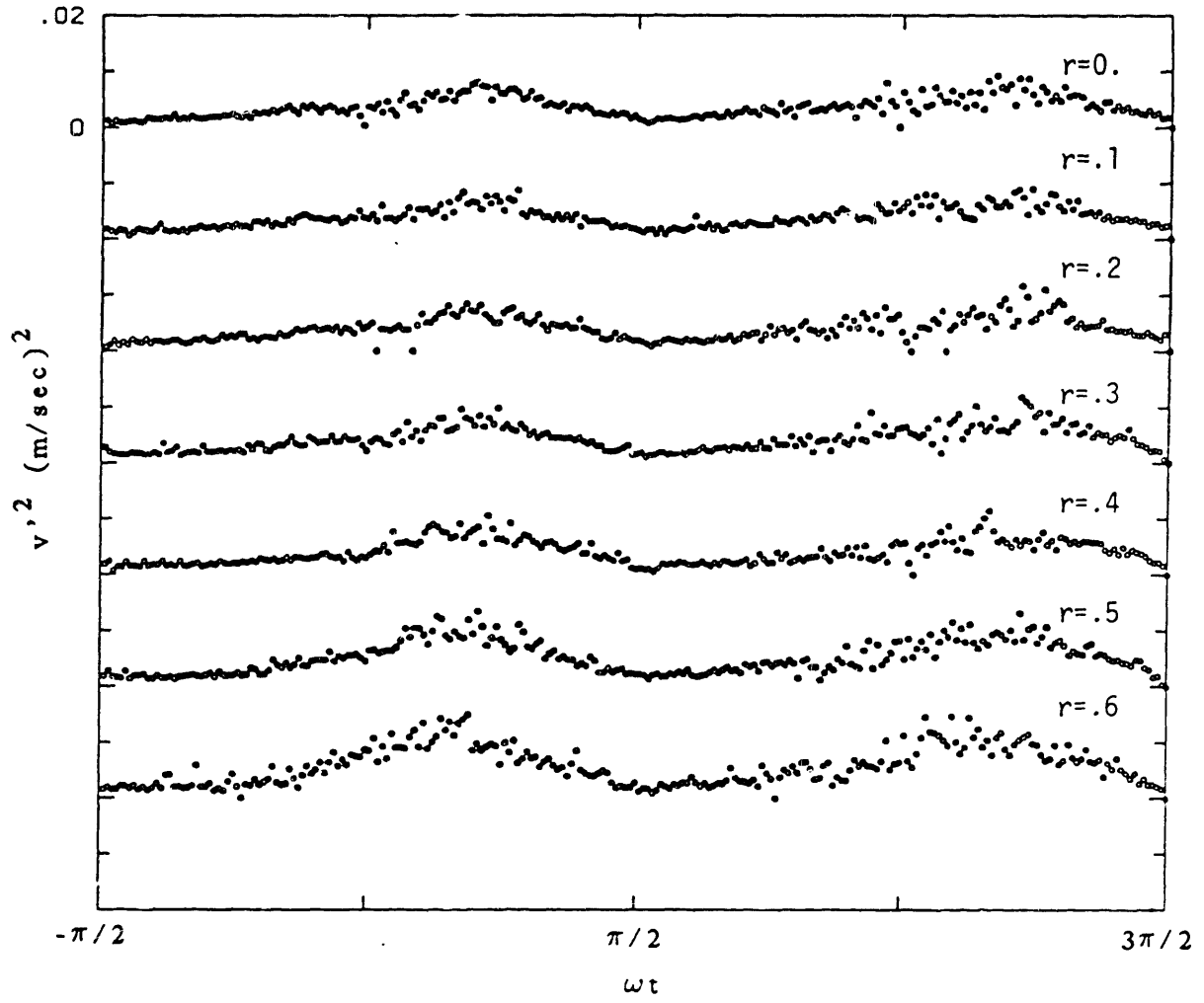

Figure 10a. For caption see figure 10c.

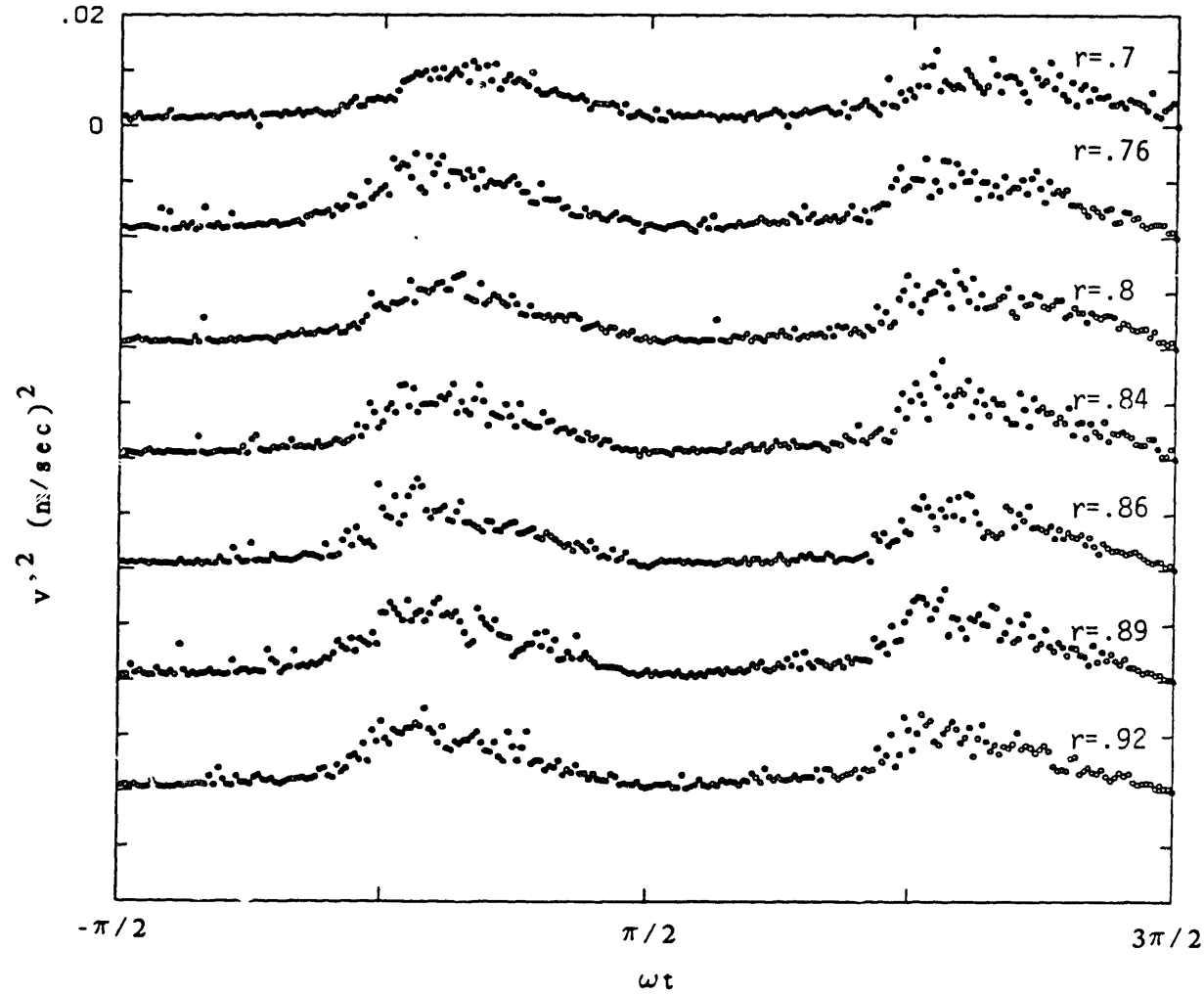

Figure 10b. For caption see figure 10c.

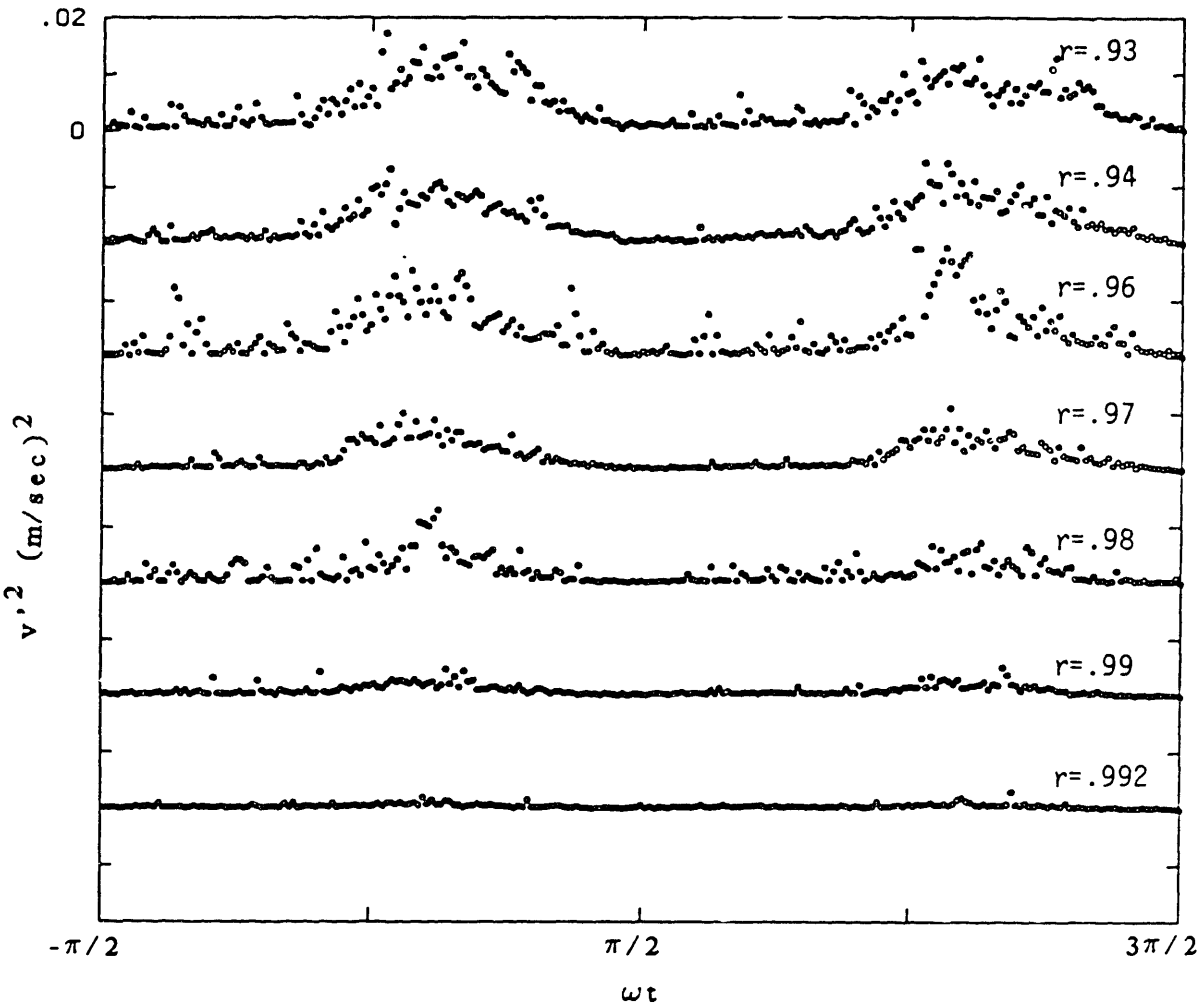

Figure 10c. Phase variation of radial turbulence intensities at various radial positions. (Re^{δ}=1080, Λ=10.6)

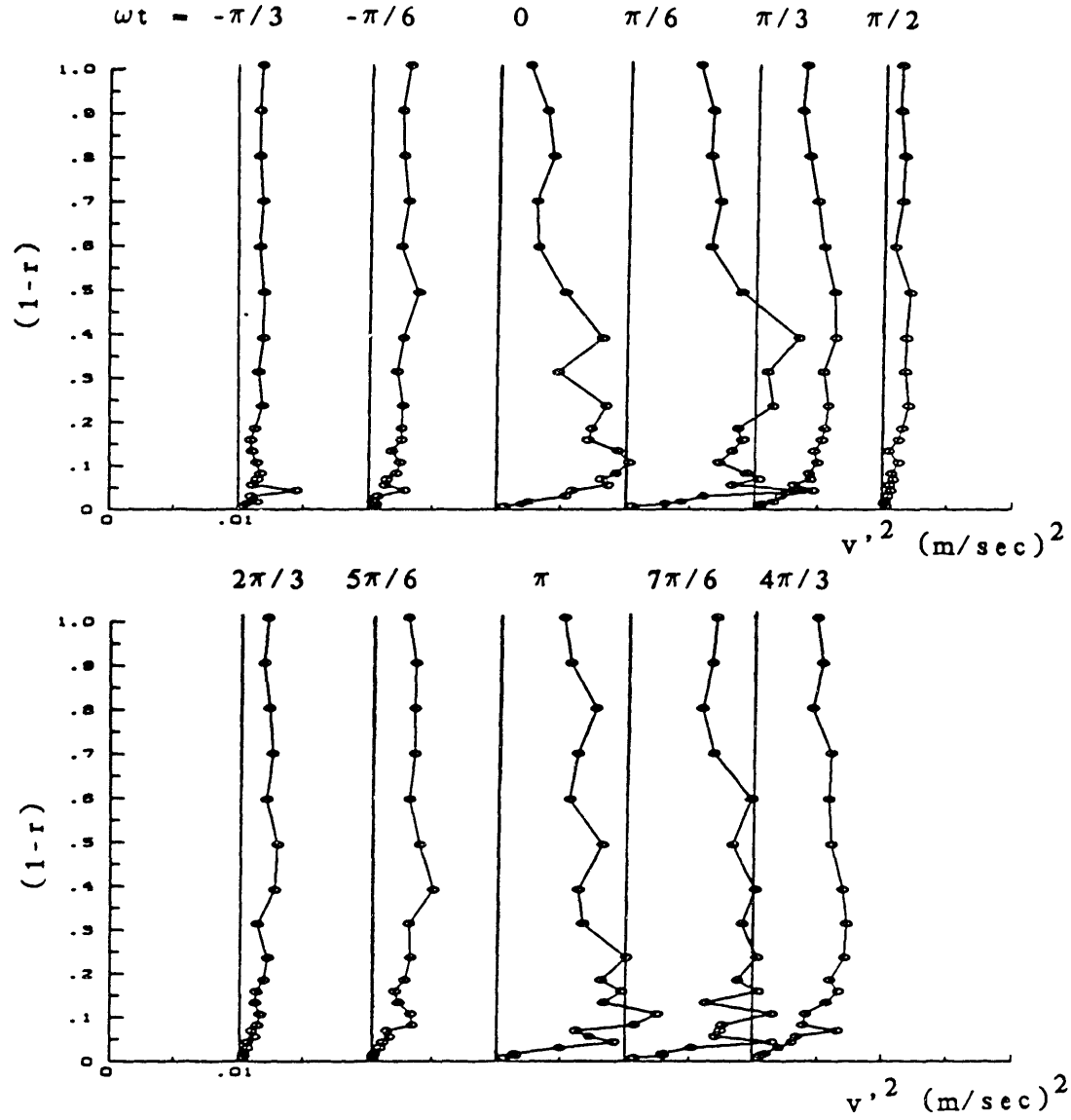

Figure 11. Distribution of radial turbulence intensity across the pipe radius for various phases. (Re^{δ}=1080, Λ=10.6)

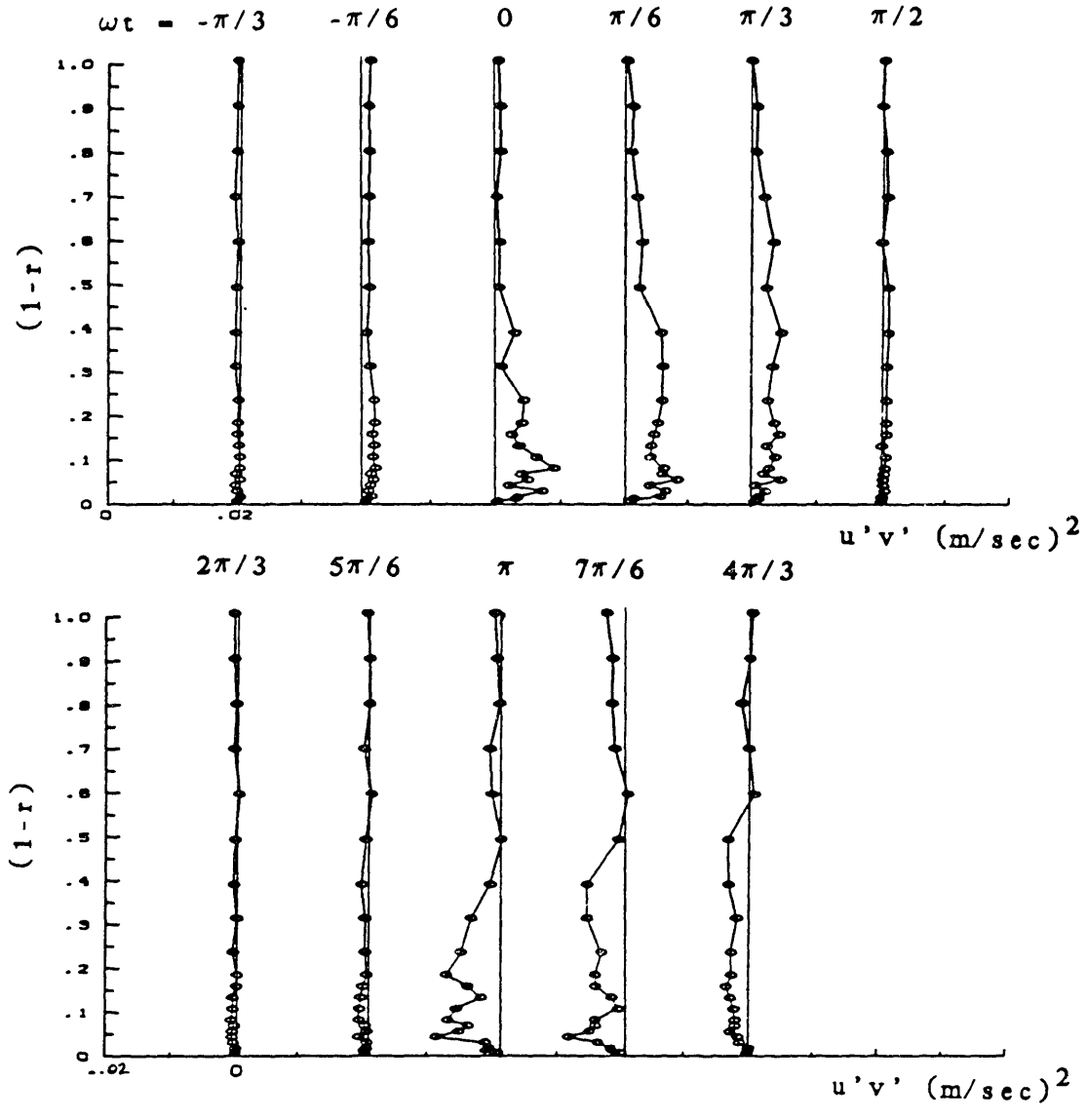

Figure 12. Distribution of Reynolds stress across the pipe radius for various phases. (Re^{δ}=1080, Λ=10.6)

2.2.3 Effect of Re^{δ} and Λ

The effect of Re^{δ} and Λ on the characteristics of the turbulent oscillatory pipe flow has been briefly considered by studying two other flows; one with the same Λ (=10.6) as the case discussed above, but at a higher Re^{δ} (=1720), and the other at roughly the same Re^{δ} (~1000) but at a lower Λ (Λ=5.7) .

The experimental results for the case Re^{δ}=957, Λ=5.7 are shown in figures 13 through 20. This flow differs from the case discussed in the previous section in that, due to the lower value of Λ, the adverse pressure gradients that are set up during the deceleration phase of the cycle are not as severe. Accordingly, turbulence is observed only during the later stages of the deceleration phase (starting at $\omega t \simeq \pi/8$, $r \simeq .93$) when adverse pressure gradients are sufficiently high. Furthermore, the observed turbulence is not as violent in the boundary layer but tends to be more spread out through the pipe cross section. The "glitches" seen in the velocity traces of Figure 13 at $\omega t = \pi/2$ are due to the backlash in the motion of the driving piston as was discussed in section 2.1 . The curves of instantaneous flow rate for this flow condition were shown in Figures 2a and 2b, and manifest the same "glitch".

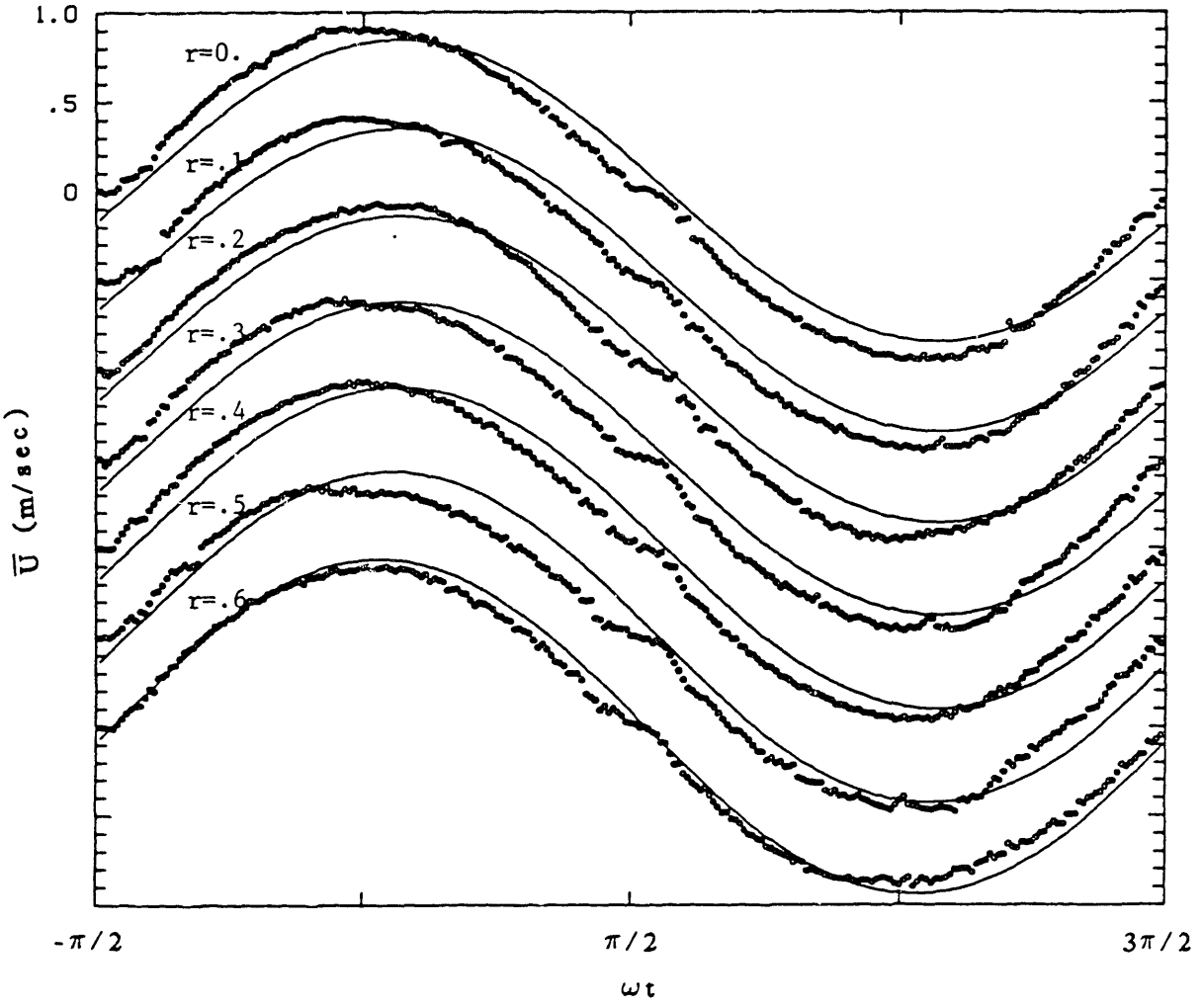

Figure 13a. For caption see Figure 13c.

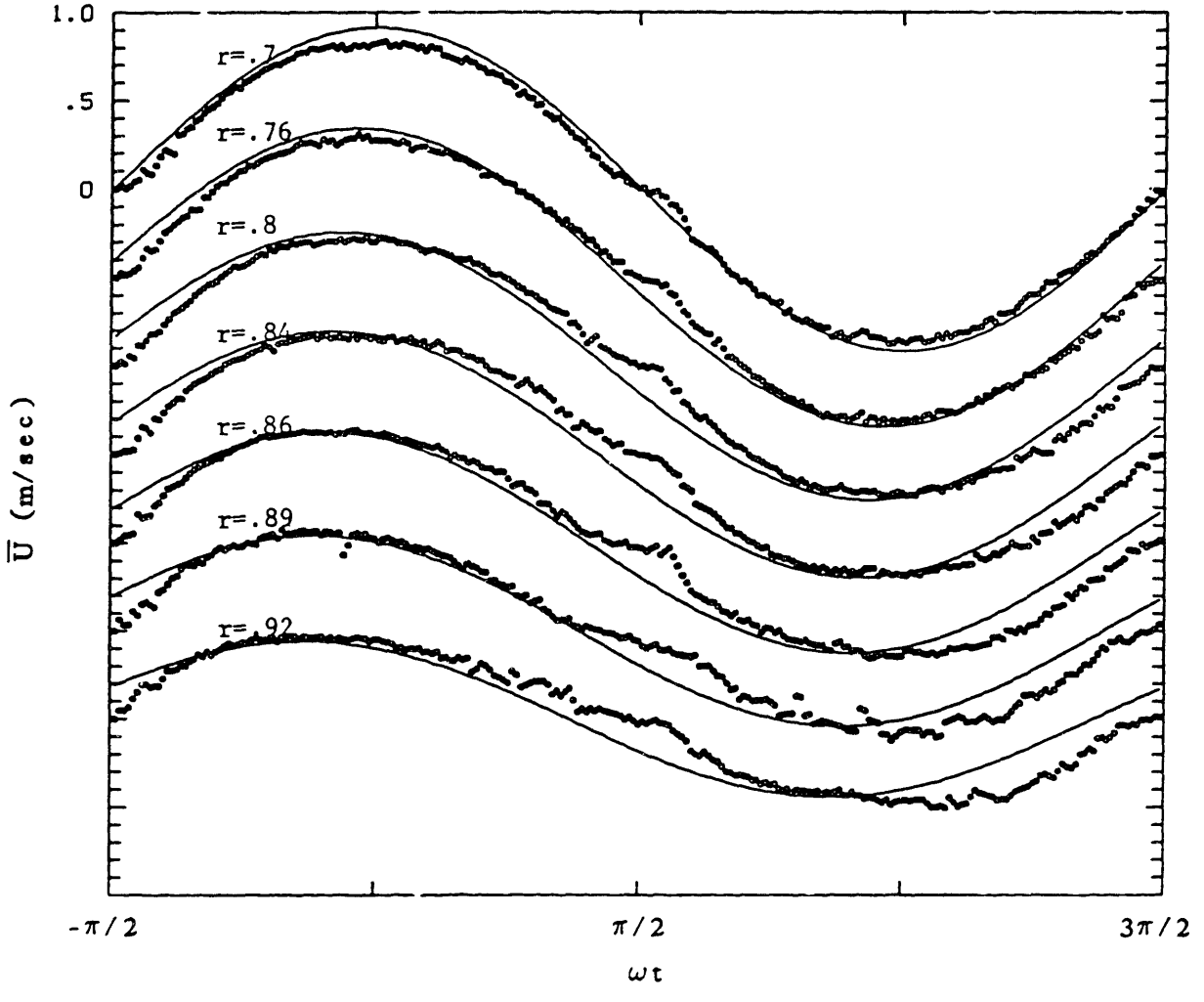

Figure 13b. For caption see Figure 13c.

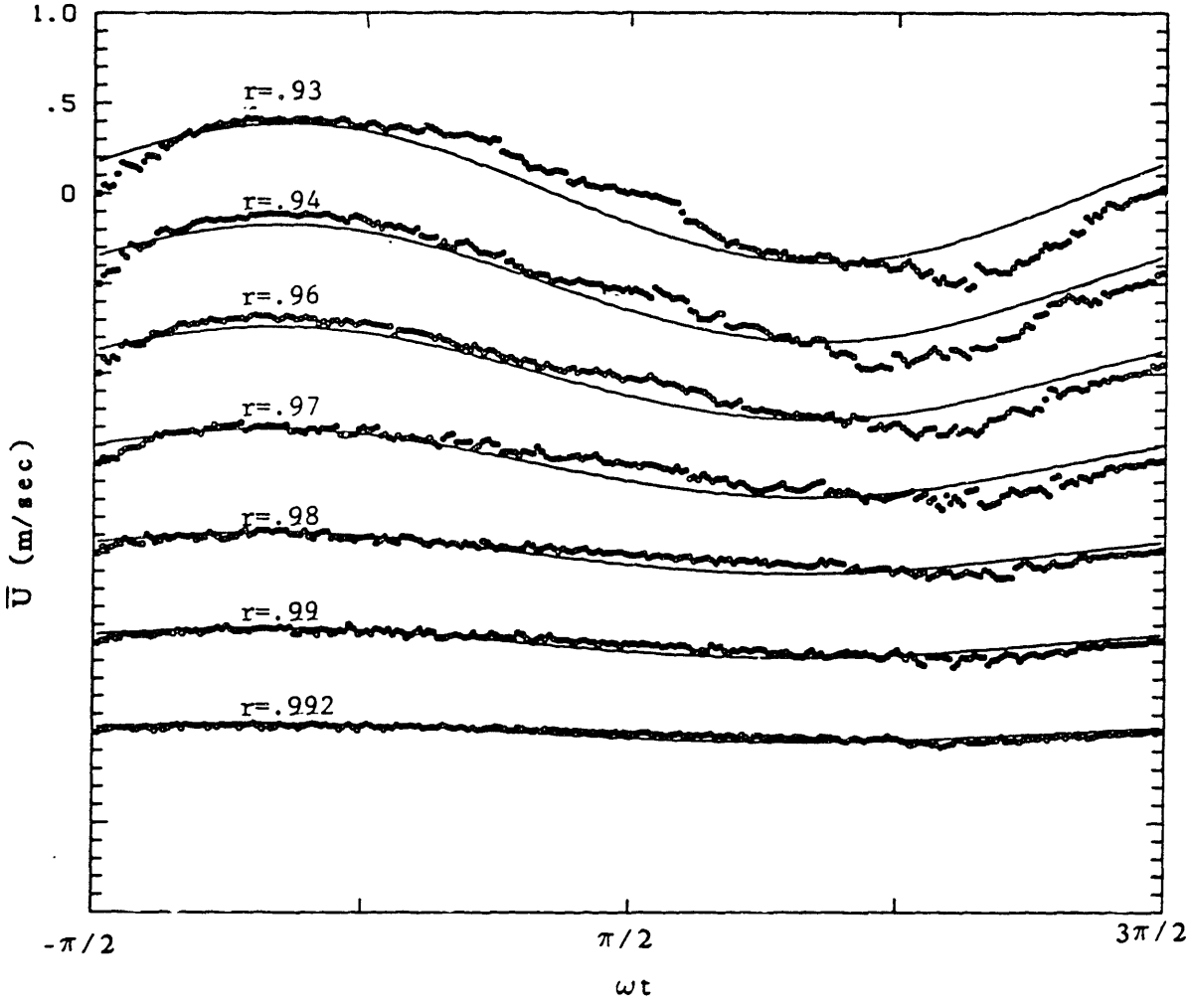

Figure 13c. Phase variation of the ensemble averaged turbulent axial velocity compared to the laminar theoretical curve for various radial positions. (Re^{δ}=957, Λ=5.7)

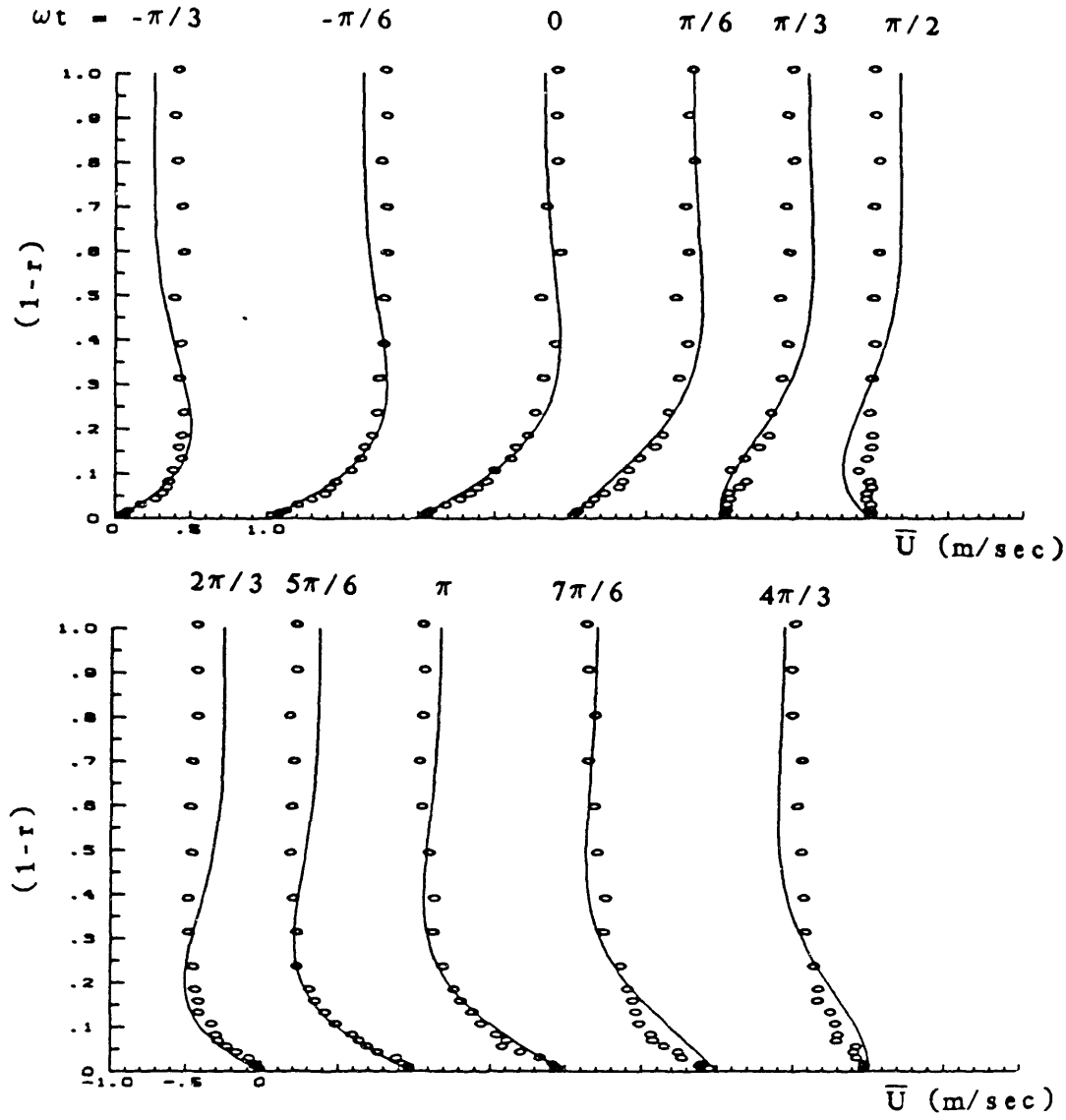

Figure 14. Instantaneous ensemble averaged velocity profiles in the turbulent flow regime compared to the laminar theoretical curve. (Re^{δ}=957, Λ=5.7)

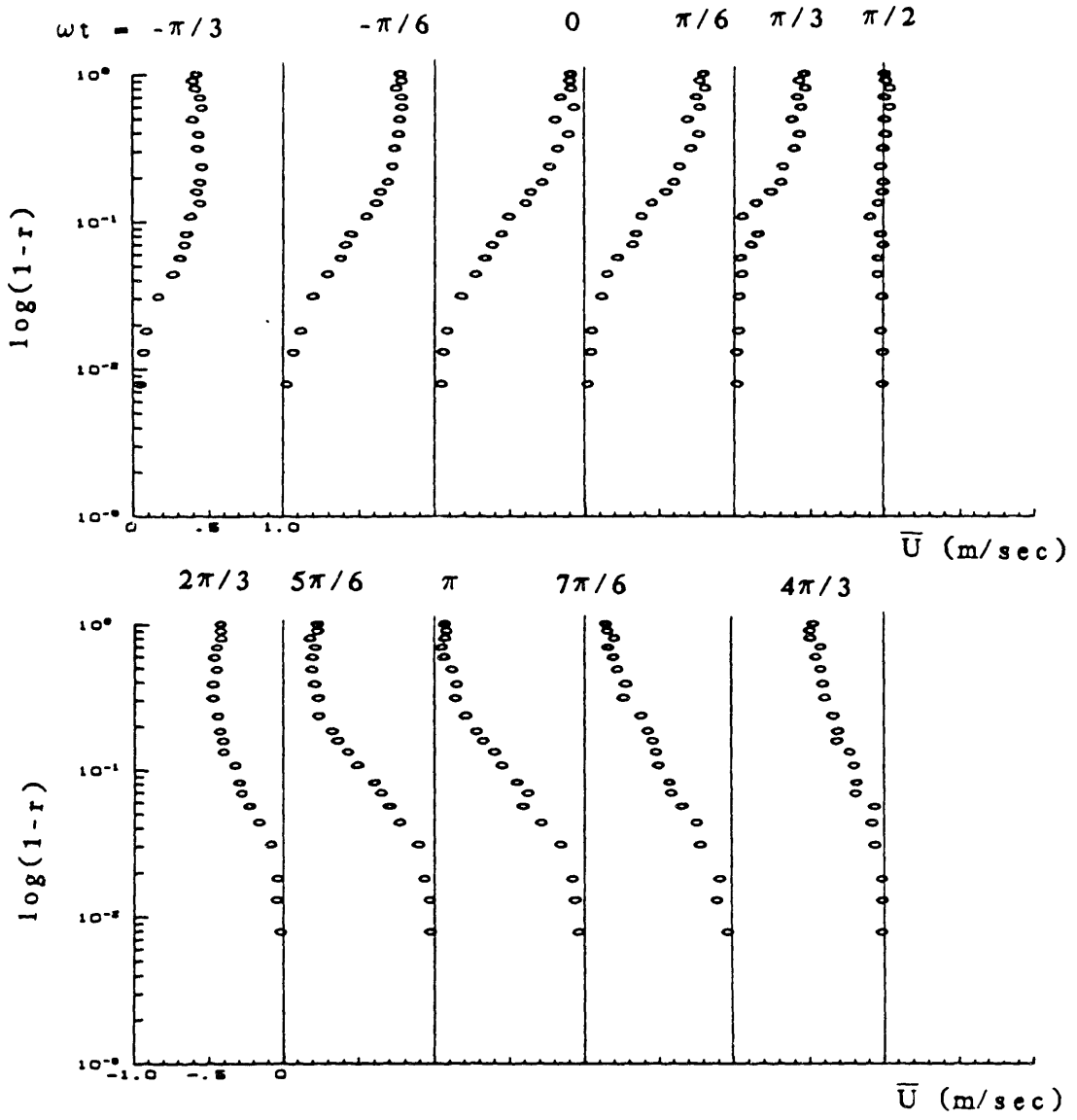

Figure 15. Semi-logarithmic plots of ensemble averaged axial velocity in the turbulent flow regime. (Re^{δ}=957, Λ=5.7)

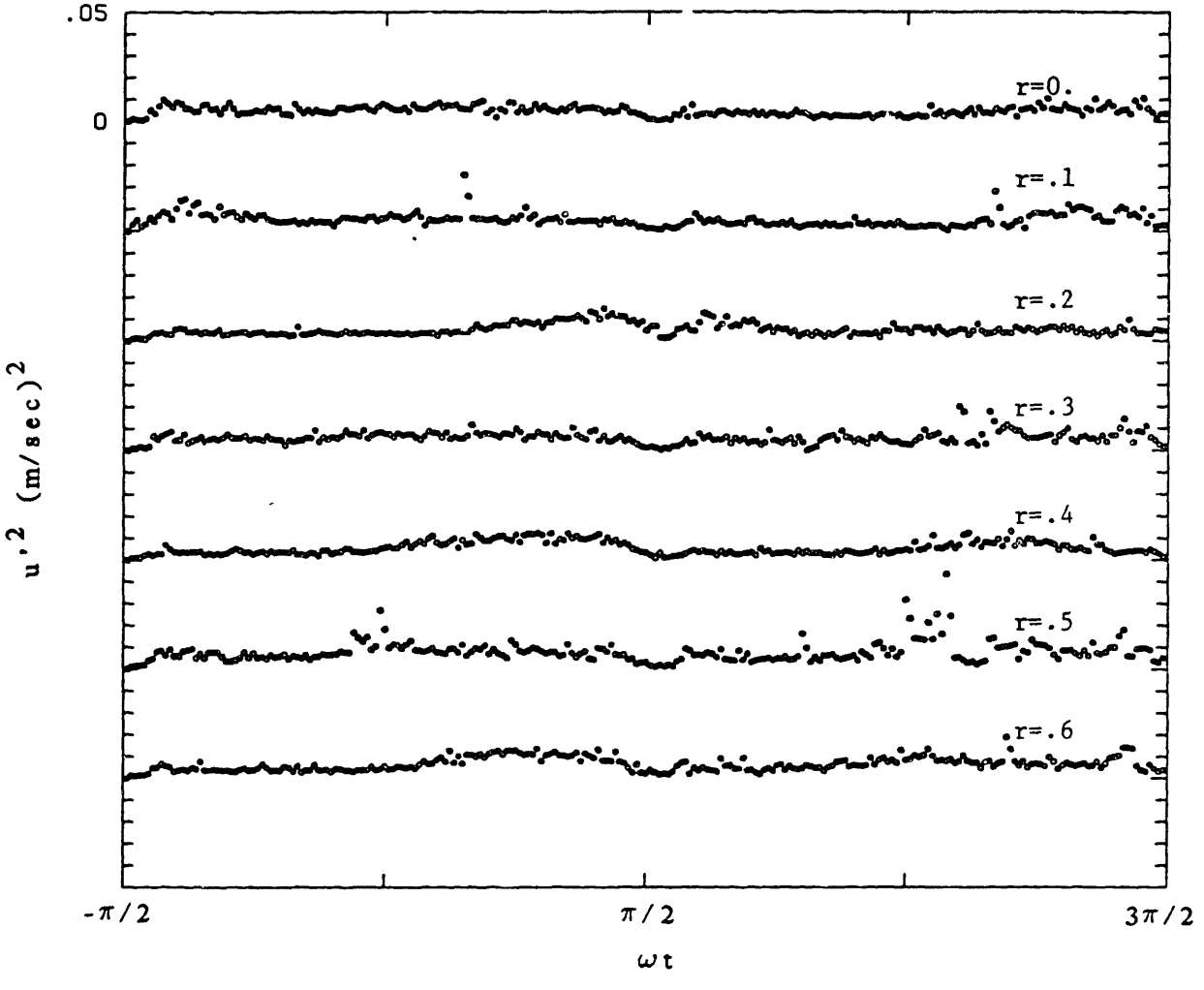

Figure 16a. For caption see Figure 16c.

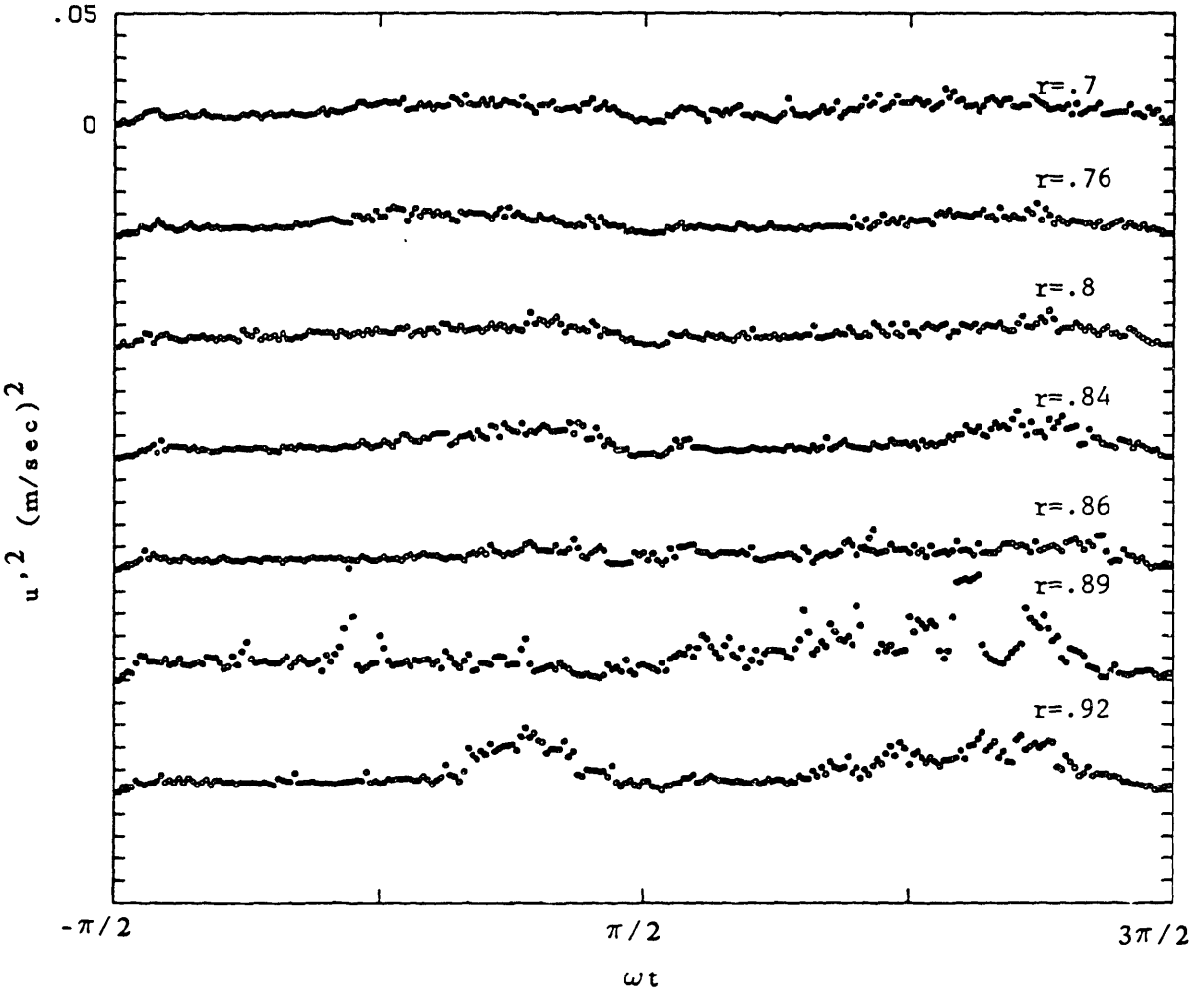

Figure 16b. For caption see Figure 16c.

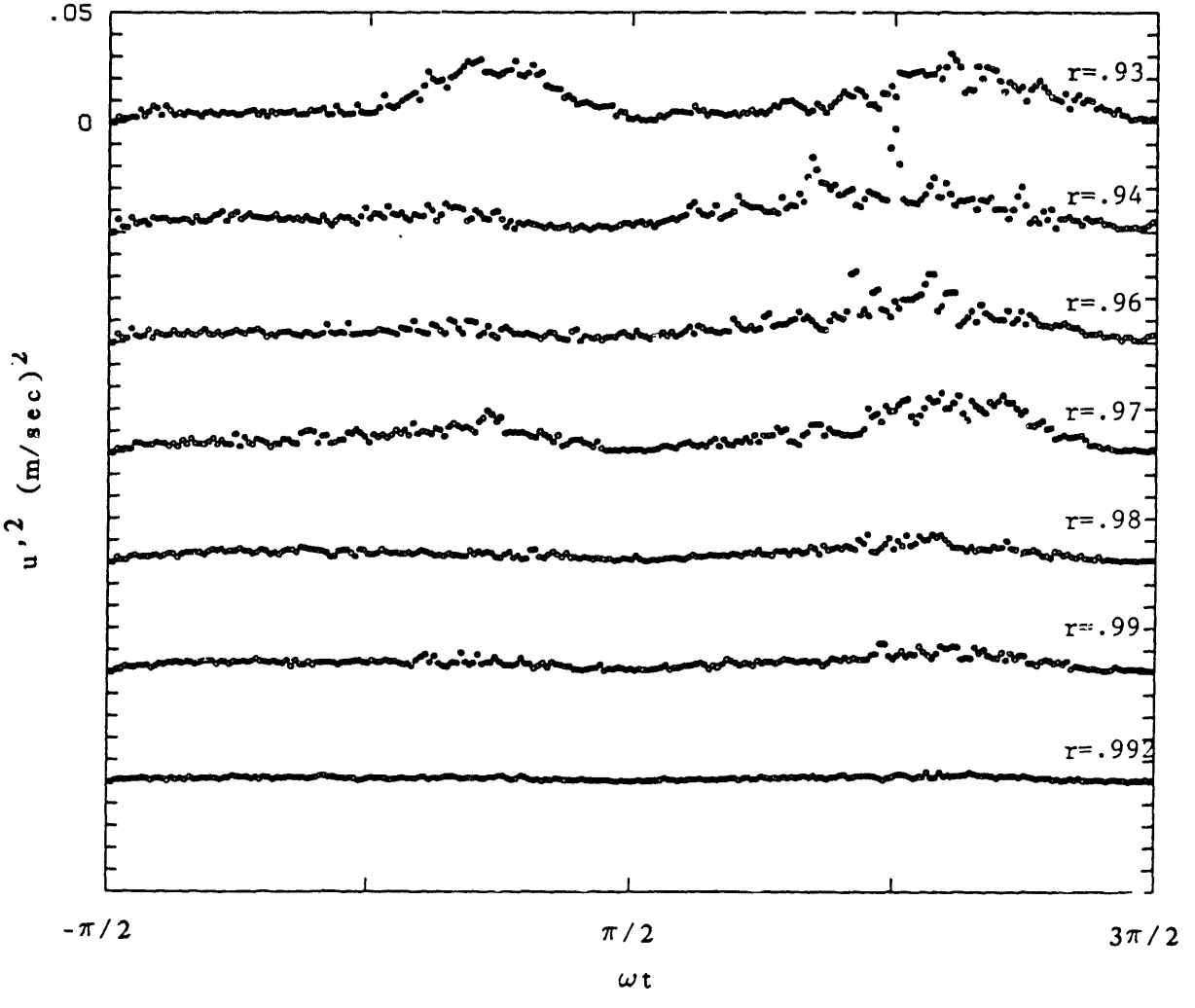

Figure 16c. Phase variation of axial turbulence intensities at various radial positions. (Re^{δ}=957, Λ=5.7)

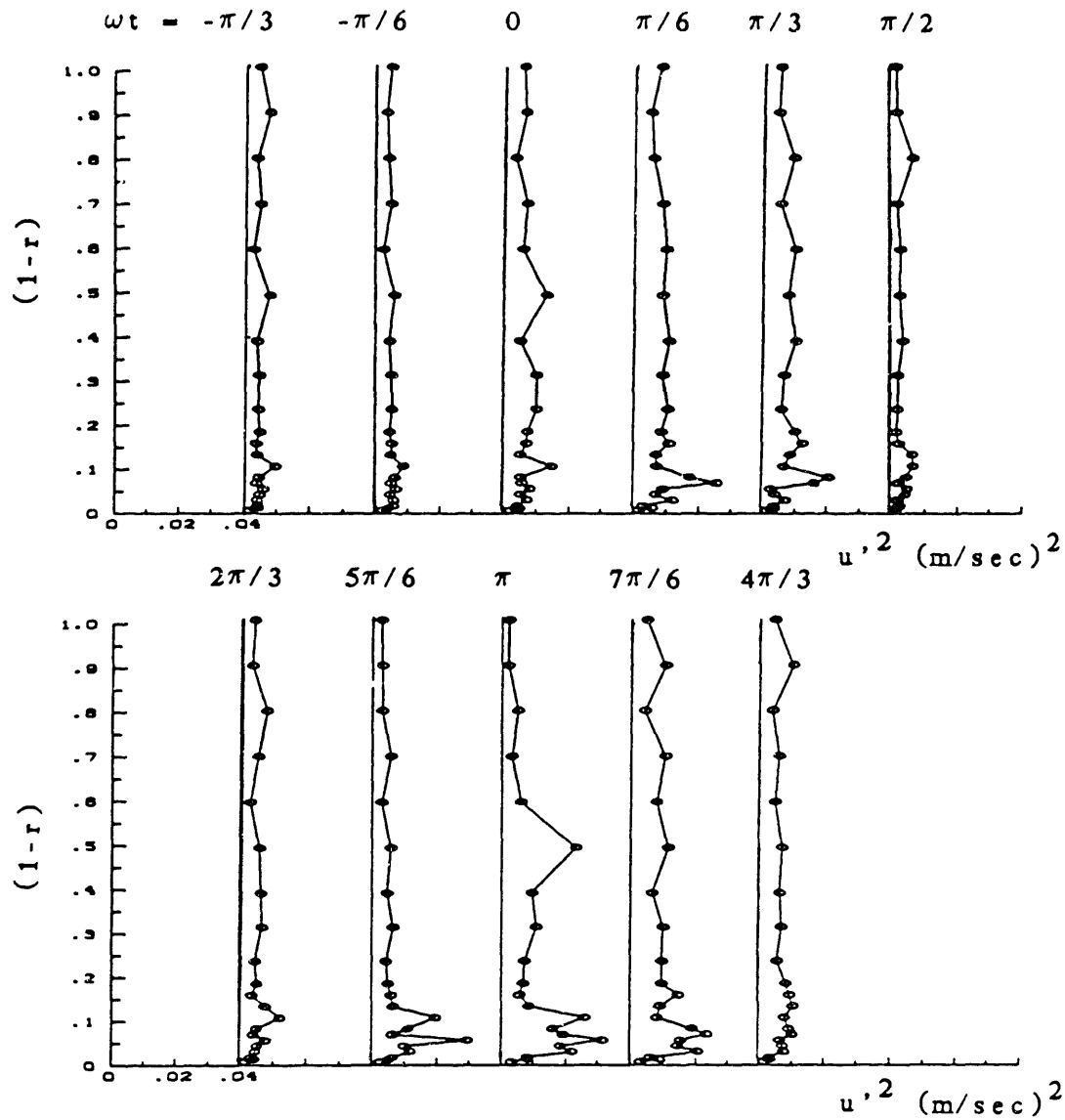

Figure 17. Distribution of axial turbulence intensity across the pipe radius for various phases. (Re^{δ}=957, Λ=5.7)

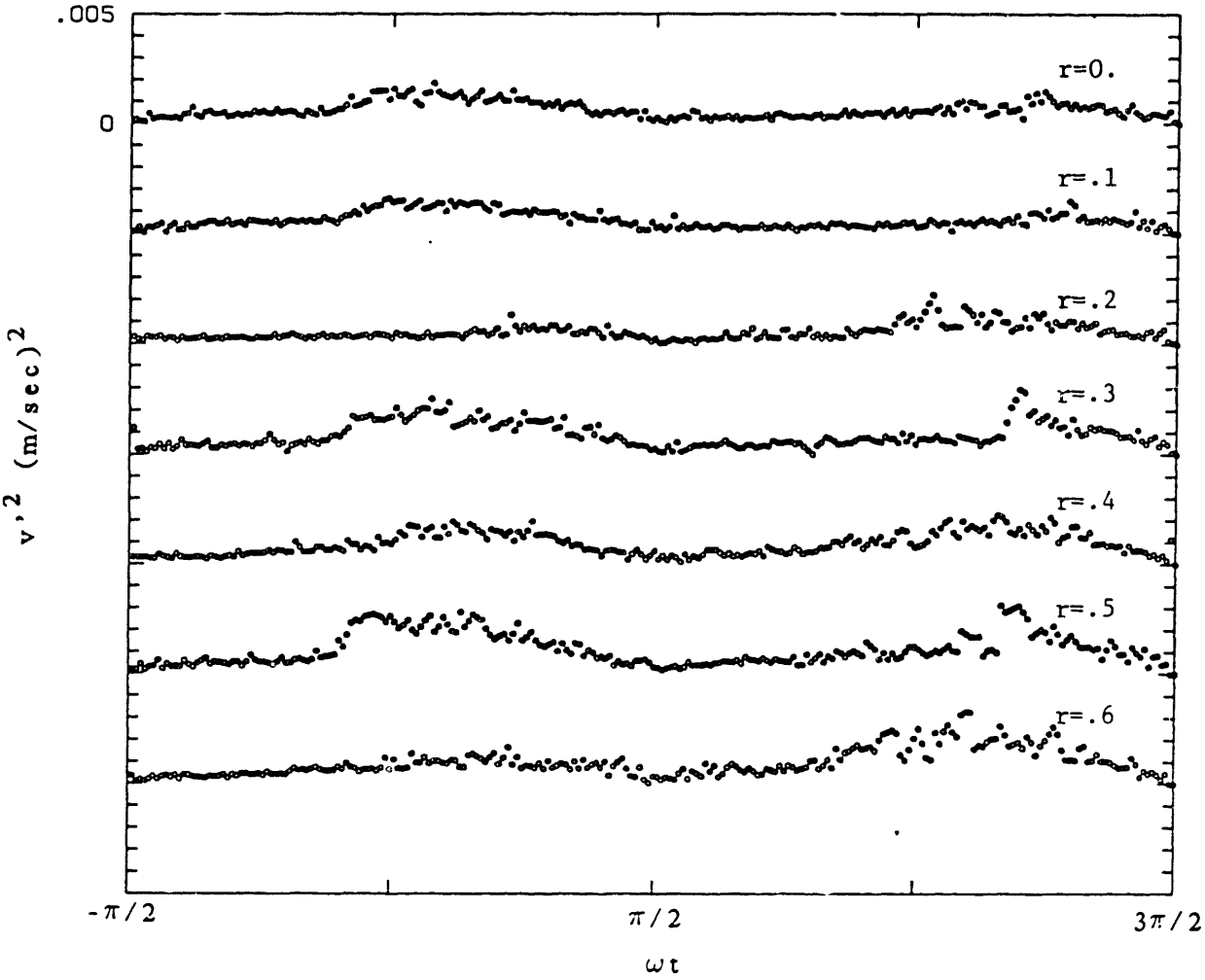

Figure 18a. For caption see figure 18c.

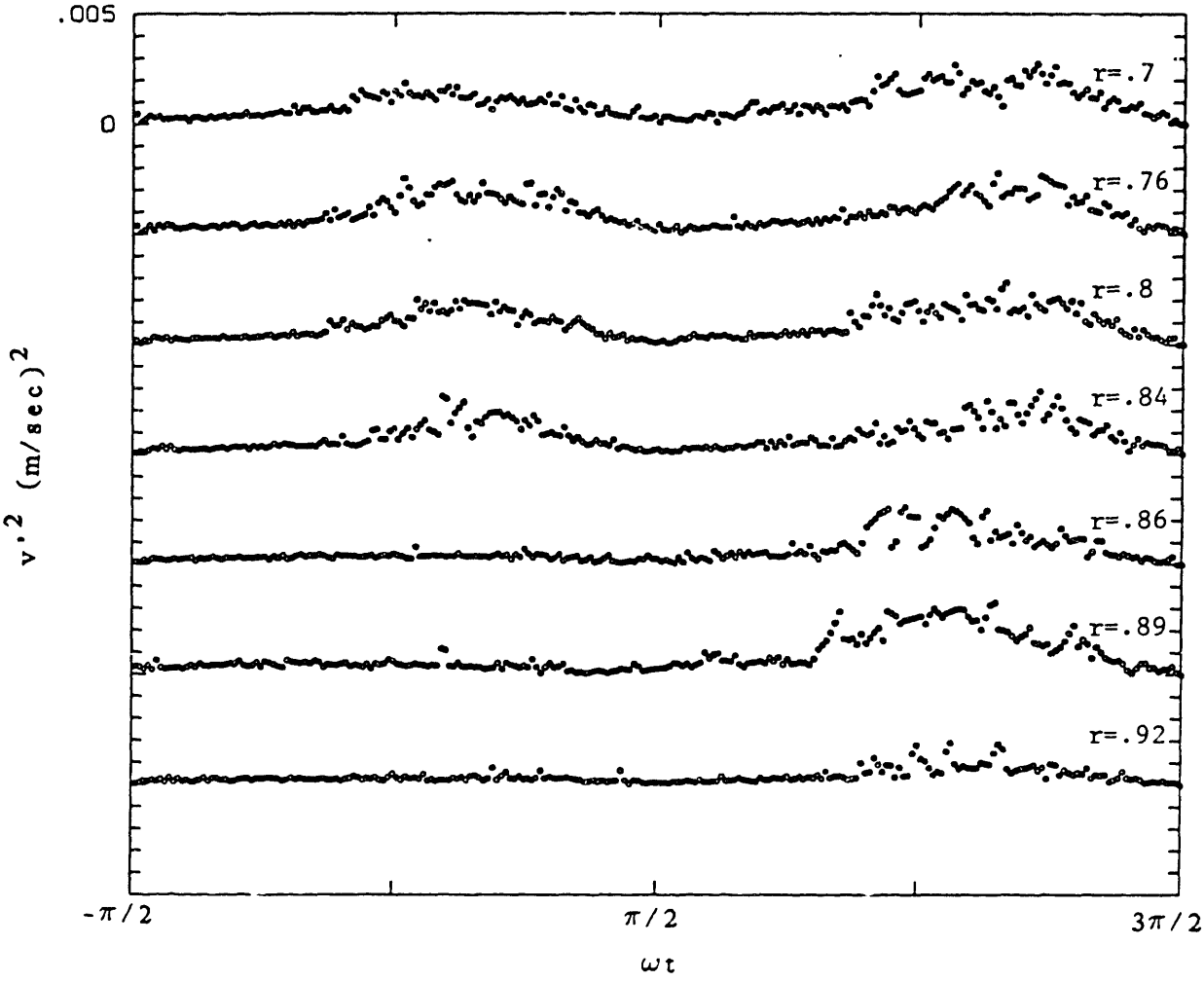

Figure 18b. For caption see figure 18c.

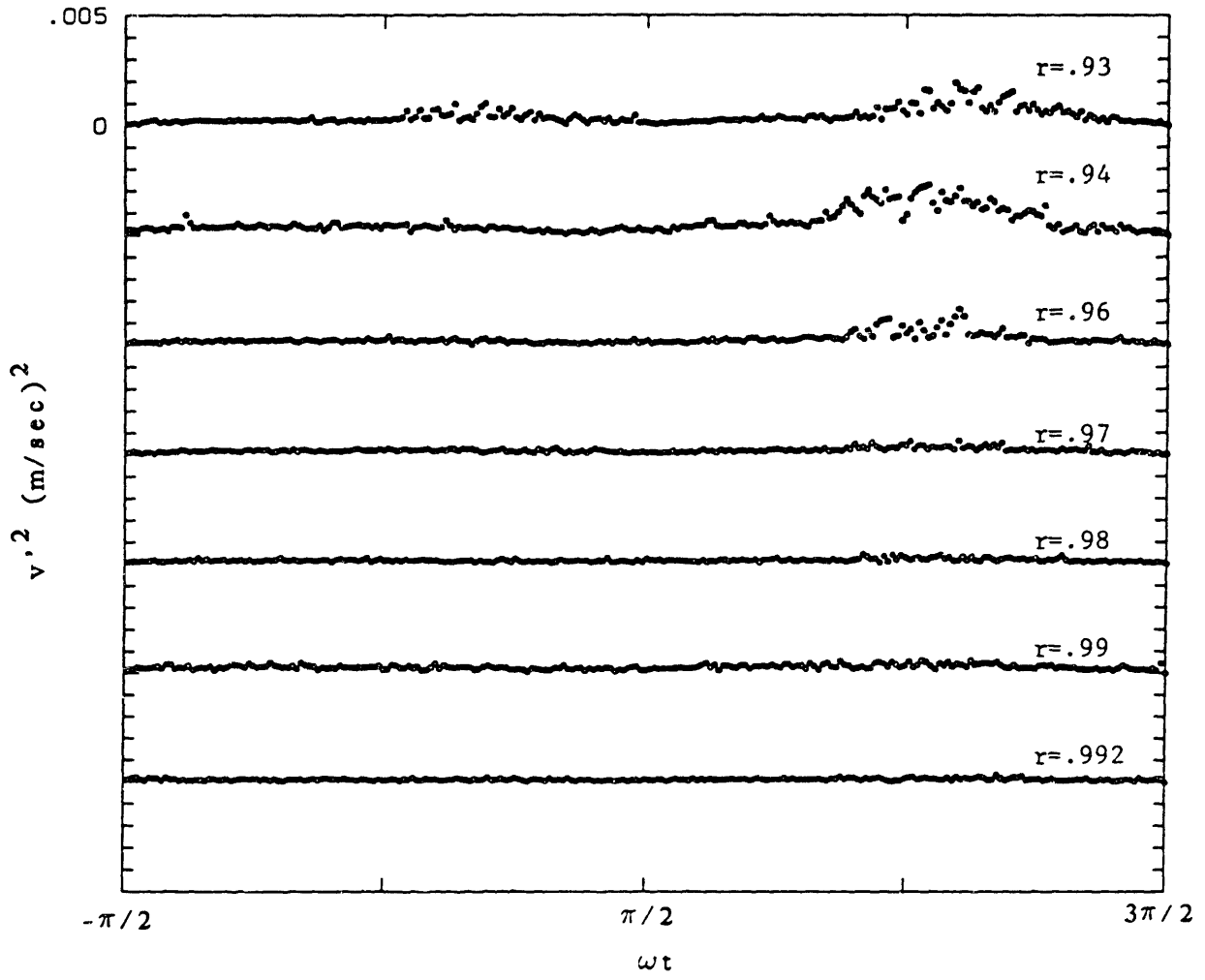

Figure 18c. Phase variation of radial turbulence intensities at various radial positions. (Re^{δ}=957, Λ=5.7)

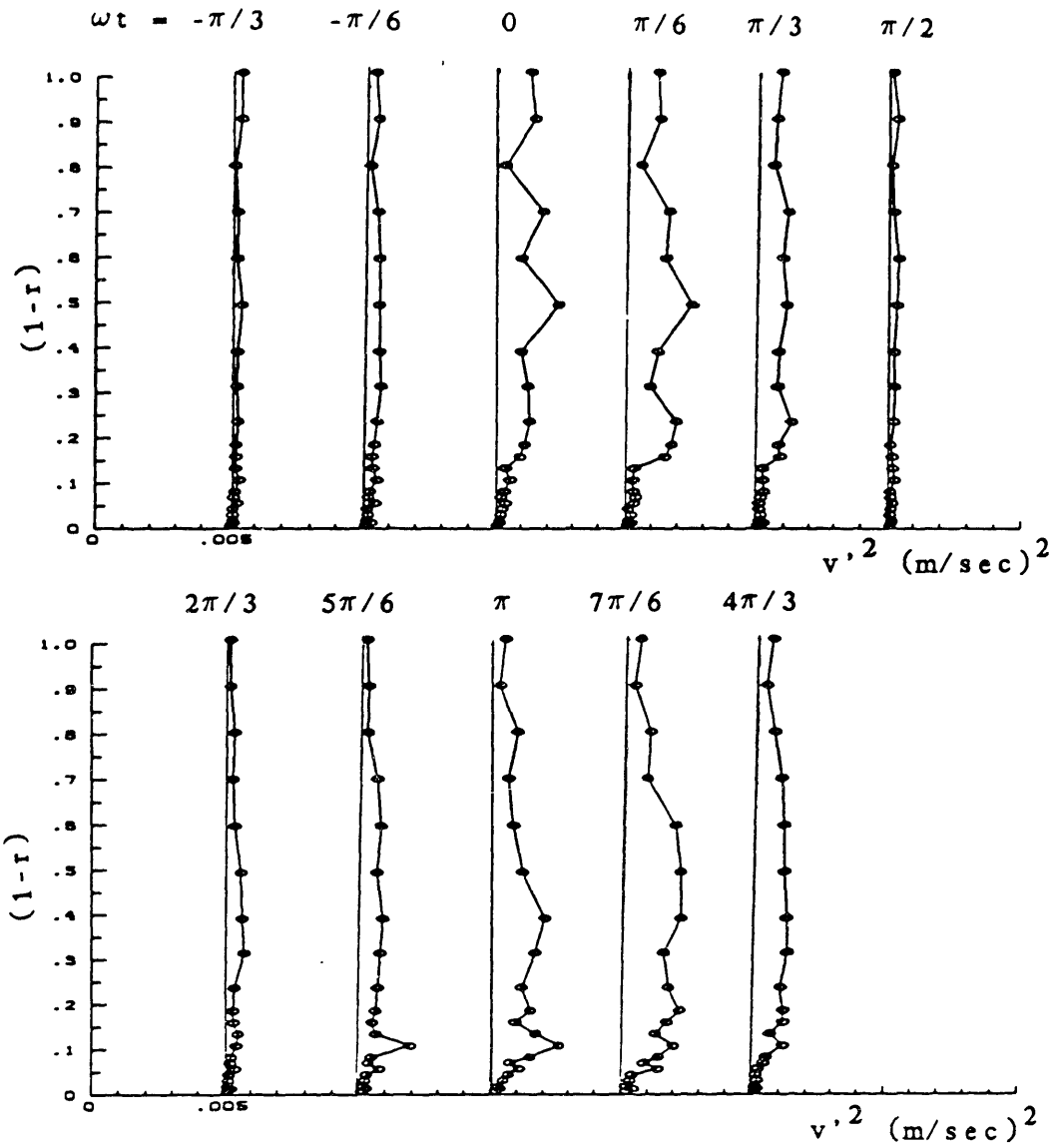

Figure 19. Distribution of radial turbulence intensity across the pipe radius for various phases. (Re^{δ}=957, Λ=5.7)

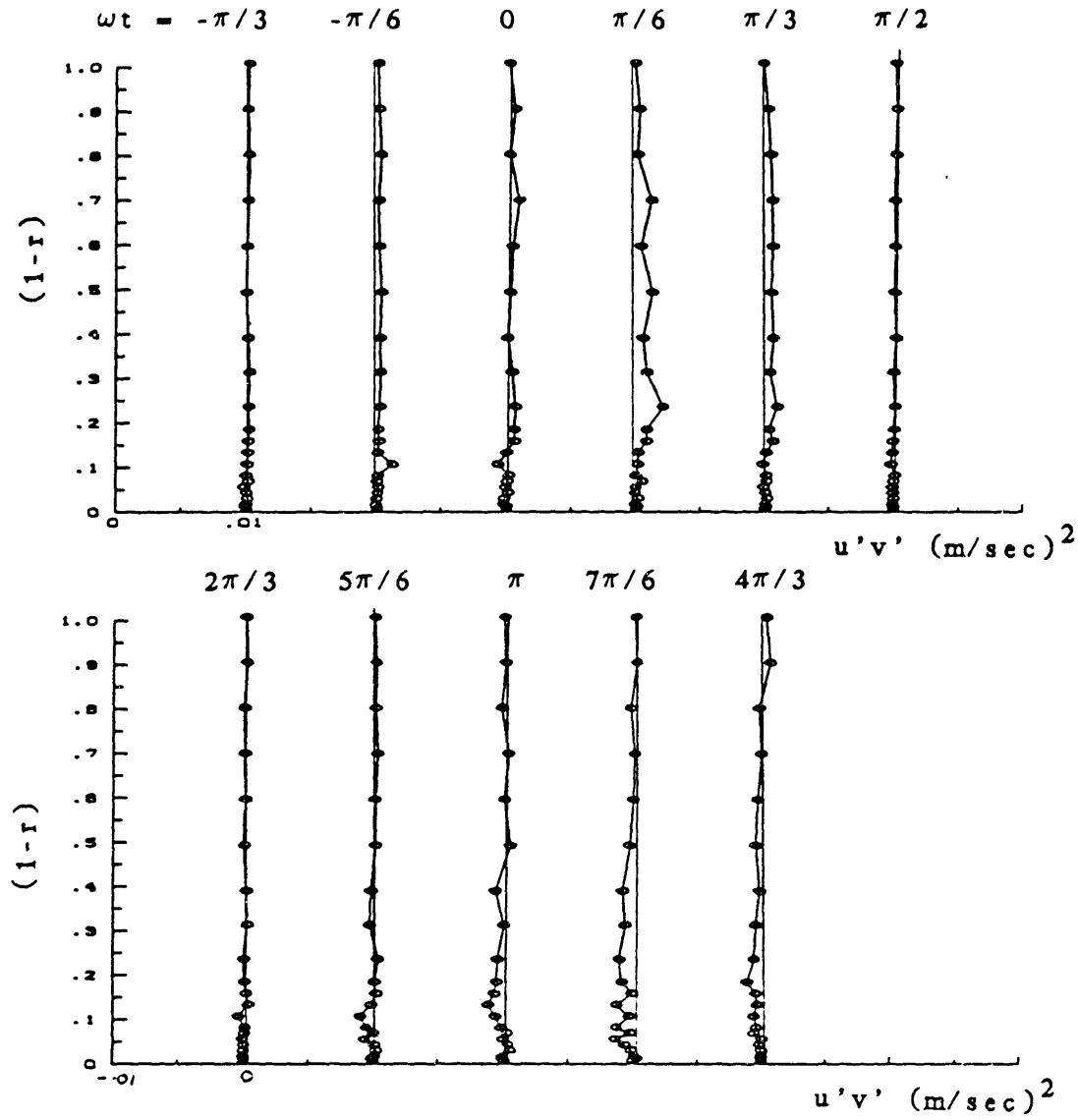

Figure 20. Distribution of Reynolds stress across the pipe radius for various phases. (Re^{δ}=957, Λ=5.7)

In contrast, the characteristics of the flow at the same Λ but at a higher Re^{δ} is shown in figures 21 through 28. In this case, the region of turbulent flow extends to the later stages of the acceleration phase (when the flow is still experiencing a mild favorable pressure gradient), suggesting that if the Reynolds number is sufficiently high the flow may remain turbulent for a substantial portion of the cycle. For an oscillatory flow, however, there will always be a region near the phase of zero flow where the instantaneous Reynolds number is low and the flow is experiencing a favorable pressure gradient, and as a result the bursting process has to stop. If the time scale of oscillation is large compared to time scale of dissipation of turbulence so that no residual turbulence is left, the flow has to relaminarize during this period. This point will be discussed in more detail later.

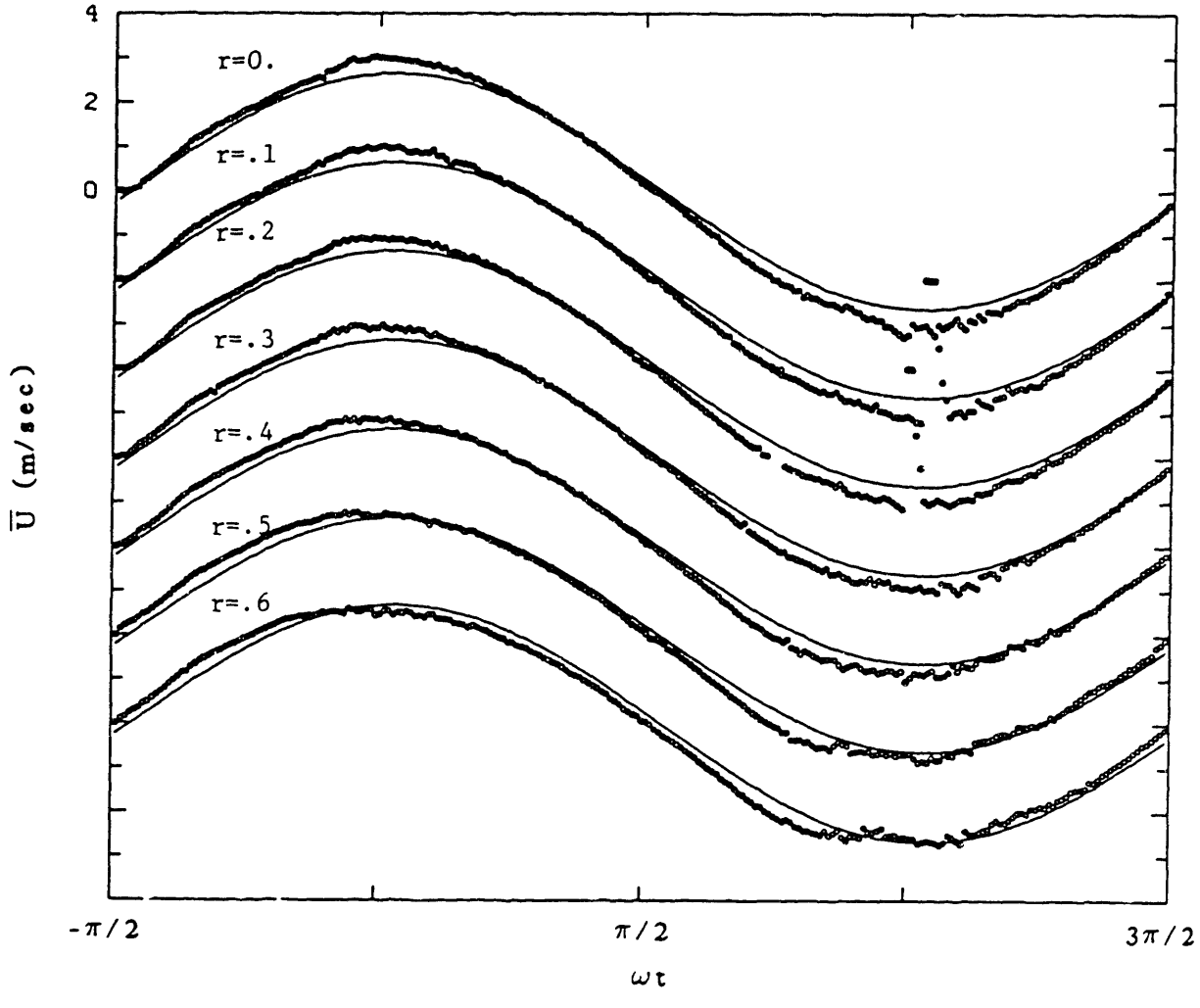

Figure 21a. For caption see Figure 21c.

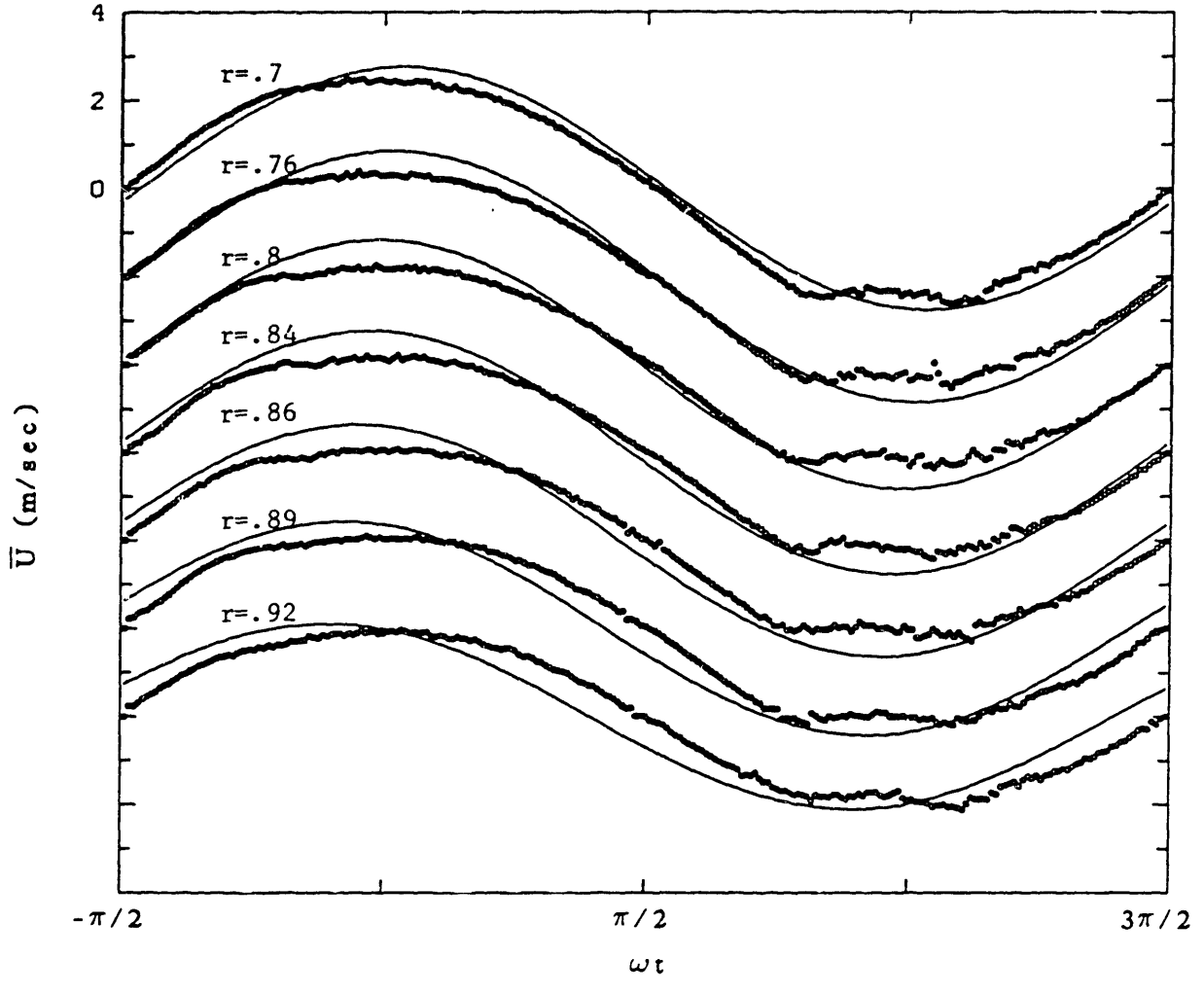

Figure 21b. For caption see Figure 21c.

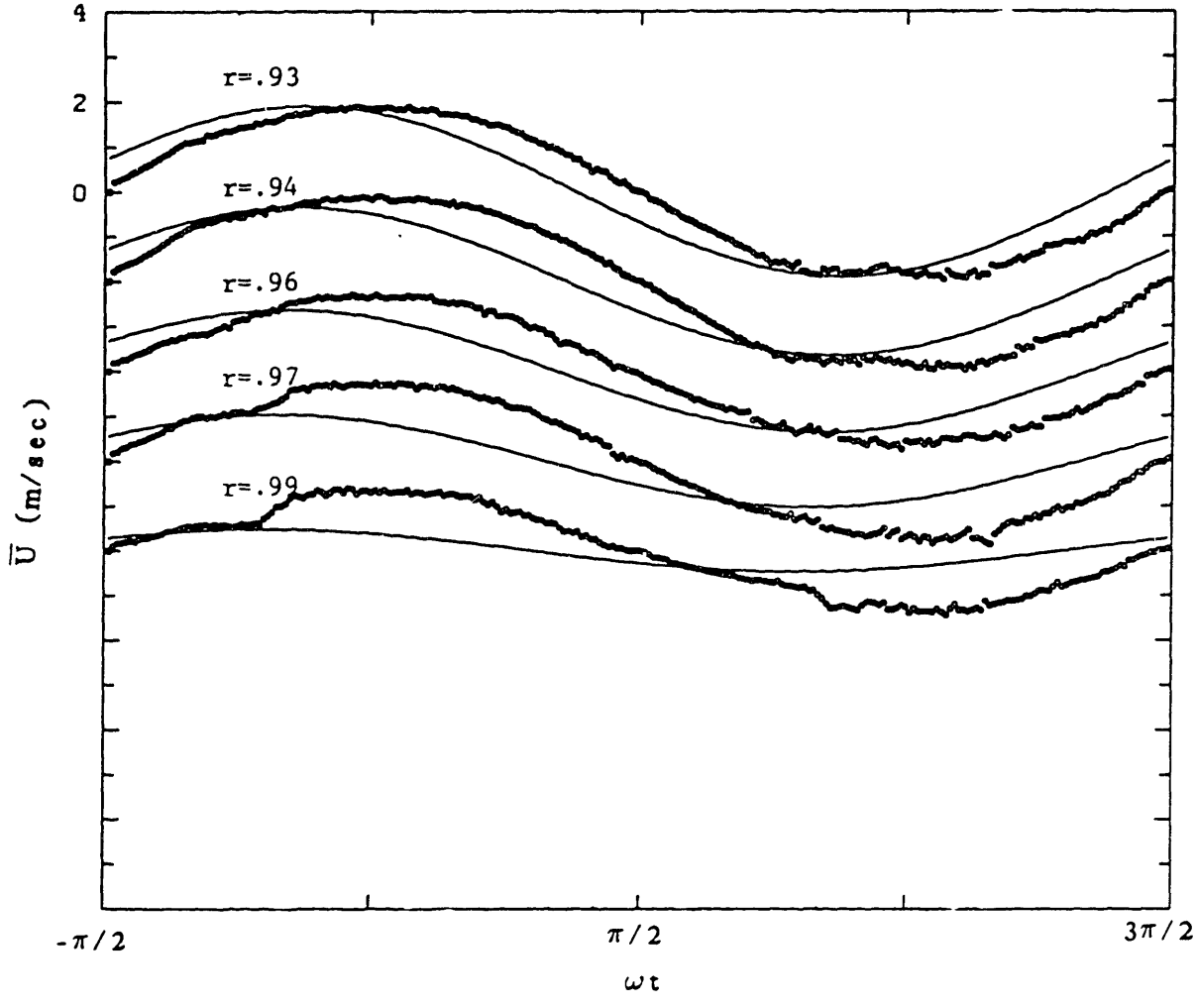

Figure 21c. Phase variation of the ensemble averaged turbulent axial velocity compared to the laminar theoretical curve for various radial positions. (Re^{δ}=1720, Λ=10.6)

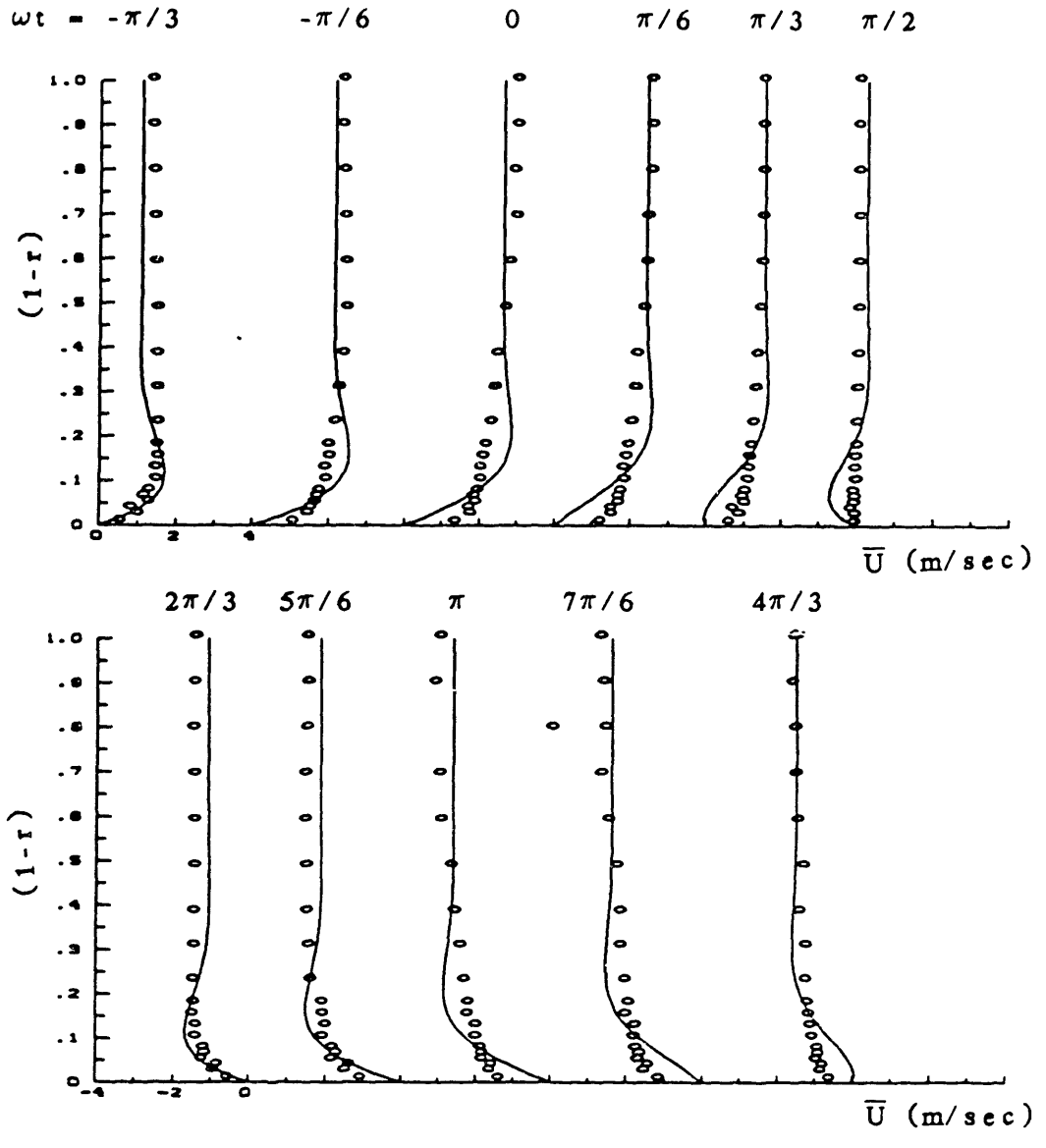

Figure 22. Instantaneous ensemble averaged velocity profiles in the turbulent flow regime compared to the laminar theoretical curve. (Re^{δ}=1720, Λ=10.6)

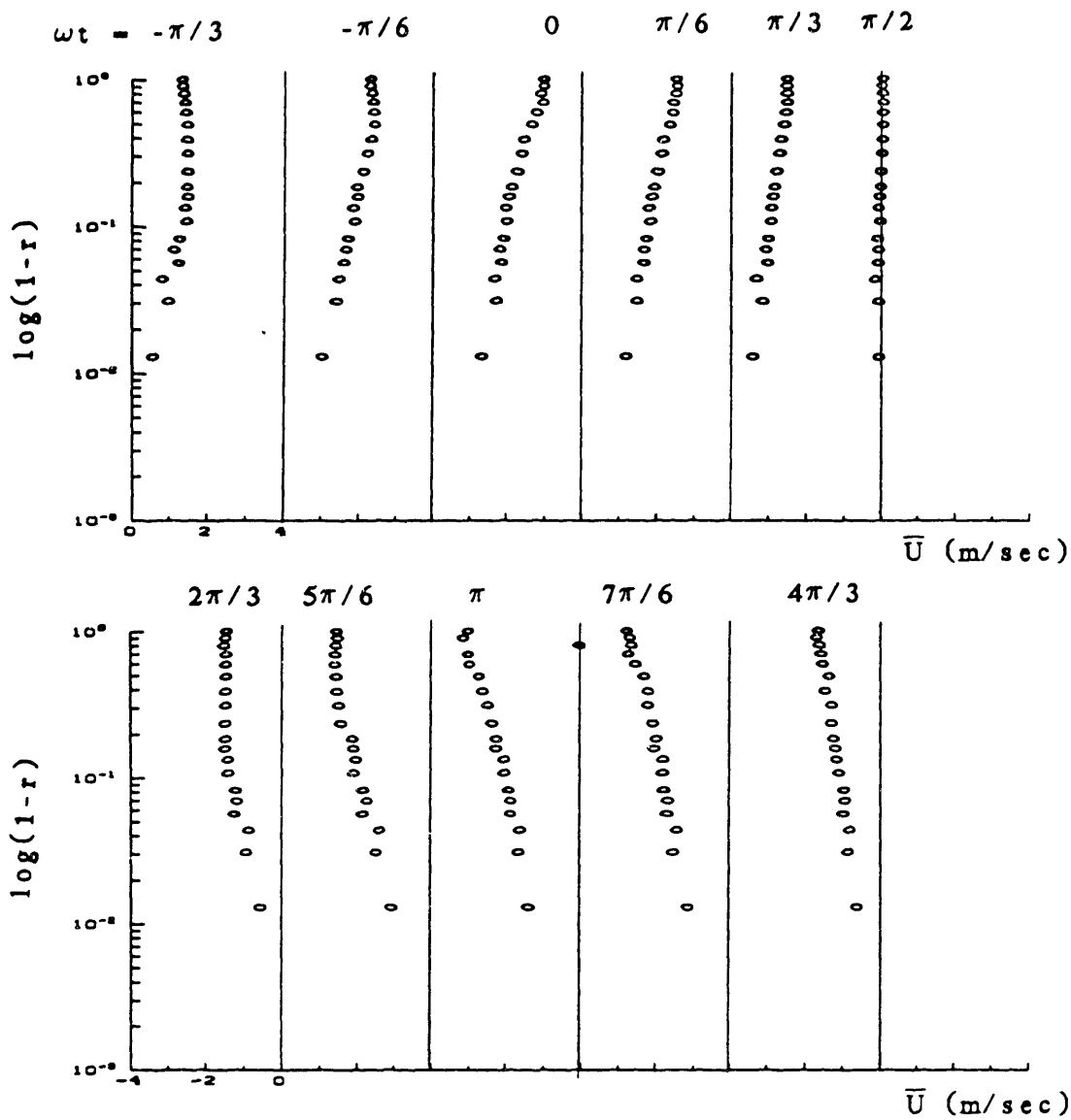

Figure 23. Semi-logarithmic plots of ensemble averaged axial velocity in the turbulent flow regime. (Re^{δ}=1720, Λ=10.6)

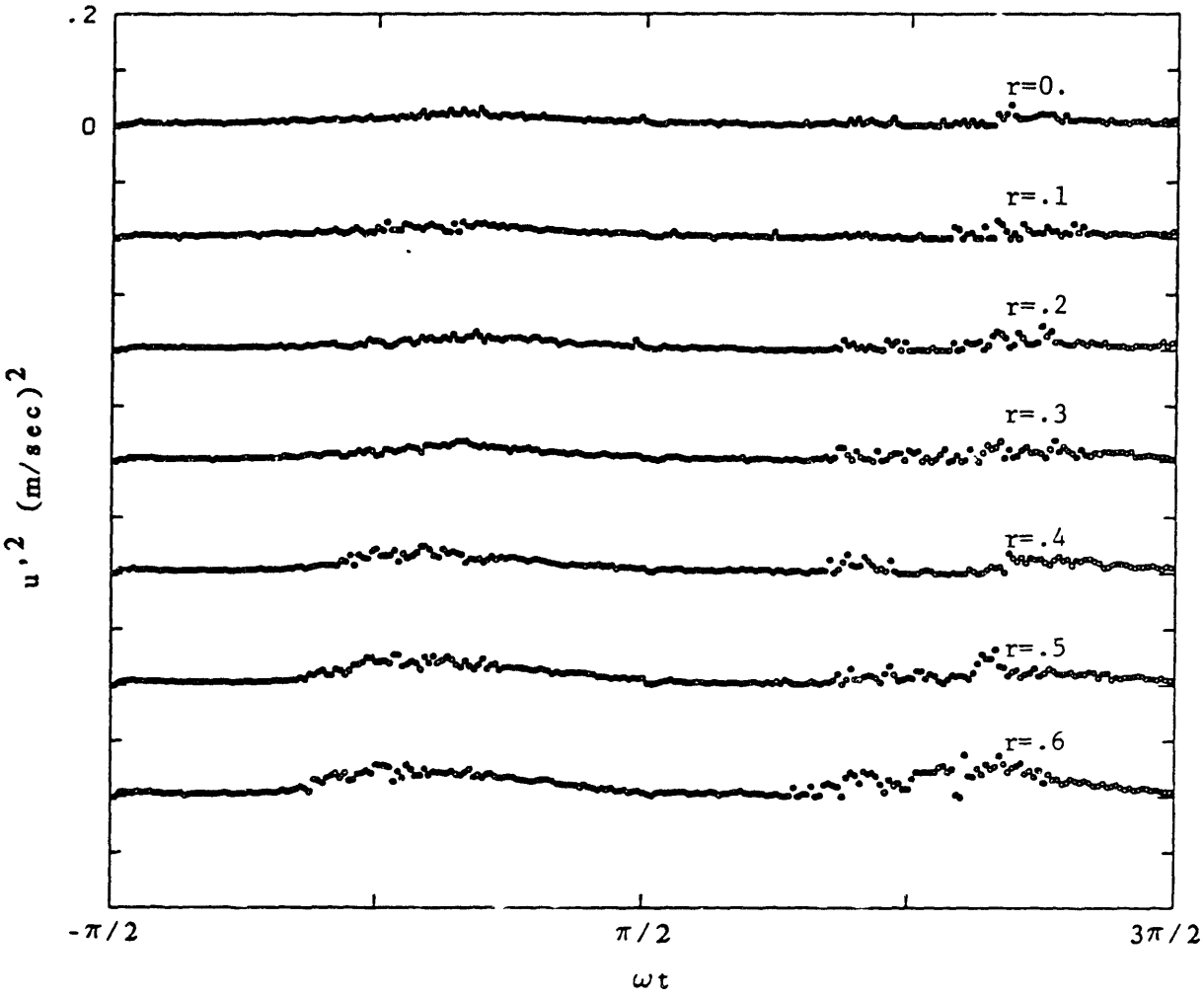

Figure 24a. For caption see Figure 24c.

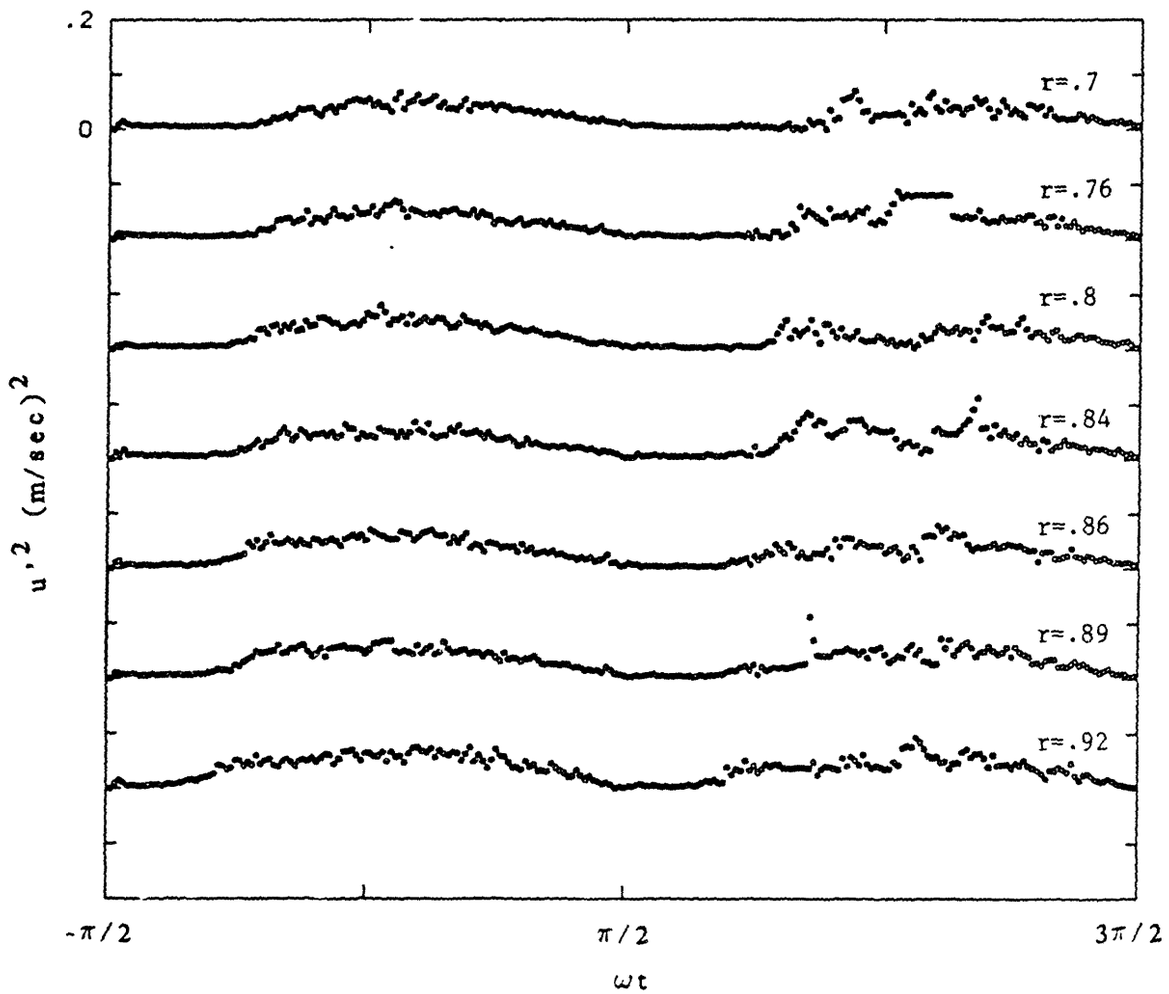

Figure 24b. For caption see Figure 24c.

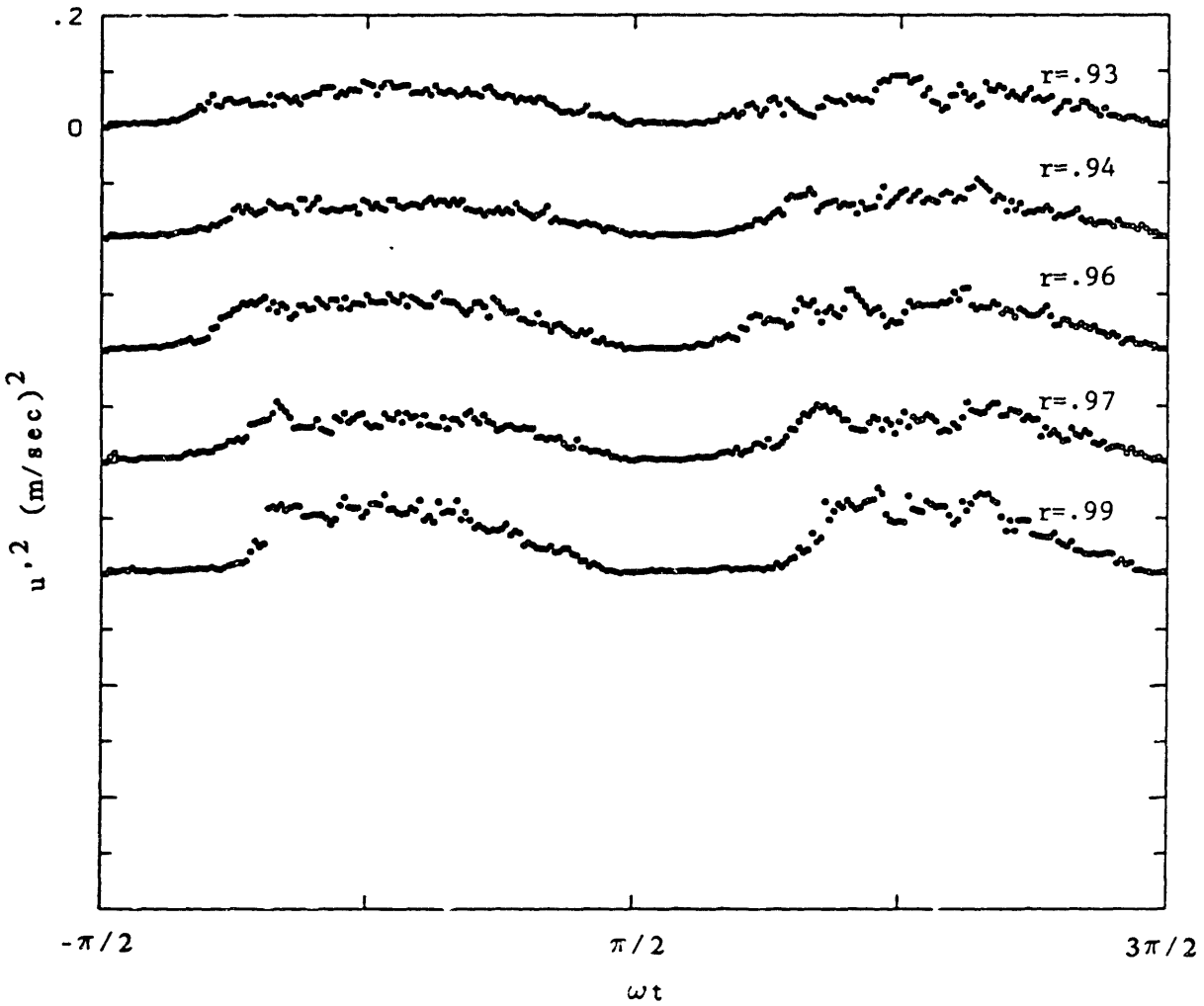

Figure 24c. Phase variation of axial turbulence intensities at various radial positions. (Re^{δ}-1720, Λ-10.6)

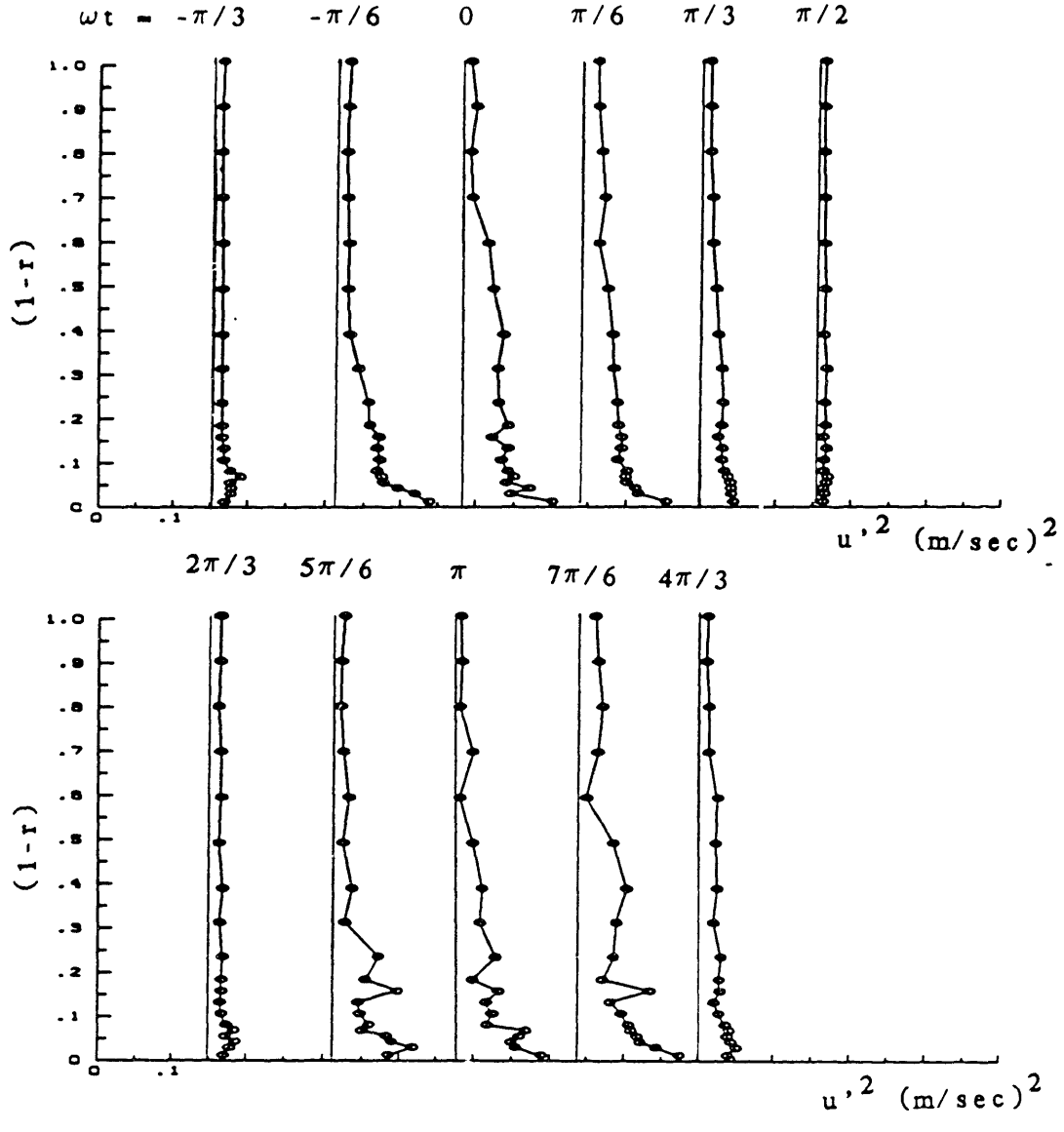

Figure 25. Distribution of axial turbulence intensity across the pipe radius for various phases. (Re^{δ}=1720, Λ=10.6)

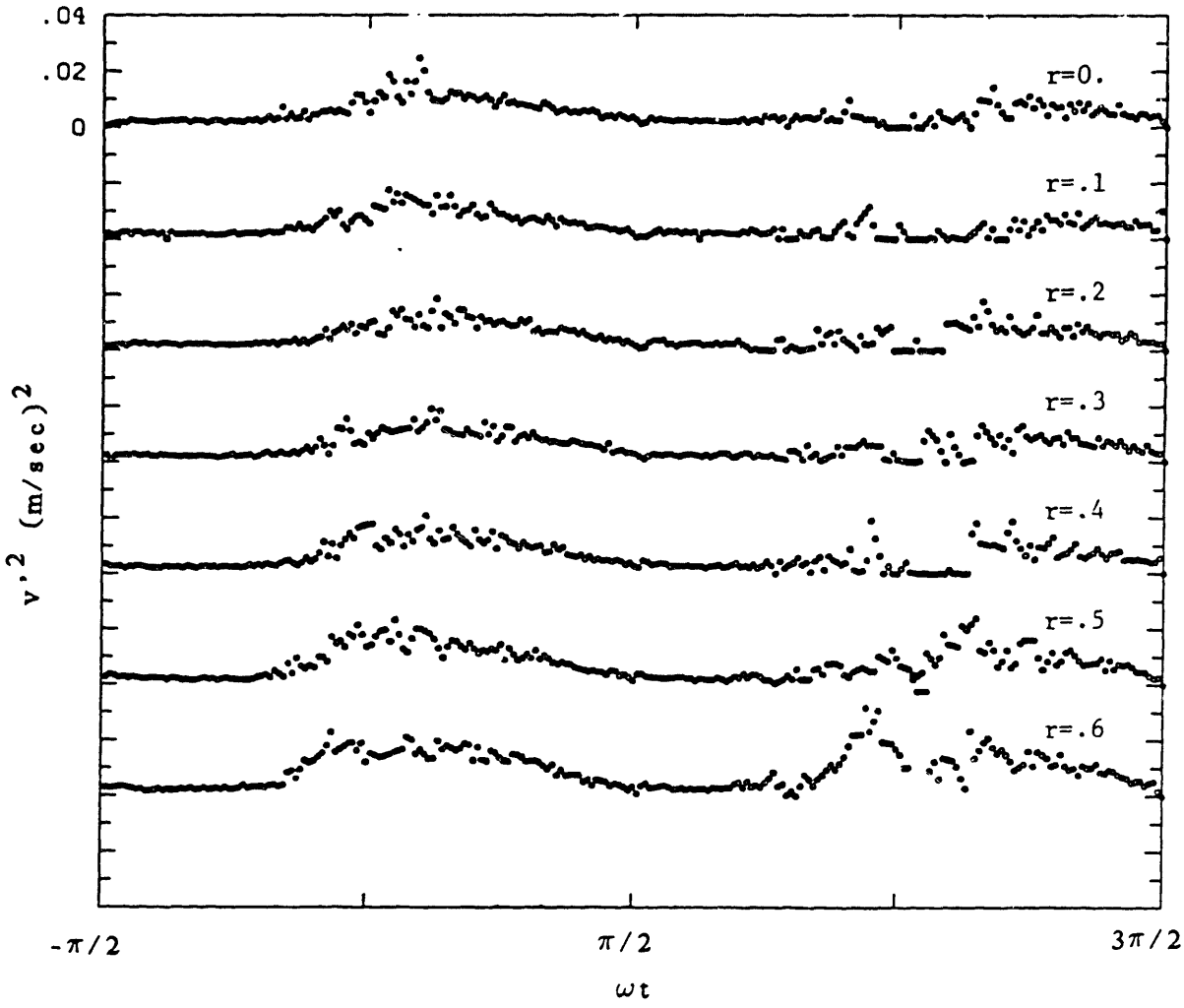

Figure 26a. For caption see figure 26c.

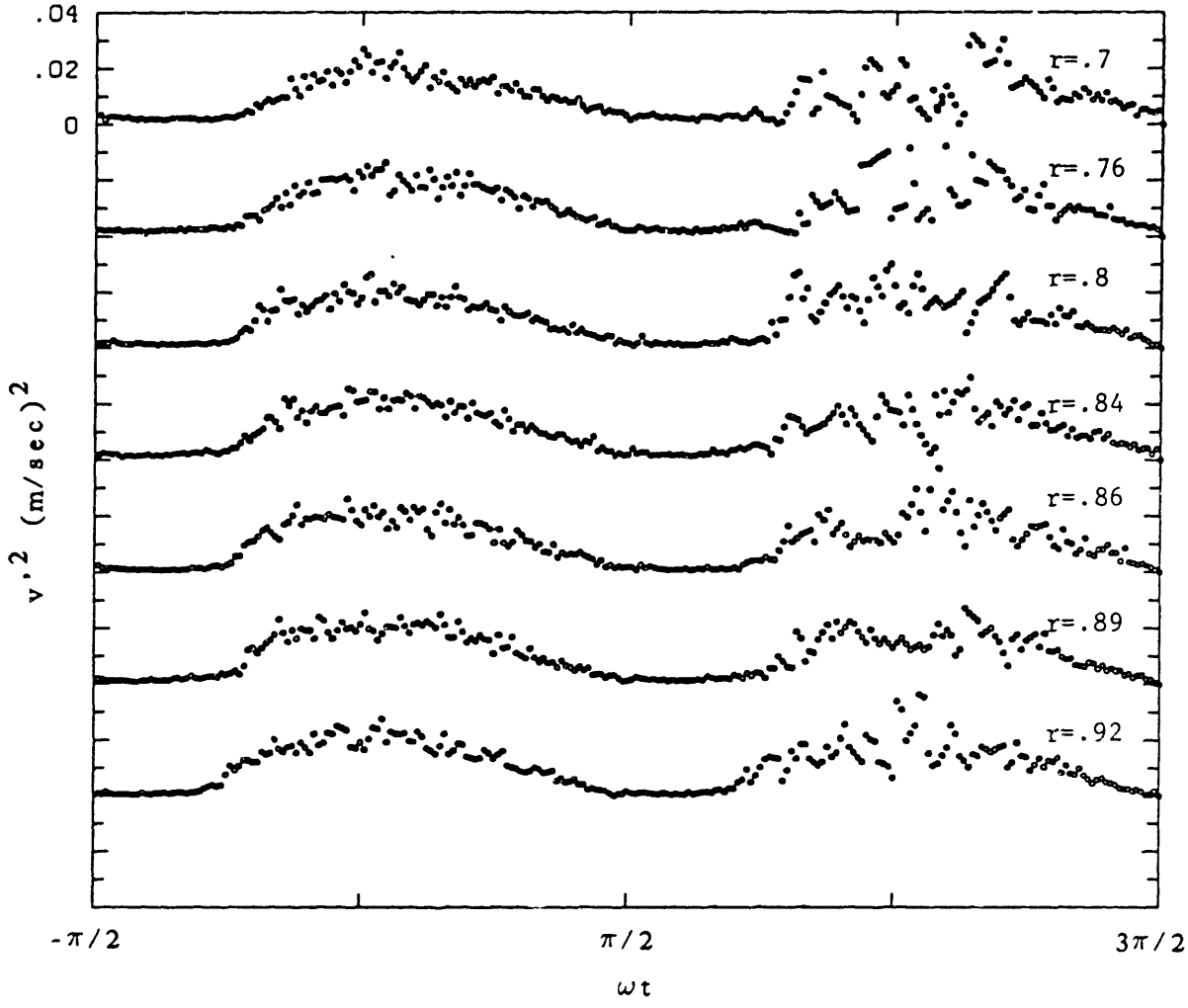

Figure 26b. For caption see figure 26c.

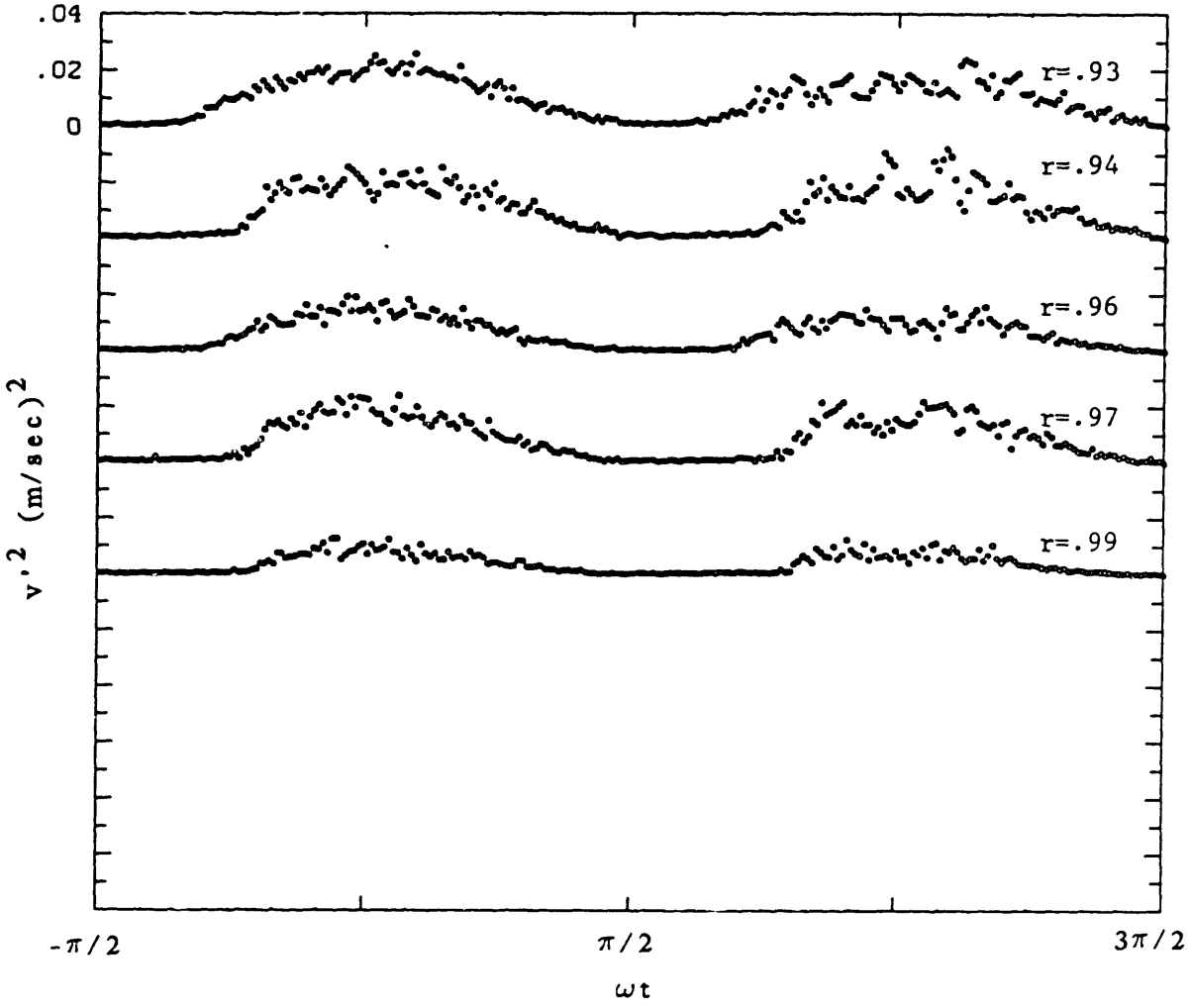

Figure 26c. Phase variation of radial turbulence intensities at various radial positions. (Re^{δ}=1720, Λ=10.6)

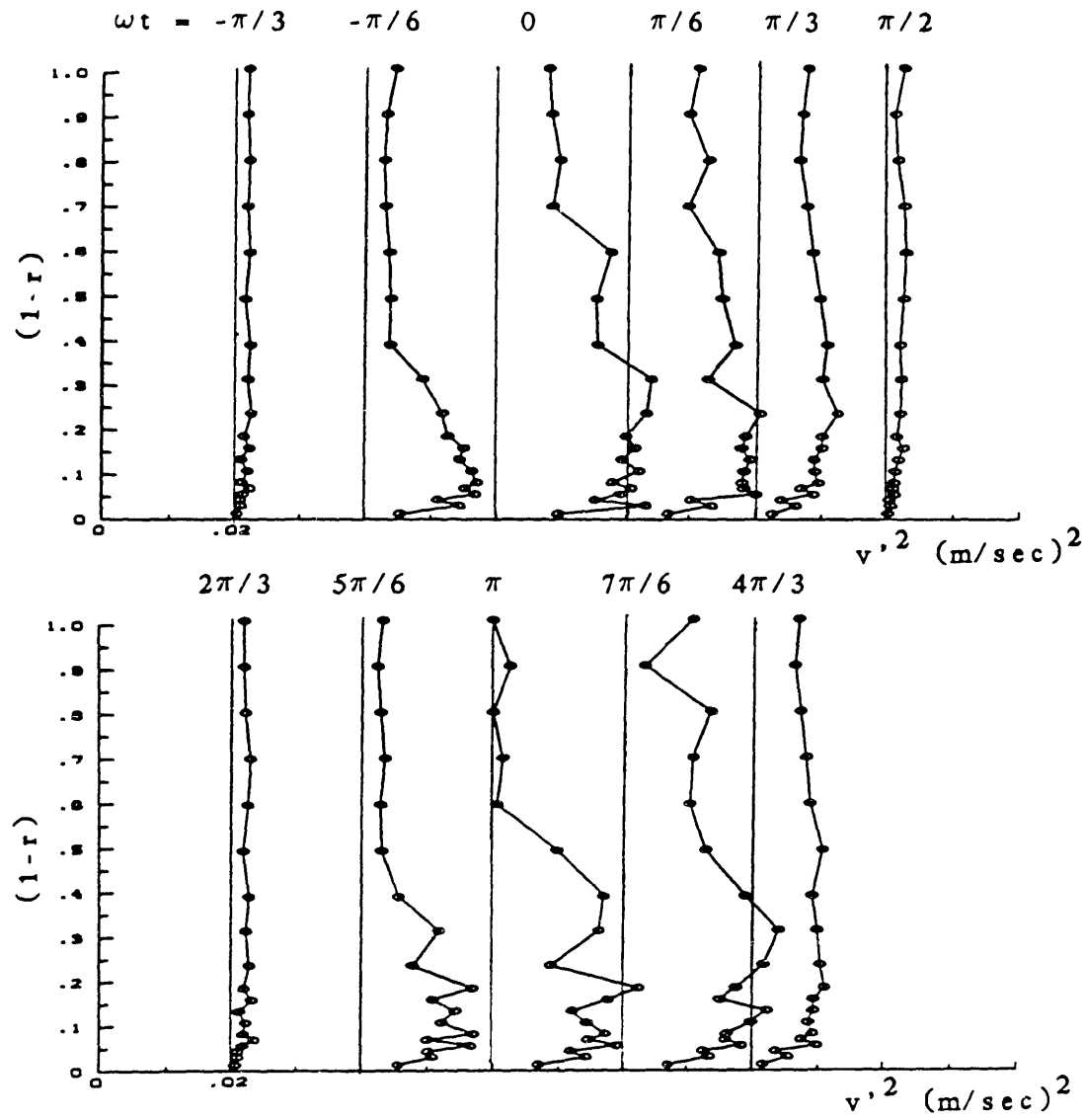

Figure 27. Distribution of radial turbulence intensity across the pipe radius for various phases. (Re^{δ}=1720, Λ=10.6)

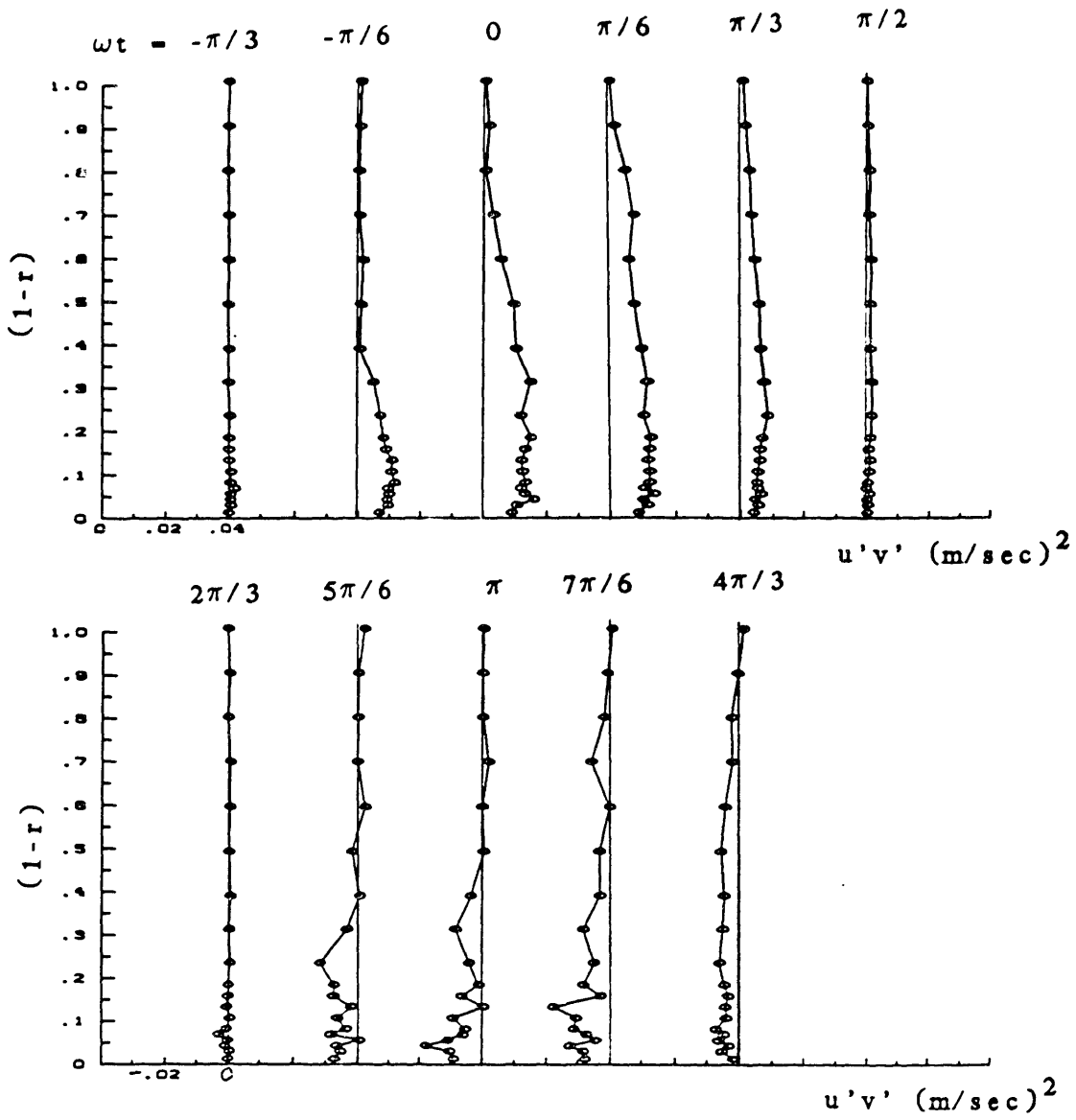

Figure 28. Distribution of Reynolds stress across the pipe radius for various phases. (Re^{δ}=1720, Λ=10.6)

2.3 Discussion

One of the major objectives of the present work is to gain some understanding of the fundamental physical processes that underlie the transition back and forth between the "laminar" and turbulent states of oscillatory pipe flow.

We have already mentioned that the ensemble averaged velocity profiles during the deceleration phase of the cycle (when the flow is turbulent) look very similar to instantaneous profiles that obtain during the ejection phase of turbulent bursts in steady wall-bounded flows [Kline,et.al (1967), Kovasznay, et.al (1962)], in that the profiles are inflectional just outside the boundary layer as a result of momentum exchange between the low speed fluid near the wall and the higher speed fluid further away. In contrast, the profiles for the acceleration phase of the cycle are full, and suggest that the relaminarization of flow during this period may be due to cessation of turbulent bursts.

Let us start by reviewing the bursting phenomenon in steady wall flows. We can then consider the effect of

acceleration or deceleration of the flow on the bursting process and decide if the assumption with regard to relaminarization of the flow because of cessation of bursting is justifiable.

Consider the (inviscid) vorticity field associated with a uniform shear flow. The vorticity field for this undisturbed flow consists of spanwise vortex lines forming sheets of transverse vorticity (Figure 29). If this flow is perturbed by a disturbance which has a streamwise vorticity component the vortex lines which were originally in the spanwise direction are deformed into U-shaped loops in the x_1-x_2 plane (see Benney and Lin [1960] for the origin of these disturbances). Due to self-induction of the U-shaped vortex a positive u_3 velocity component is induced at the tip of the loop (points T) while a negative u_3 velocity component is induced at points V (valleys). This induced velocity lifts up the tip of the vortex bringing it into regions of higher axial velocity, and pushes down the vortex filament near the valleys into regions of low velocity. As a result, the tip of the vortex loop ends up in a region of higher axial velocity relative to the valleys and therefore would have to move faster compared to the valleys, giving rise to further stretching of the vortex filament and the formation of an Ω-shaped filament. At the same time, the the original vortex filament is no more purely in the spanwise direction but acquires a strong streamwise component

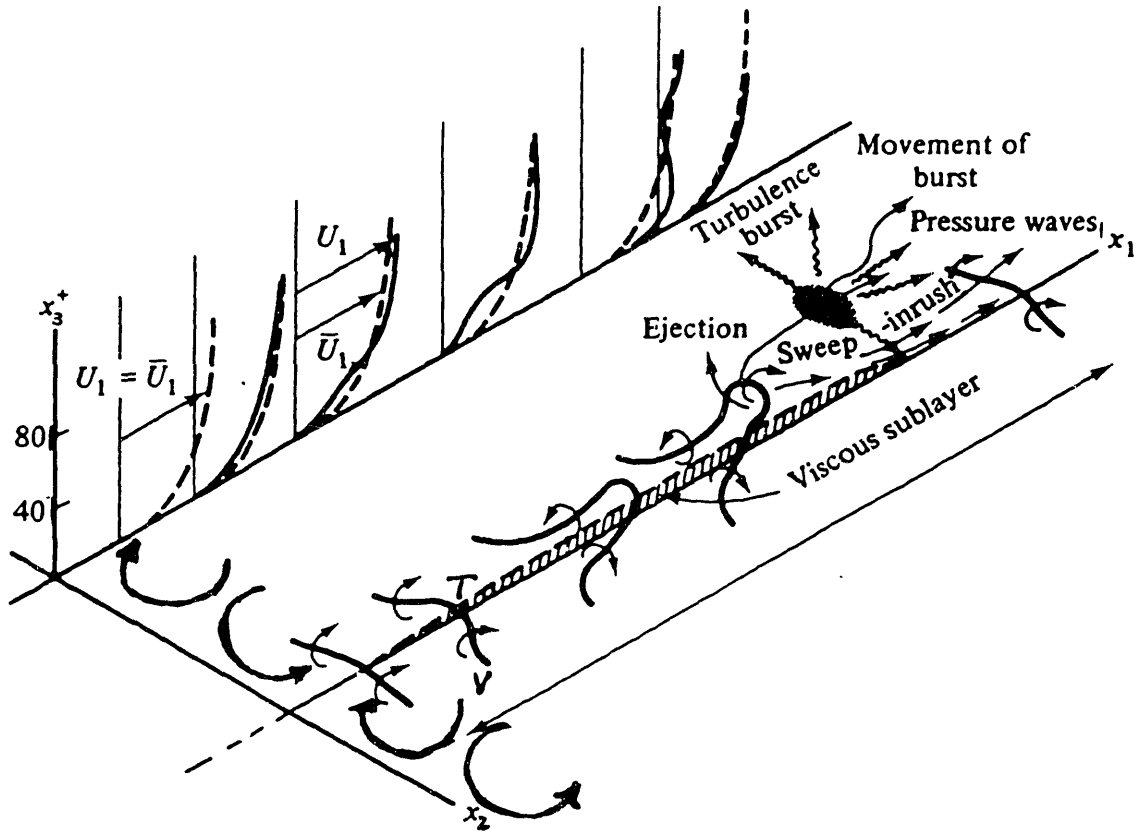

Figure 29. Conceptual model of the bursting process in steady wall-bounded shear flows (from Hinze, Turbulence).

especially around the legs of the vortex loop. This streamwise vorticity pumps the low speed fluid away from the wall and results in a defect in instantaneous axial velocity profiles which is accompanied by very intense shear layers in the velocity profiles. A turbulent burst is the result of local inflectional instability of these intense shear layers.

When the flow is accelerating, because of the favorable pressure gradients that are superimposed on the flow the profiles at the "peaks" cannot become as inflectional. As a result, the streamwise vortex filaments cannot lift and stretch as effectively and the bursting process does not occur.

Deceleration of the fluid, on the other hand, would tend to enhance the "defect" in the velocity profiles at the "peaks", and would result in more violent bursting.

For the oscillatory pipe flow, the (adverse or favorable) pressure gradients are not constant, but vary with time. This variation, however, is immaterial during an individual bursting process because the time scale of the burst is much shorter that the time variation of the flow. To see this point, recall that the turbulent burst has convective time scales on the order of (d/U), whereas the oscillatory pipe flow varies on a time scale $(1/\omega)$. The

ratio of these two time scales is the Strouhal number = $U/\omega d$ which is of the same order as $Re^{\delta}/\Lambda \gg 1.0$.

The relaminarization of the flow during the acceleration phase requires, in addition to cessation of bursting during this period, that no residual turbulence is left in the flow from the deceleration phase. Thus we need to estimate the time scale of decay of turbulence. In this regards, one must recall that dissipation is a very passive process in the sense that it proceeds at a rate that is dictated by the inviscid inertial behavior of the large eddies (Tennekes and Lumley). In other words the time limiting step in the dissipation process is the rate at which large eddies can transfer their energy to the smaller scales. This time scale is given by u'/l, where l represents the size of the largest eddies. These eddies, on the other hand, maintain their vorticity as a result of interaction with the mean shear flow and thus have characteristic vorticities of the same order as the mean shear; $u'/l \sim U/d$. This reasoning is the basis of mixing length theories in steady flows, and can be extended to our nonsteady problem because $d/U \gg 1/\omega$. From the above arguments, the time scale for decay of turbulence can be estimated as d/U, which again is much shorter than $1/\omega$ if $Re^{\delta}/\Lambda \gg 1$. Therefore, as long as the Strouhal number $= U/\omega d = Re^{\delta}/\Lambda \gg 1$, the turbulence generated during the deceleration phase does not get carried over to the acceleration phase, and in the absence of bursting during this period the flow has to relaminarize.

In summary, it appears that the transition back and forth between the laminar and turbulent states is mainly due to cessation of "bursting" during portions of the acceleration phase of the cycle, as a result of favorable pressure gradients superimposed on the boundary layer. Our experiments present indirect evidence that the fundamental bursting process is the same as that for steady wall-bounded flows. Further experimentation, (in particular in the form of Lagrangian flow visualization) can provide better evidence for this claim.

We will instead proceed to investigate the transition process by direct numerical simulations of the Navier-Stokes equations. These results will be discussed in the next section.

III. NUMERICAL SIMULATIONS

3.1 Problem Formulation and Numerical Methods

In this section we present results of a numerical investigation of the stability of oscillatory flow in a channel which is subjected to various classes of infinitesimal and finite-amplitude two- and three-dimensional disturbances. The full three-dimensional time-dependent Navier-Stokes equations are solved in each case, using the pseudospectral formulation suggested by Orszag [1971].

The flow geometry is a two-dimensional channel which has rigid walls at $z = \pm h$ and extends to infinity in the x and y directions. In all that follows the channel half width, h, is taken to be ten times the Stokes boundary layer thickness ($h \equiv 10\sqrt{2\nu/\omega}$). The flow rate per unit width into this channel is imposed as $Q^* = Q_o \cos(\omega t^*)$.

The choice of a channel geometry for the theoretical study versus a pipe for experiments is mainly a matter of convenience. The characteristics of the turbulent flow in a pipe and a channel are very similar, because the turbulent flow structures are in general much smaller than the curvature of the pipe. For steady flows the large pool of

experimental data is in support of this fact. For the Stokes problem, we base this argument on the close similarity between our experimental results for flow in a pipe and the results of Hino and coworkers which were obtained in a channel.

We solve the Navier-Stokes equations expressed in rotation form,

$$\frac{\partial \mathbf{v}^*}{\partial t^*} = \mathbf{v}^* \times \omega^* - \nabla\left(\frac{p^*}{\rho} + \frac{|\mathbf{v}^*|^2}{2}\right) + \nu\nabla^2\mathbf{v}^* + f^*\hat{\mathbf{x}}$$

where $\omega^* = \nabla \times \mathbf{v}^*$ is the vorticity and $\left(\frac{p^*}{\rho} + \frac{|\mathbf{v}^*|^2}{2}\right)$ is the pressure head. The mean pressure gradient is not included in p^* but is represented by the external forcing f^*, $(f^* = -\nabla P^*/\rho)$. Here, * denotes dimensional quantities.

If one further introduces the non-dimensional quantities,

$$t = \omega t^*$$

$$\mathbf{v} = \frac{\mathbf{v}^*}{U_o}, \quad \text{where} \quad U_o = \frac{Q_o}{2h}$$

$$\mathbf{x} = \frac{\mathbf{x}^*}{\delta}, \quad \text{where} \quad \delta = \sqrt{2\nu/\omega}$$

$$\Pi = \frac{\left(\frac{p^*}{\rho} + \frac{|\mathbf{v}^*|^2}{2}\right)}{U_o^2}$$

$$f = \frac{f^*}{\left(\frac{U_o^2}{\delta}\right)}$$

the Navier-Stokes equations can be represented in the nondimensional form,

$$\frac{\partial \mathbf{v}}{\partial t} = \left(\frac{Re^{\delta}}{2}\right)(\mathbf{v}\times\omega) - \left(\frac{Re^{\delta}}{2}\right)\nabla\Pi + \frac{1}{2}\nabla^2\mathbf{v} + \left(\frac{Re^{\delta}}{2}\right)f\,\hat{\mathbf{x}}$$

This equation is solved numerically subject to no slip boundary conditions at $z=\pm 1$0, and with periodic boundary conditions in the horizontal directions;

$$\mathbf{v}\left(\mathbf{x} + \frac{2\pi n}{\alpha}, y + \frac{2\pi m}{\beta}, z, t\right) = \mathbf{v}(\mathbf{x},y,z,t)$$

for all integers n and m, and specified streamwise and spanwise wavenumbers α and β.

The numerical scheme is that used in earlier studies of transition in steady wall-bounded flows by Orszag and coworkers. Various details of the the numerical code may be found in the literature [Orszag and Kells (1980), Orszag and Patera(1983)]. Here we summarize the basic discretization and time-stepping procedures.

The velocity field is represented using Fourier series in x and y and Chebyshev polynomials in z,

$$\mathbf{v} = \sum_{p=0}^{P}\sum_{n=-N}^{N}\sum_{m=-M}^{M} \mathbf{v}_{nmp}(t)\, e^{i\alpha n x}\, e^{i\beta m y}\, T_p(z)$$

$$= \sum_{n=-N}^{N}\sum_{m=-M}^{M} \mathbf{v}_{nm}(z,t)\, e^{i\alpha n x}\, e^{i\beta m y}$$

The time-stepping procedure uses a fractional step (or splitting technique), where incompressibility and viscous boundary conditions are imposed in different fractional time steps. The time-stepping procedure is given by,

$$(i)\quad \frac{\hat{\mathbf{v}}^{n+1}-\mathbf{v}^{n}}{\left(\frac{Re^{\delta}}{2}\Delta t\right)} = \frac{3}{2}(\mathbf{v}\times\omega)^{n} - \frac{1}{2}(\mathbf{v}\times\omega)^{n-1} + f\,\hat{\mathbf{x}}$$

$$(ii)\quad \frac{\hat{\hat{\mathbf{v}}}^{n+1} - \hat{\mathbf{v}}^{n+1}}{\left(\frac{Re^{\delta}}{2}\Delta t\right)} = -\nabla\Pi$$

$$\nabla\cdot\hat{\mathbf{v}}^{n+1} = 0$$

$$||\hat{\mathbf{w}}^{n+1}=0 \text{ at } z=\pm 10$$

$$(iii)\quad \frac{\mathbf{v}^{n+1} - \hat{\hat{\mathbf{v}}}^{n+1}}{\Delta t} = \frac{1}{2}\nabla^{2}\mathbf{v}^{n+1}$$

$$||\mathbf{v}^{n+1} = 0 \text{ at } z=\pm 10$$

The first step incorporates nonlinear effects. The time stepping procedure is an Adams-Bashforth explicit scheme, which incurs errors of $O(\Delta t^{2})$.

The second step imposes incompressibility. The vector equations are reduced to a Poisson equation for $\hat{w}$ which is

solved subject to the inviscid boundary conditions (i.e, $\hat{\hat{w}}=0$ at $z=\pm 10$). At the end of this step the flow is incompressible but the viscous boundary conditions are not satisfied.

The last step incorporates the viscous effects and imposes the viscous boundary conditions. The time-stepping scheme is only first order but implicit.

In the present problem the flow rate (Q=cost) rather than the external forcing (pressure gradient) is specified. This can be implemented by noting that since f is divergence-free, it merely has an additive effect on $\hat{v}^{n+1}$ and $\hat{\hat{v}}^{n+1}$ in steps (i) and (ii). In other word the effect of the external forcing is to introduce a contribution to v^{n+1} in step (iii) given by v'^{n+1} where,

$$\frac{v'^{n+1}}{\Delta t} = \frac{1}{2}\nabla^2 v'^{n+1} + \left(\frac{Re^{\delta}}{2}\right) f^{n+1}\,\hat{x}$$

$$|| v'^{n+1} = 0 \quad \text{at } z = +10$$

One could thus solve for v^* corresponding to a unit forcing in a pre-processing stage,

$$\frac{v^*}{\Delta t} = \frac{1}{2}\nabla^2 v^{*n+1} + \hat{x}$$

$$|| \; v^* = 0 \quad \text{at} \quad z = +10$$

At each time step, equations (i) thru (iii) are then solved without the effect of external forcing to give v''^{n+1}. The correct solution to v^{n+1} is then,

$$v^{n+1} = v''^{n+1} + (Re^{\delta}/2)\, f^{n+1}\, v^{*}$$

where f^{n+1} is determined by the imposed flow rate at time (n+1), i.e;

$$\int v''^{n+1}\, dA + (Re^{\delta}/2)\, f^{n+1} \int v^{*}\, dA = Q^{n+1}$$

or,

$$\left(\frac{Re^{\delta}}{2}\right) f^{n+1} = \frac{Q^{n+1} - \int v''^{n+1}\, dA}{\int v^{*}\, dA}$$

This completes the description of the main part of the program.

Initial conditions for the runs reported in this study generally consist of an unperturbed laminar flow on which are superposed various combinations of infinitesimal or finite-amplitude two- and three-dimensional eigenmodes of the (time-independent) Orr-Sommerfeld equation for the "frozen" initial profile. Note that even though the initial disturbance is strictly valid only if the flow was time-independent, the results obtained in the steady state using the full time-dependent simulation and the initial

disturbances described above should accurately represent the full time-dependent behavior of the flow.

A number of tests have been performed to verify the accuracy of the direct numerical simulation. As a start, the evolution of the least stable eigenmode of the Orr-Sommerfeld equation is followed for a frozen profile using the direct simulation and the results are compared to those predicted by the Orr-Sommerfeld equation. A few of these results are summarized in table 1. In other tests results of the full simulation for small disturbances were compared with those of the linearized equations; and finally direct simulations of two- and three-dimensional infinitesimal disturbances were compared to verify that they correspond to each other according to Squires' theorem. These results will be discussed in later sections.

Typical parameter values for direct simulations are P=64(or 128), 2N=32, 2M=2, Courant number = 0.1 . Convergence in all these parameters has been verified by either halving or doubling the resolution.

	frozen profile of $\omega t=0$		frozen profile of $\omega t=\pi/2$	
	2D disturbance	3D disturbance	2D disturbance	3D disturbance
Re^{δ}	1000	$1000\sqrt{2}$	1000	$1000\sqrt{2}$
α	0.5	$0.5/\sqrt{2}$	0.5	$0.5/\sqrt{2}$
β	—	$0.5/\sqrt{2}$	—	$0.5/\sqrt{2}$
Real(ω)	.54467293	.38514192	-.06858357	-.04849591
Im(ω)	.00175319	.00121291	.02015786	.01425378
Resolution 2N x (P+1)	8x65	8x65	8x65	8x65
Courant #	.1	.1	.1	.1
Final Time	$\pi/10$	$\pi/10$	$\pi/10$	$\pi/10$
predicted amp. chng $e^{(Re/2)Im(\omega)t}$	1.309	1.309	23.722	23.722
computed amp. chng	1.346	1.341	23.406	23.446
predicted phase chng $e^{-i(Re/2)Real(\omega)t}$	-85.557	-85.557	10.773	10.773
computed phase chng	-85.813	-85.813	10.772	10.772

Table 1. Comparison of evolution of small-amplitude disturbances for frozen profiles to prediction of Orr-Sommerfeld equation.

3.2 Small Amplitude Disturbances (Linear Theory)

The linear stability of oscillatory Stokes layers has been the subject of a number of investigations. The simplest and most popular approach is the quasi-static assumption, where the time dependence of the basic profile is ignored and the stability of instantaneous "frozen" profiles is studied using the the classical (time-independent) Orr-Sommerfeld eigenvalue equation. One question is the choice of which frozen profile to use. For the particular example of oscillatory flow in a channel with an imposed flow rate of $Q = \cos t$, two such quasi-steady stability maps, one for a time of $t=0$ and the other for $t=\pi/2$, are shown in Figures 30a and 30b. As one would expect, the two stability maps are quite different. The minimum critical Reynolds number, for example, has a value $Re^{\delta}_{crit.} \sim 80$ for the profile at $t=\pi/2$; but a significantly larger value ($Re^{\delta}_{crit.} \sim 500$) for $t=0$. The most dangerous streamwise wavenumbers, however, are in both cases close to α of 0.5. If the quasi-steady problem is at all relevant to the problem of stability of oscillatory Stokes layers, the stability maps of Figure 30 suggest a search for unstable modes (in the full time-dependent problem) in the range of wavenumbers $\alpha \sim 0.2$ to 0.7.

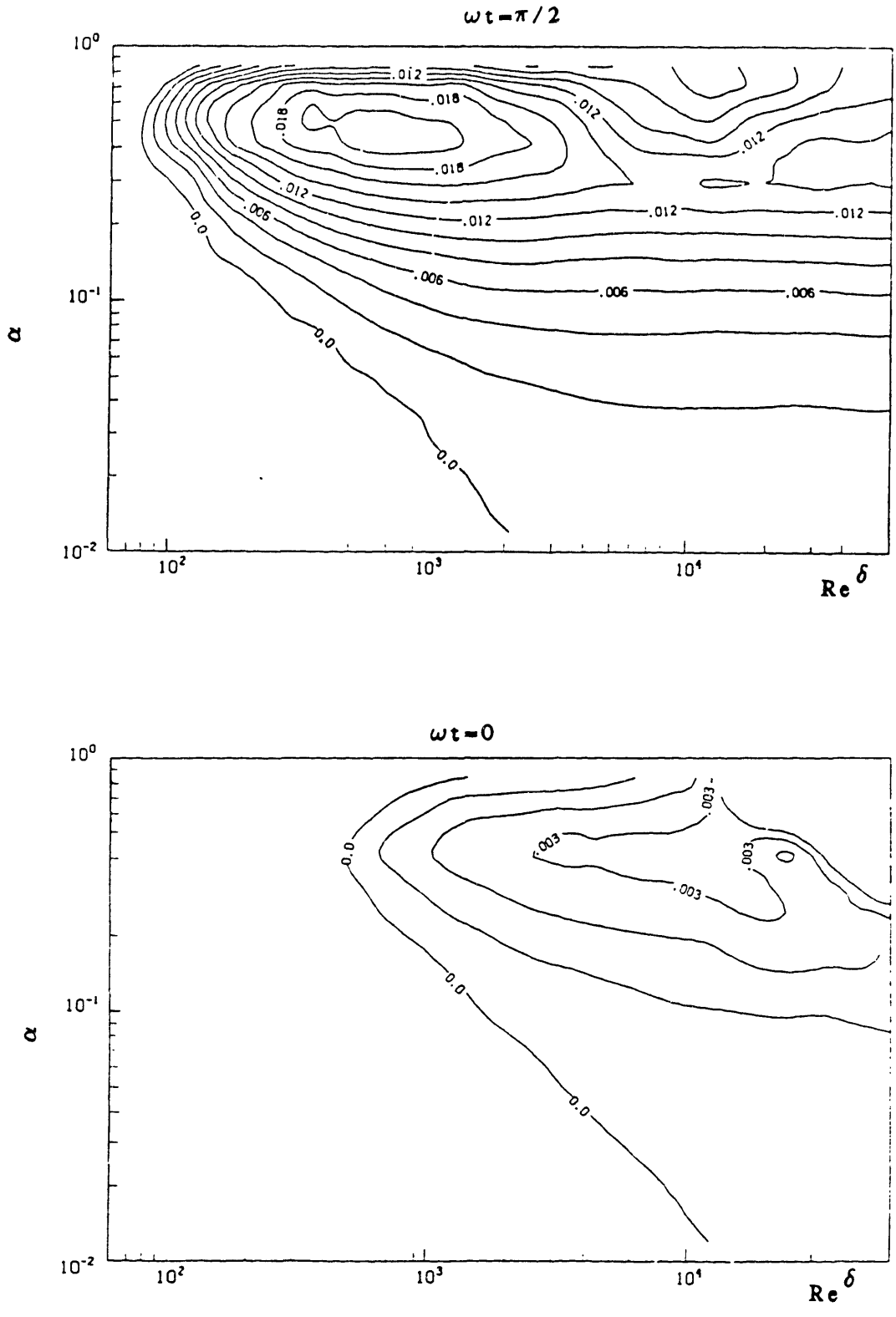

Figure 30. Iso-growth curves for the frozen profiles at $\omega t=\pi/2$ and $\omega t=0$.

3.2.1 Two and Three-Dimensional Disturbances

Squire's theorem provides a very useful transformation for the linear stability problem of "steady" unidirectional shear flows, which reduces the linear stability problem of any 3-D disturbance to that of 2-D disturbance at a lower Reynolds number [Drazin and Reid,1981]. Exactly the same transformation can be used in the "unsteady" linearized equations [von Kerczek & Davis,1974] with the conclusion that the evolution of any infinitesimal 3-D disturbance is related to a 2-D one at a lower Reynolds number. This is confirmed in the results of the numerical simulation, one example of which is shown in Figure 31. In this figure the evolution of a 3-D disturbance and its equivalent 2-D disturbance are compared. Here En2 is the total two-dimensional disturbance energy (in all the streamwise fourier modes $1<n<N$) and is given by,

$$En2 = \sum_{n=1}^{N} \int_{-10}^{10} (\mathbf{v}_n(2) . \mathbf{v}_n^*(2)) \, dz$$

where * denotes complex conjugate.

Similarly En3 is the total three-dimensional energy,

$$En3 = \sum_{m=-M}^{M} \sum_{n=-N}^{N} \int_{-10}^{10} (\mathbf{v}_{nm}(3) . \mathbf{v}_{nm}^*(3)) \, dz$$

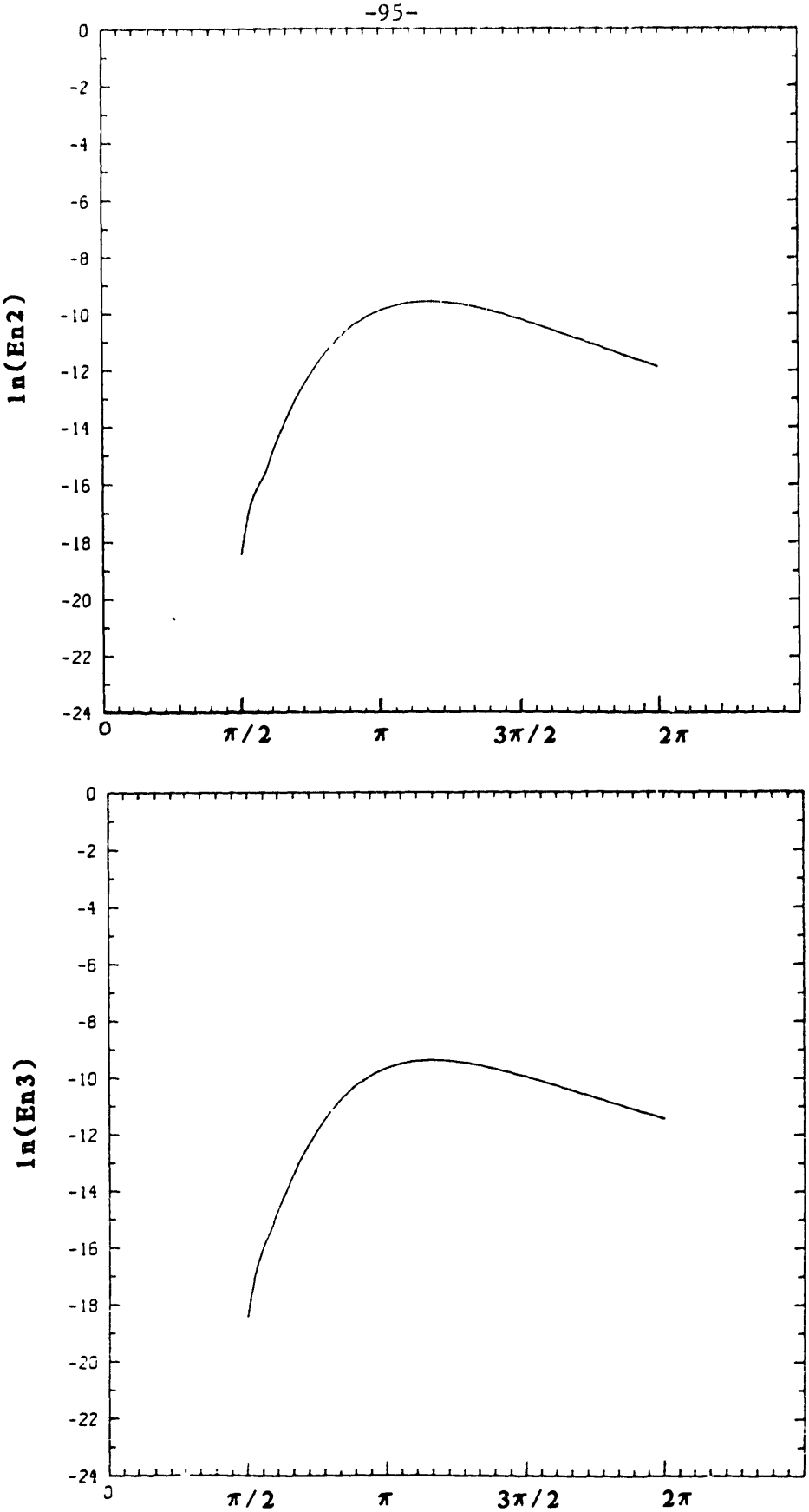

Figure 31. Equivalence of two- and three-dimensional infinitesimal disturbances by Squires Theorem. For 2D disturbances Re^{δ}=1000., α=0.5 . For 3D disturbances $Re^{\delta}=1000\sqrt{2}$, $\alpha=\beta=0.5/\sqrt{2}$. Initial conditions are the least stable eigenmodes of O-S equation for the frozen initial profile.

The comparison also serves as an extra check on the integrity of the numerical code.

Consequently, only two-dimensional infinitesimal disturbances will be considered in this section.

3.2.2 The Linearized Problem

For infinitesimal disturbances, a substantial savings in computation time is achieved by solving, instead of the full nonlinear problem, the linearized disturbance equations given by:

$$\frac{\partial}{\partial t}(u',v',w') = -\frac{Re^{\delta}}{2}(\bar{U}u'_x + w'\bar{U}_z \ , \ \bar{U}v'_x \ , \bar{U}w'_x) - \frac{Re^{\delta}}{2}(\Pi_x, \Pi_y, \Pi_z) + \frac{1}{2}\nabla^2(u',v',w')$$

Here $\mathbf{v}'$ is the disturbance velocity, and only one fourier mode is kept in the streamwise direction;

$$\mathbf{v}' = \sum_{n=-1,+1} \mathbf{v}'(t)\, e^{i\alpha n x}\, T_p(z) = \sum_{n=-1,+1} \mathbf{v}'(z,t)\, e^{i\alpha n x}$$

Except for the implementation of the nonlinear terms, the method of solution is the same as that described earlier.

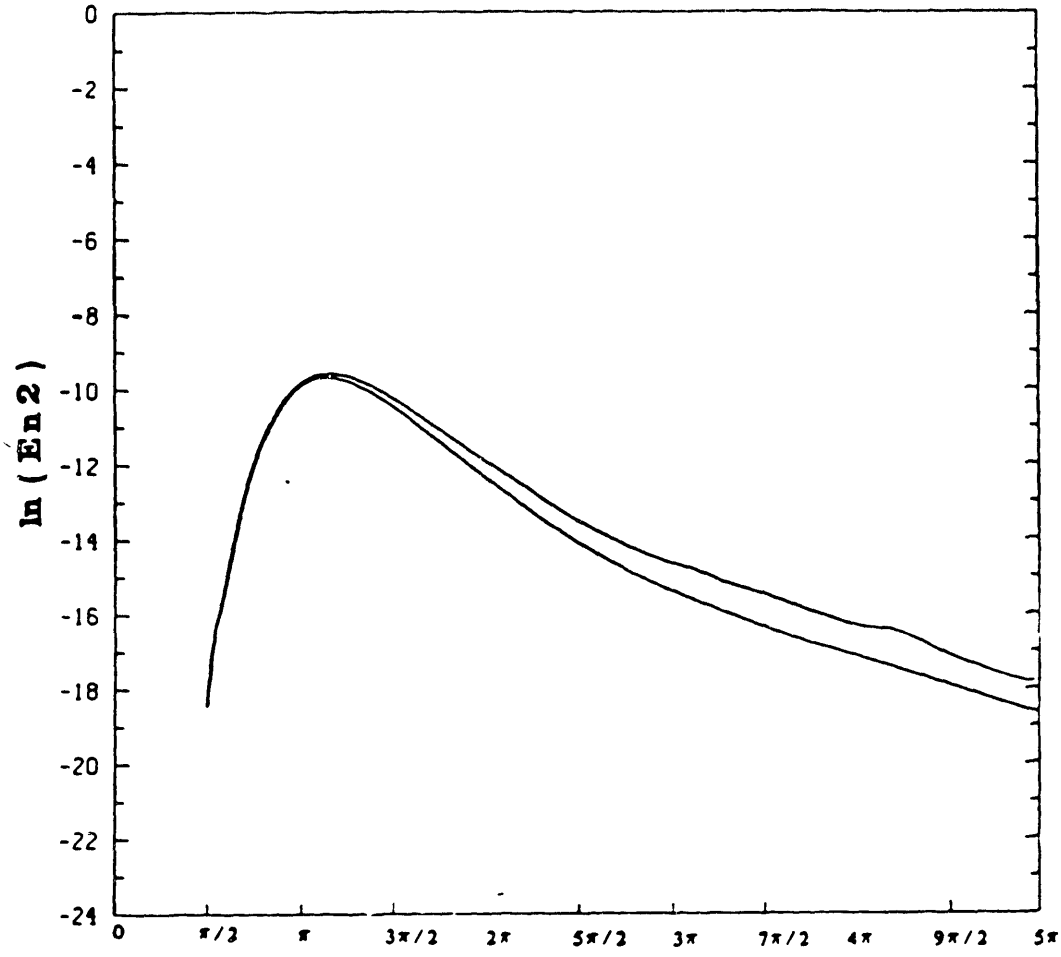

Figure 32. Comparison of the results of the full three-dimensional simulation to the linearized problem for the evolution of two-dimensional disturbances at Re^{δ}=1000.0 α=0.5 .

For infinitesimal disturbances, the results of the linearized equations should, of course, be in agreement with the full nonlinear problem. A comparison of the two is shown in Figure 32 for $Re^{\delta}=1000$ and $\alpha=0.5$. The slight wiggles at large times in the full simulation are due to the excitation of higher order modes by roundoff errors.

The results to be discussed in the rest of this section were obtained using the linearized equations.

3.2.3 Effect of Initial Conditions

It was mentioned earlier that the Navier-Stokes equations are solved subject to initial conditions that are the least stable eigenmodes of the Orr-Sommerfeld equation for the initial "frozen" profile. It was also mentioned that for large times the solution becomes independent of the initial condition. This point is verified by the results shown in Figures 33(a-d), where the flow is started at two different times ($t=0$, and $t=\pi/2$) and in each case subjected to the least stable disturbance of the initial "frozen" profile. In addition to the overall energy of the disturbance, the distribution of the disturbance energy across the channel width is also shown for selected times. Comparison of the growth rates in the two cases (as shown in Figures 33a,b), or the distributions of the disturbance energy for large times (as shown in Figures 33c and 33d)

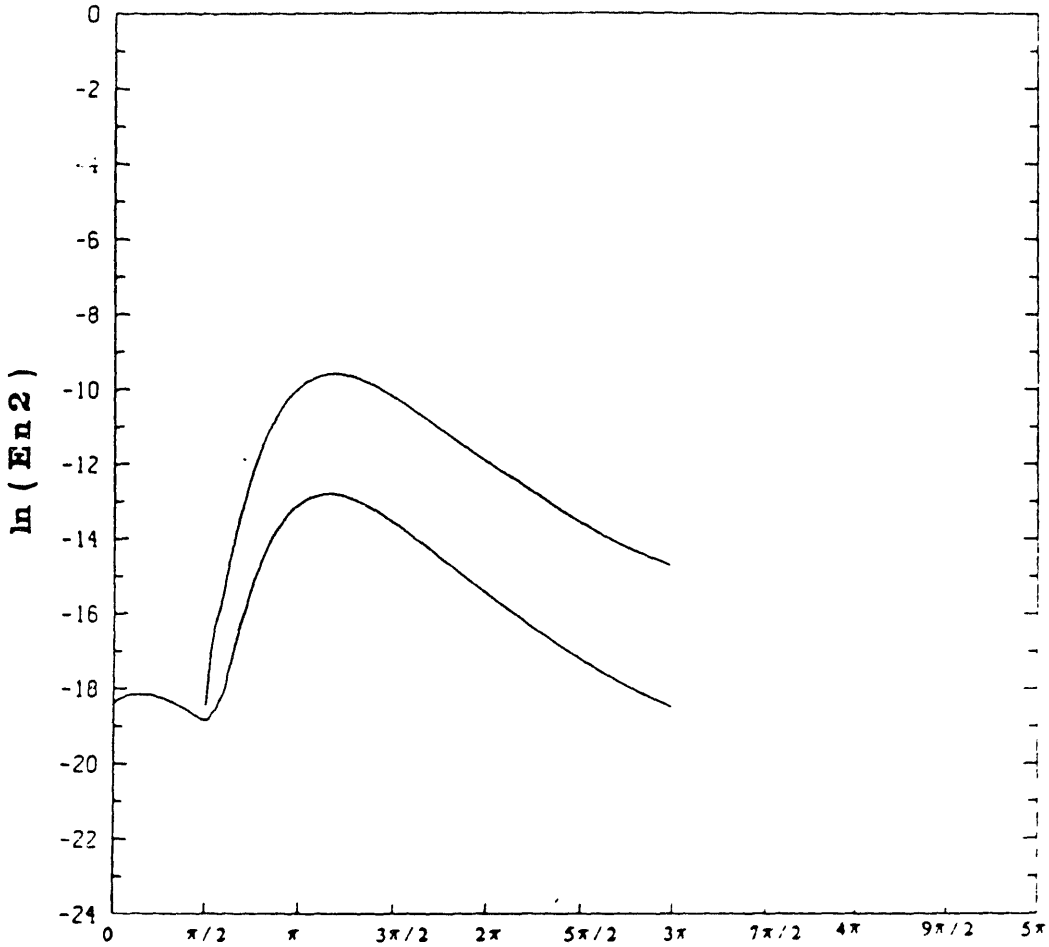

Figure 33(a,b). Evolution of two-dimensional disturbances at $Re^{\delta} = 1000.0$, $\alpha = 0.5$ for two distinct initial conditions. Note that at large times the growth rates (Figures 33a , b) and distributions of the disturbance energy across the channel width (Figures 33c , d) become independent of the initial condition.

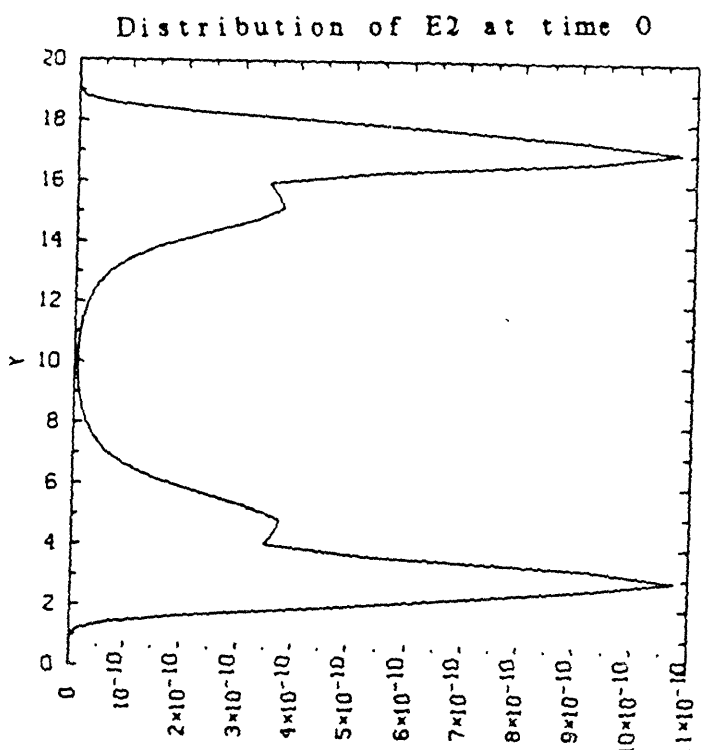

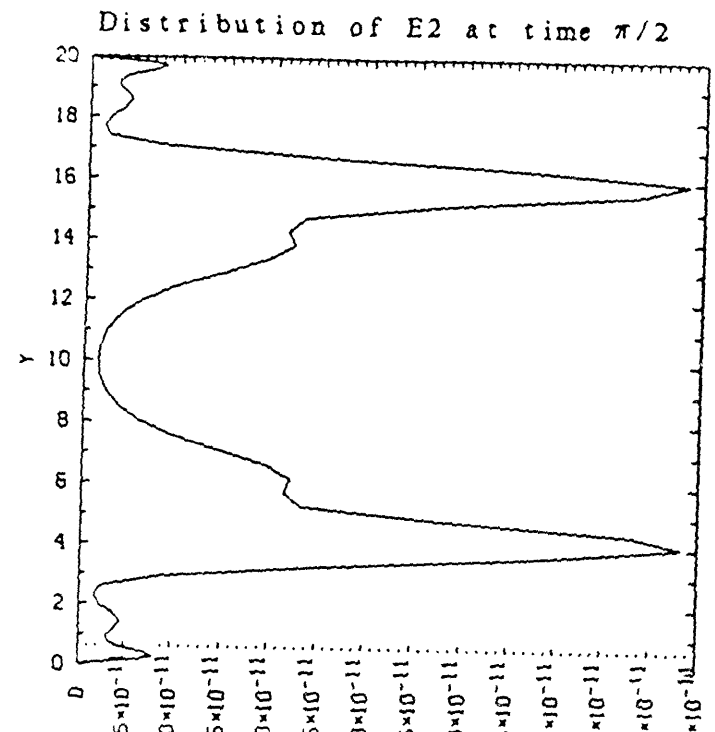

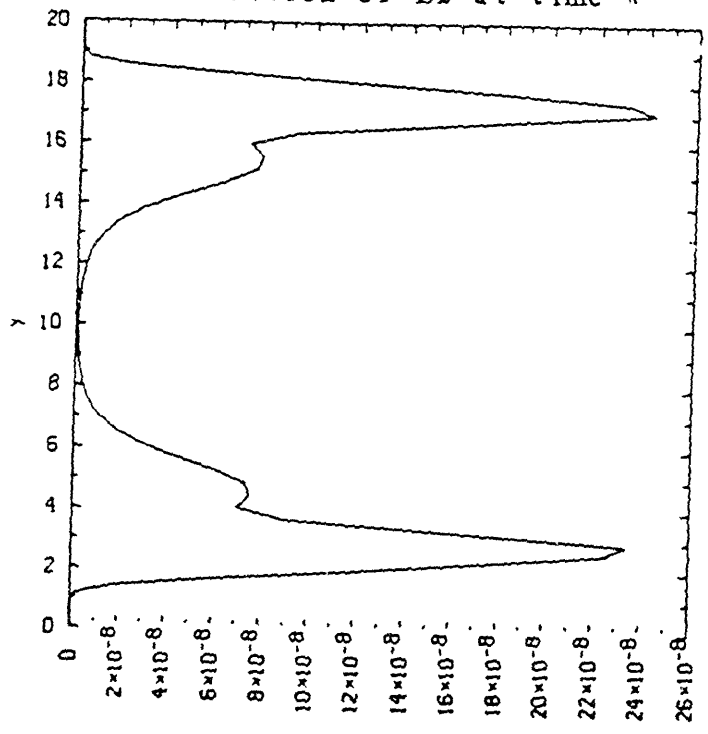

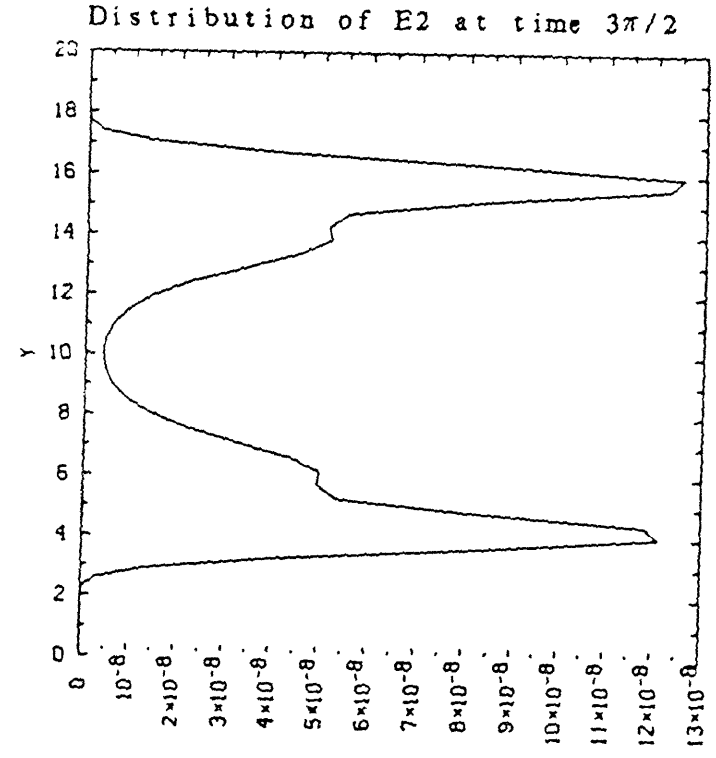

Figure 33c. For caption see Figure 33a.

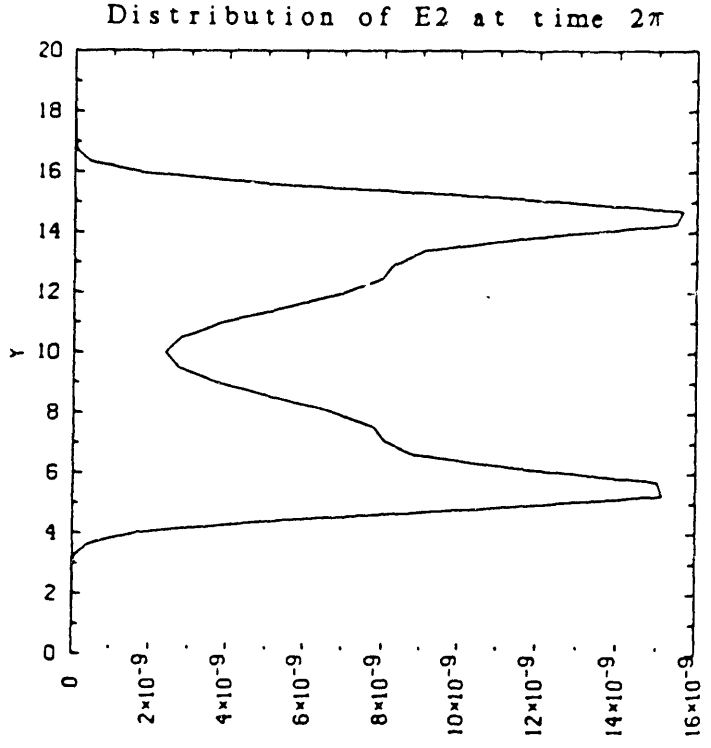

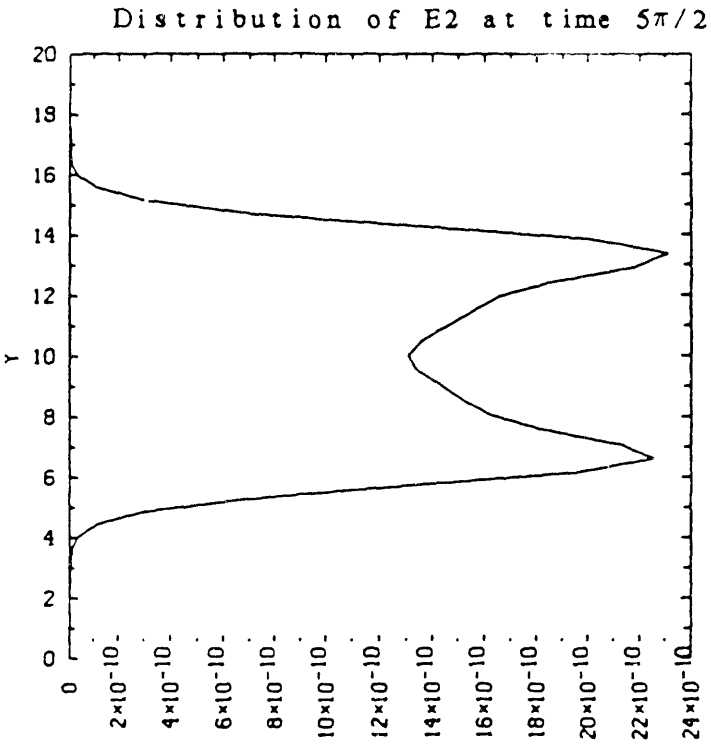

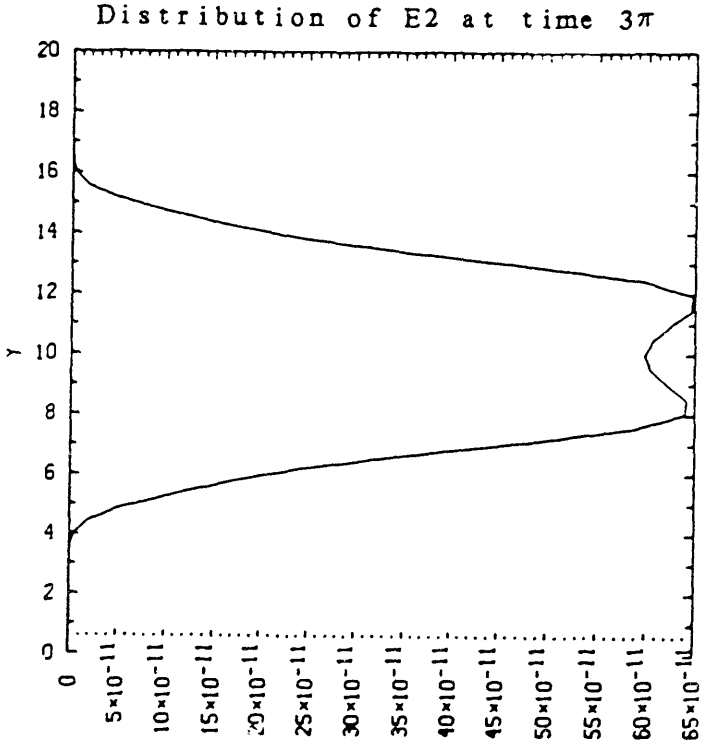

Figure 33c. For caption see Figure 33a.

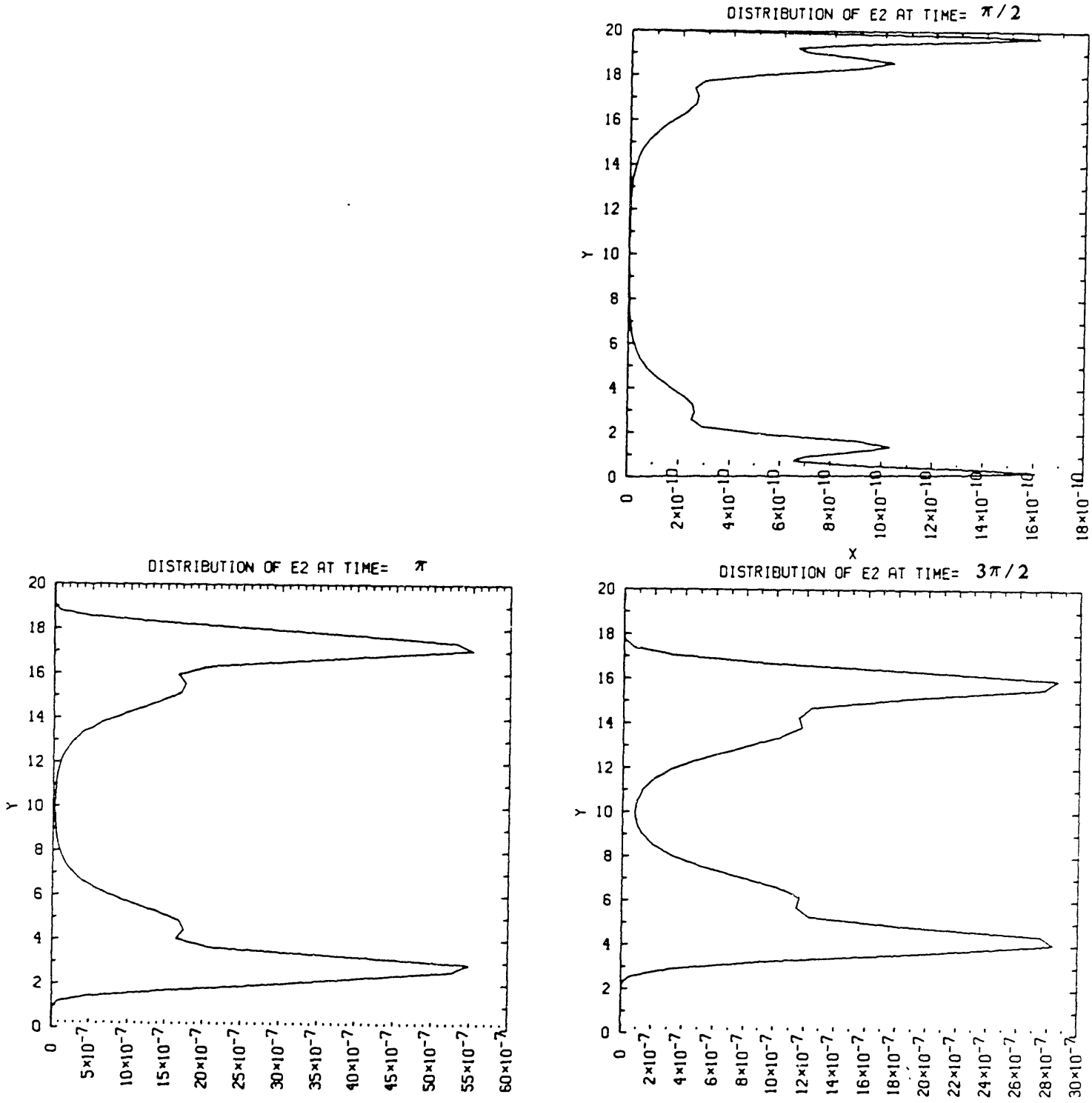

Figure 33d. For caption see Figure 33a.

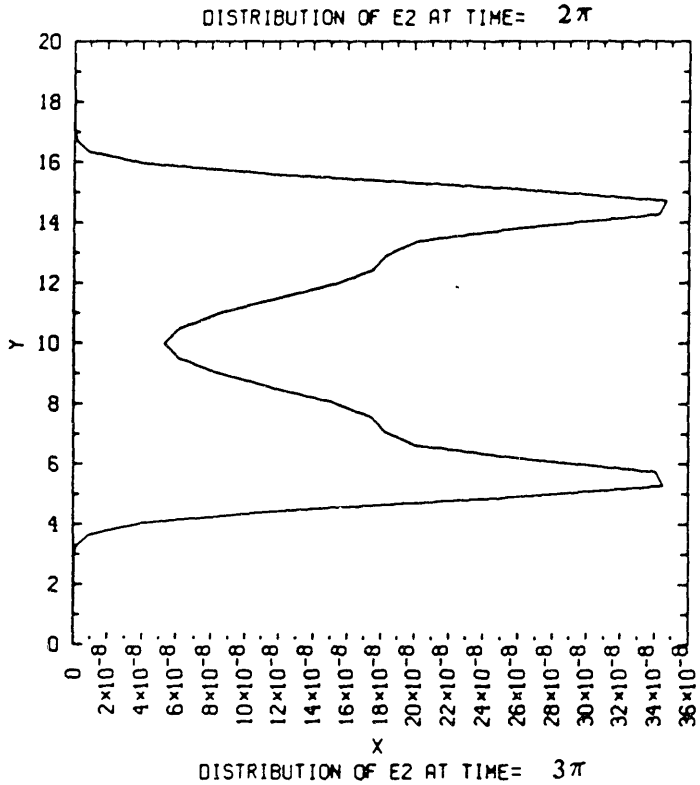

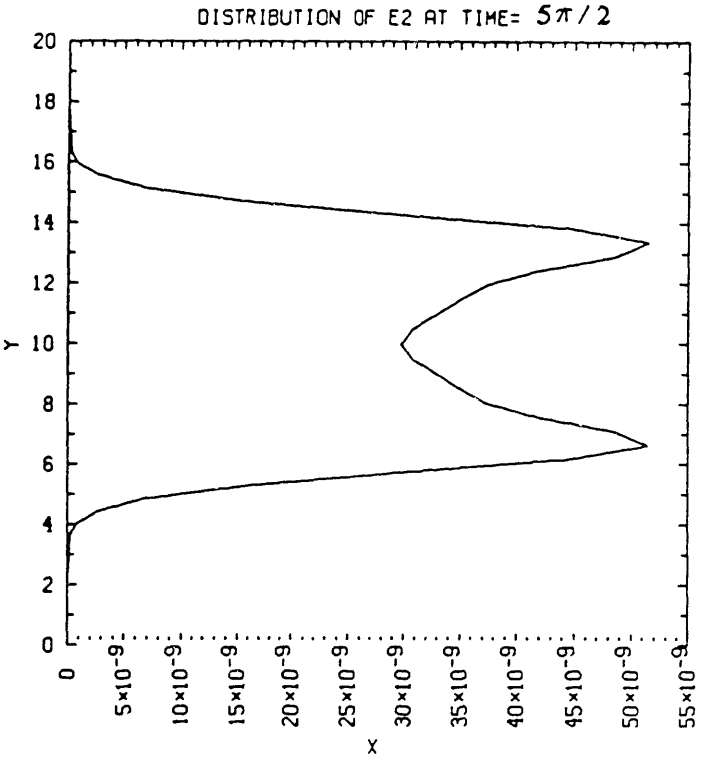

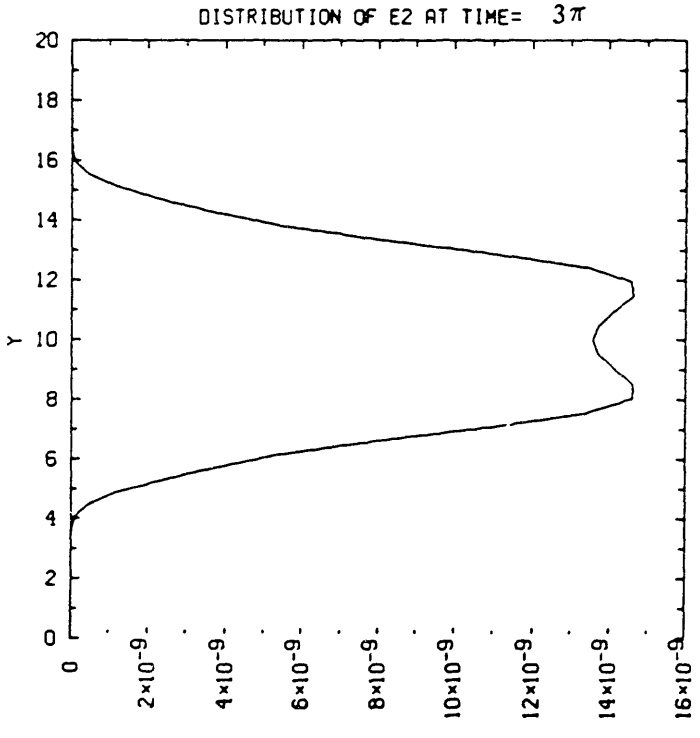

Figure 33d. For caption see Figure 33a.

proves that the final solution is independent of the form of the initial disturbance.

3.2.4 Results

In Figures 34 and 35 we show how a typical two-dimensional disturbance which starts off as the least stable eigenmode of the (time-independent) Orr-Sommerfeld equation for the initial "frozen" profile, evolves to a steady state solution which is that predicted by a Floquet analysis of the time-dependent Orr-Sommerfeld equation.

In addition to the overall energy of the disturbance (shown in Figure 34), we find it useful to consider the distribution of the disturbance energy across the channel width at various times (Figure 35). From Figure 35 it immediately becomes obvious why quasi-steady theories give results that are so different from those of the Floquet analysis of the Orr-Sommerfeld equation.

The initial disturbance field (at time $\pi/2$) is specified as the least stable eigenmode of the Orr-Scmmerfeld equation for the "frozen" initial profile. The plot of distribution of energy for this time has a major peak at the "critical layer", with two less prominent peaks at successive inflexion points. Between $\pi/2$ and π, the

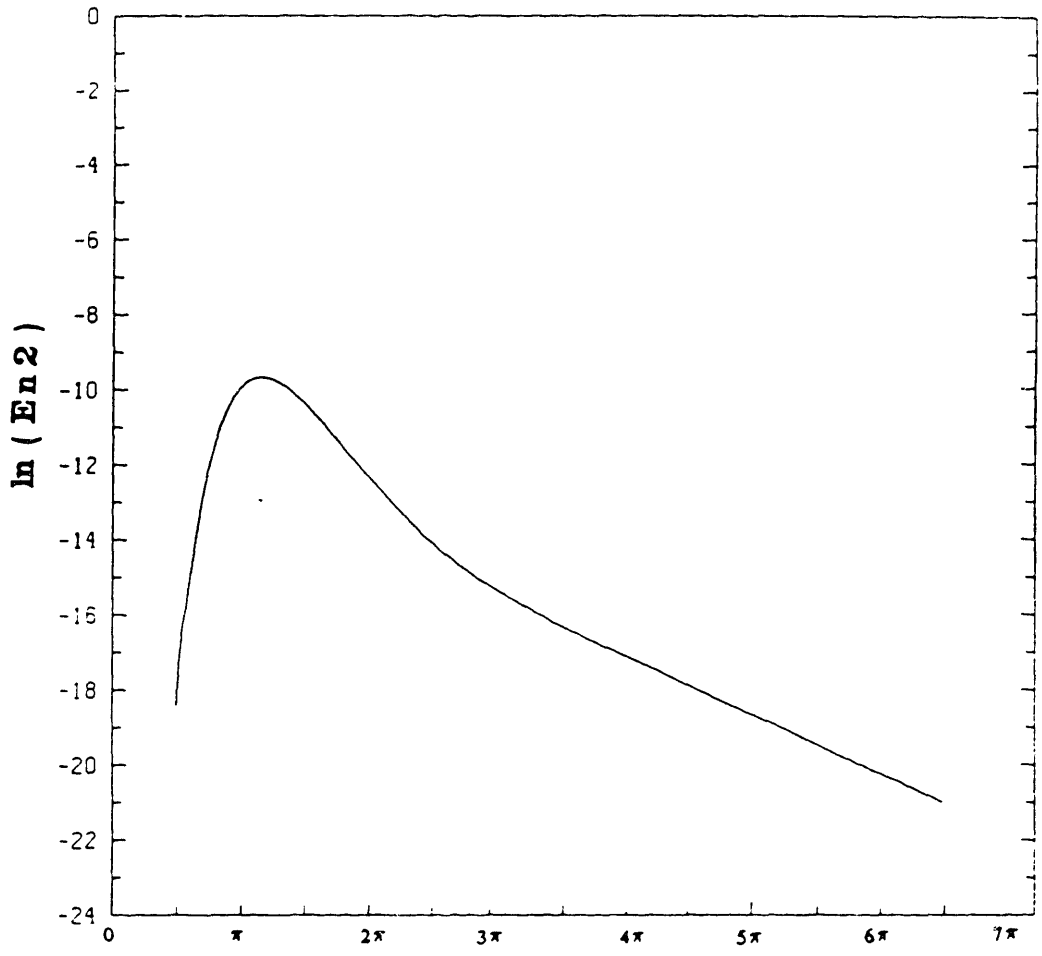

Figure 34. Evolution of the energy of two-dimensional disturbances at Re^{δ}=1000.0, α=0.5 . The initial conditions correspond to the least stable eigen modes of the Orr-Sommerfeld equation for the frozen initial profile.

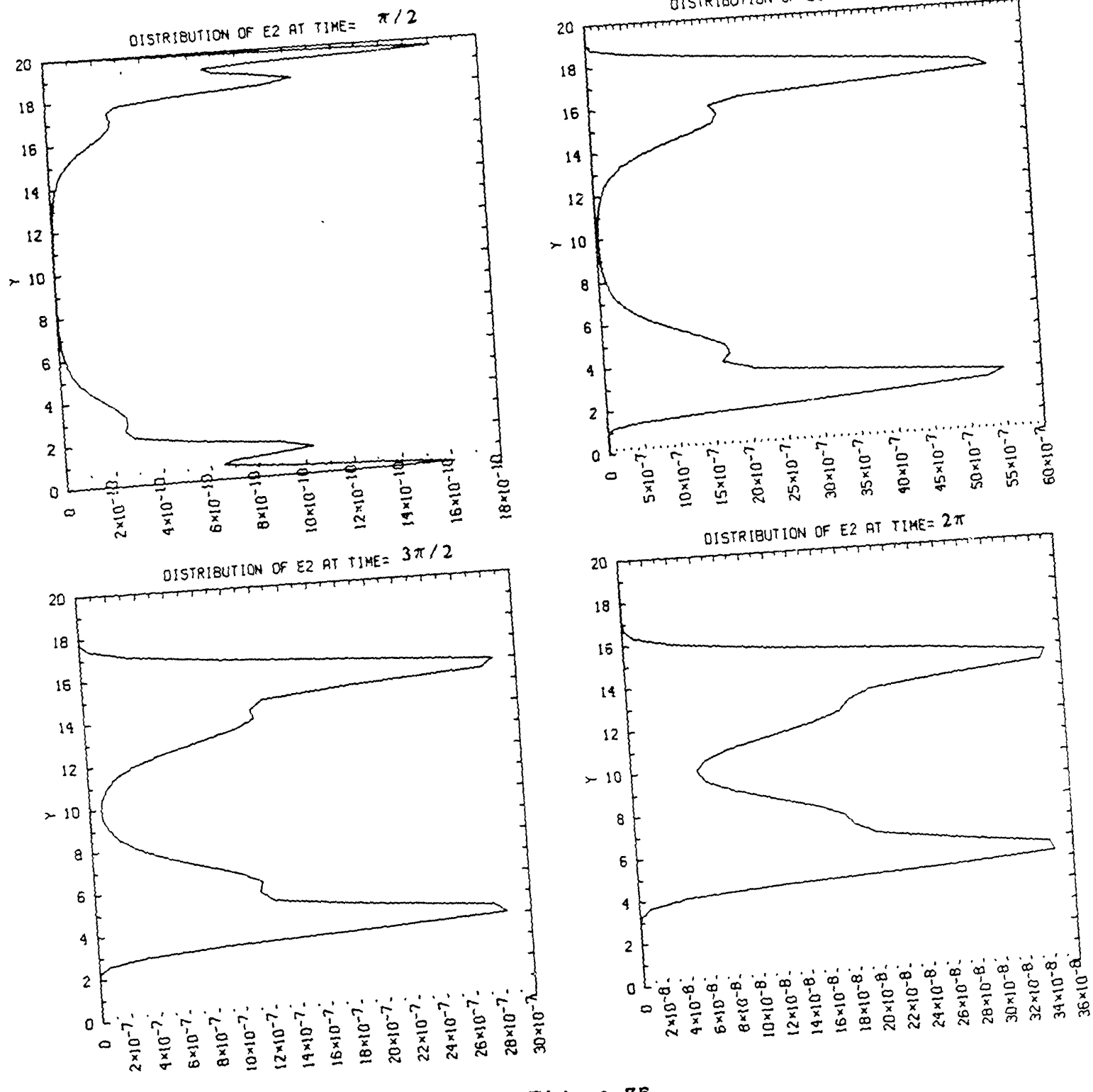
DISTRIBUTION OF E2 AT TIME= π/2
DISTRIBUTION OF E2 AT TIME= π
DISTRIBUTION OF E2 AT TIME= 3π/2
DISTRIBUTION OF E2 AT TIME= 2π
Y

Figure 35.

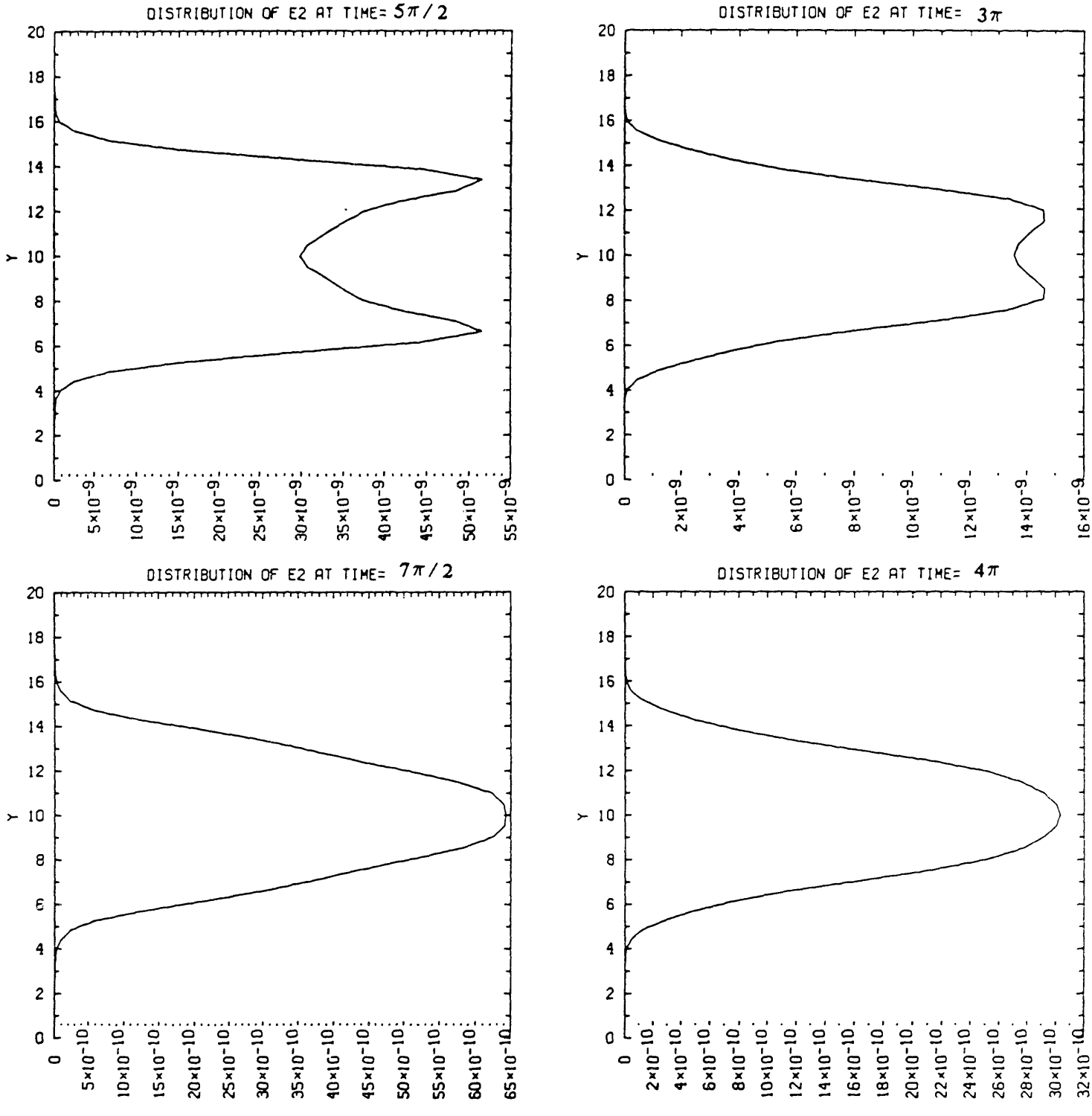
DISTRIBUTION OF E2 AT TIME= 5π/2
DISTRIBUTION OF E2 AT TIME= 3π
DISTRIBUTION OF E2 AT TIME= 7π/2
DISTRIBUTION OF E2 AT TIME= 4π
Y

Figure 35.

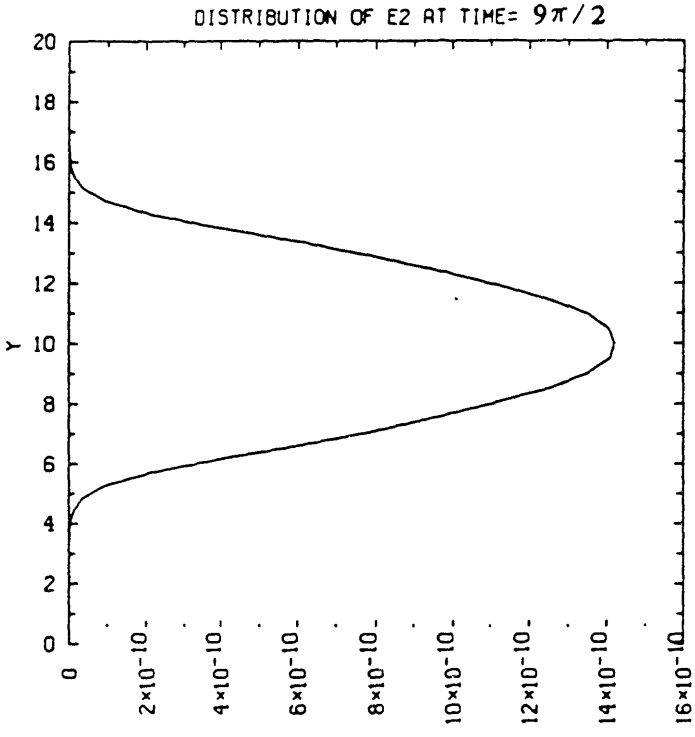
DISTRIBUTION OF E2 AT TIME= 9π/2
Y
0
2
4
6
8
10
12
14
16
18
20
2×10⁻¹⁰
4×10⁻¹⁰
6×10⁻¹⁰
8×10⁻¹⁰
10×10⁻¹⁰
12×10⁻¹⁰
14×10⁻¹⁰
16×10⁻¹⁰

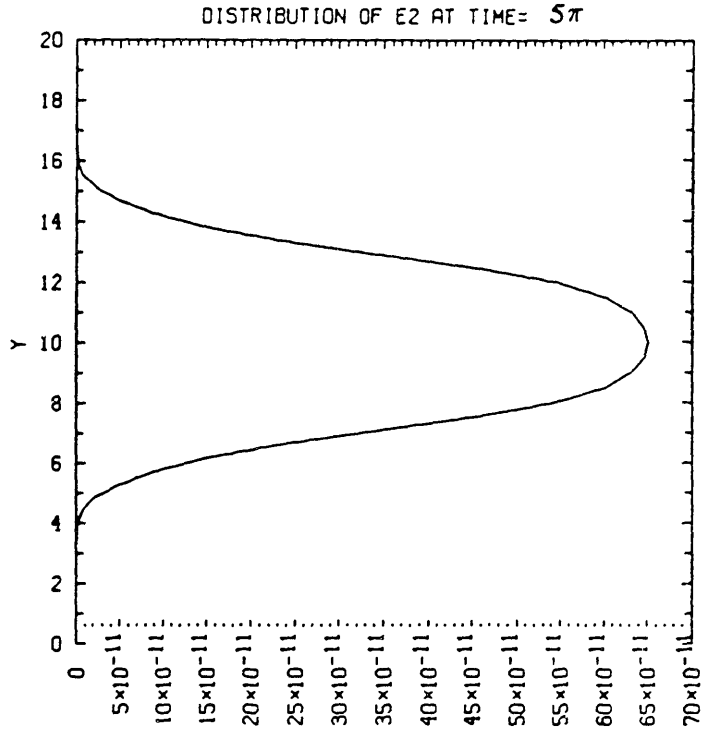
DISTRIBUTION OF E2 AT TIME= 5π
Y
0
2
4
6
8
10
12
14
16
18
20
5×10⁻¹¹
10×10⁻¹¹
15×10⁻¹¹
20×10⁻¹¹
25×10⁻¹¹
30×10⁻¹¹
35×10⁻¹¹
40×10⁻¹¹
45×10⁻¹¹
50×10⁻¹¹
55×10⁻¹¹
60×10⁻¹¹
65×10⁻¹¹
70×10⁻¹¹

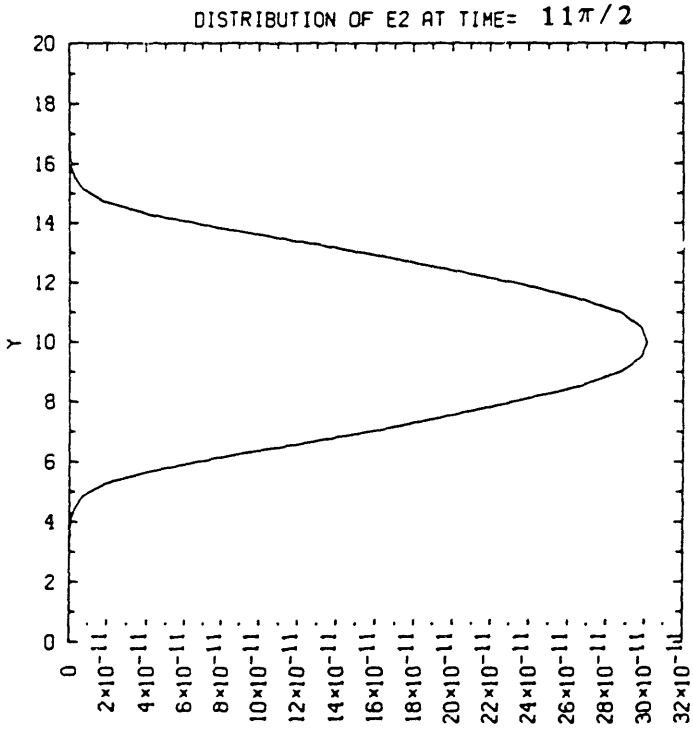
DISTRIBUTION OF E2 AT TIME= 11π/2
Y
0
2
4
6
8
10
12
14
16
18
20
2×10⁻¹¹
4×10⁻¹¹
6×10⁻¹¹
8×10⁻¹¹
10×10⁻¹¹
12×10⁻¹¹
14×10⁻¹¹
16×10⁻¹¹
18×10⁻¹¹
20×10⁻¹¹
22×10⁻¹¹
24×10⁻¹¹
26×10⁻¹¹
28×10⁻¹¹
30×10⁻¹¹
32×10⁻¹¹

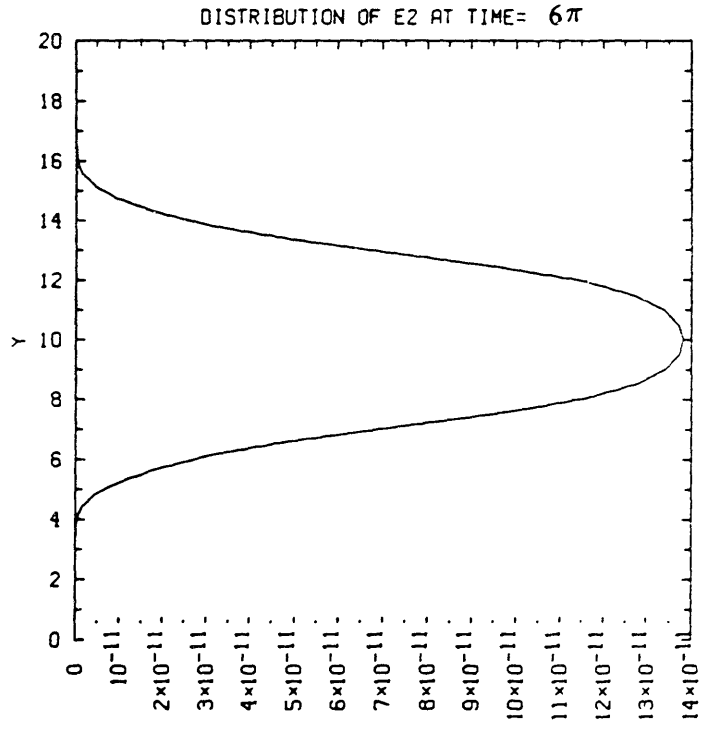
DISTRIBUTION OF E2 AT TIME= 6π
Y
0
2
4
6
8
10
12
14
16
18
20
10⁻¹¹
2×10⁻¹¹
3×10⁻¹¹
4×10⁻¹¹
5×10⁻¹¹
6×10⁻¹¹
7×10⁻¹¹
8×10⁻¹¹
9×10⁻¹¹
10×10⁻¹¹
11×10⁻¹¹
12×10⁻¹¹
13×10⁻¹¹
14×10⁻¹¹

Figure 35.

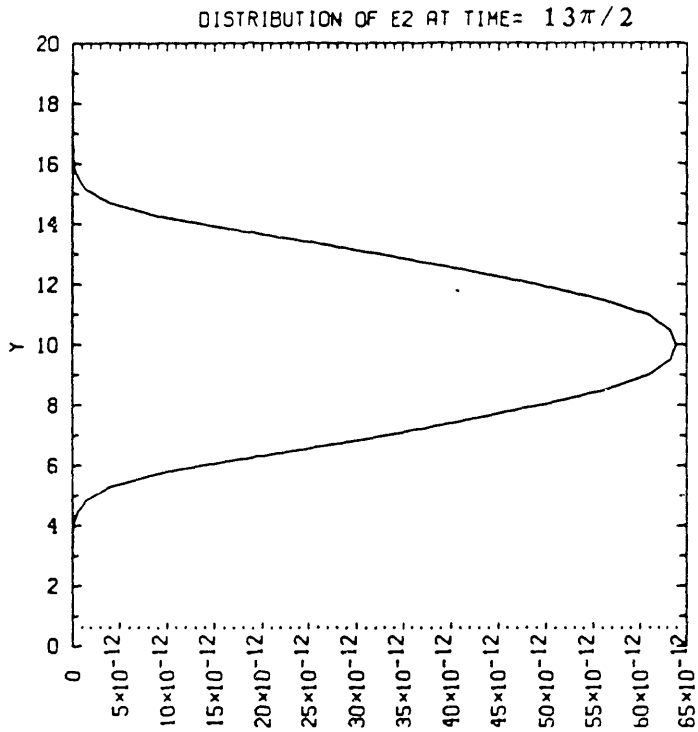

Figure 35. Evolution of two-dimensional disturbances at Re^{δ}=1000.0, α=0.5 .

disturbance evolves in ways not too different from what would be predicted by quasi-steady theories; with the growth rates of the same order of magnitude and distributions of disturbance energy across the channel similar to the "least" stable eigenmode of the Orr-Sommerfeld equation (see Figure 36 for a comparison). During this period, because of the intrinsic nature of the the basic velocity profiles, the disturbance has moved away from the wall and towards the center. In the next half period (for example at a time of $3\pi/2$), the disturbance is too far away from the wall to be able to excite the same modes that were excited earlier. Instead, it excites modes that are localized further away from the wall. This "mode-hopping" continues until the disturbance has travelled all the way to the center of the channel, at which point the flow settles into a steady-state. It is this steady-state behavior that a Floquet analysis of the time-dependent Orr-Sommerfeld equation would predict.

In the steady-state, the disturbances are synchronous with the basic flow,i.e; the disturbance at time $t+2\pi$ differs from that at time t only by an exponential factor (with no phase change). This means the Floquet exponents are real, in agreement with the results found by von Kerczek & Davis. This is to be expected, since it can be shown from the Orr-Sommerfeld equation that if λ is an eigenvalue, so is its complex conjugate,λ^*. Thus the solution should either

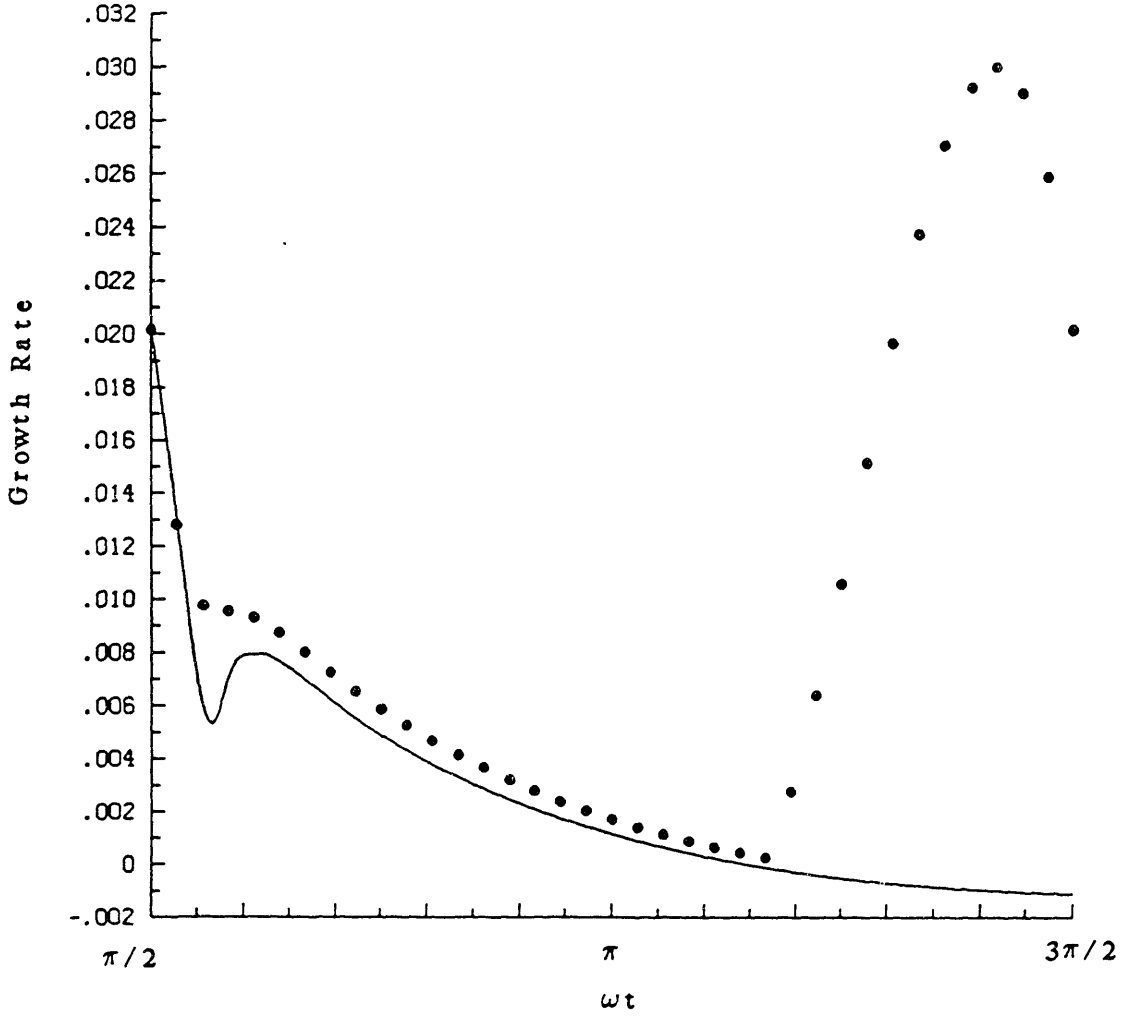

Figure 36. Comparison of the growth rates predicted by the time-dependent simulation (solid line), to the least stable eigenmode of the Orr-Sommerfeld equation (dots) for $\pi/2<t<3\pi/2$. (Two-dimensional disturbances α=0.5, Re^{δ}=1000)

$\omega t = 4\pi$

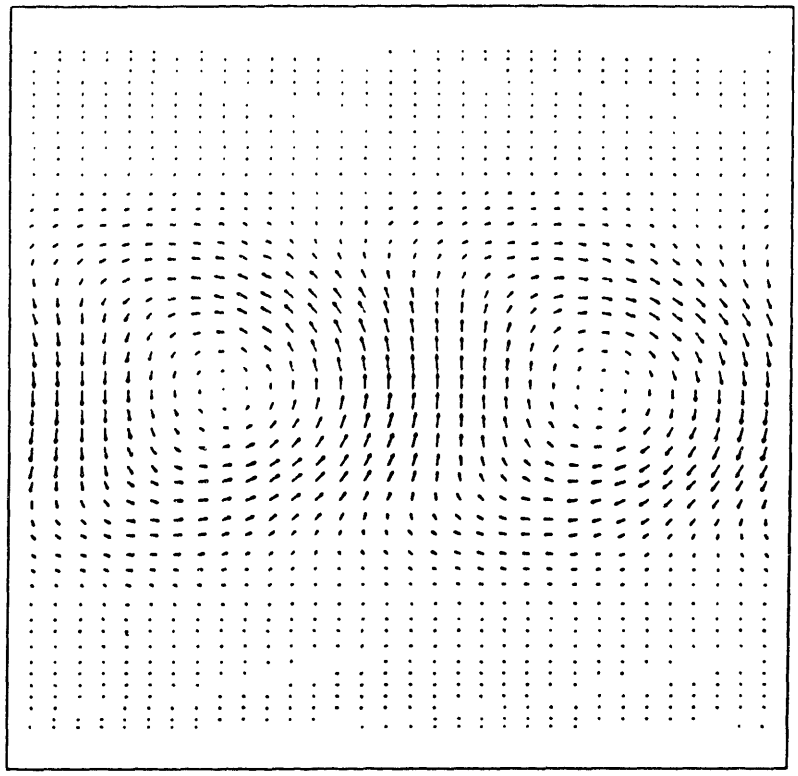

$\omega t = 9\pi / 2$

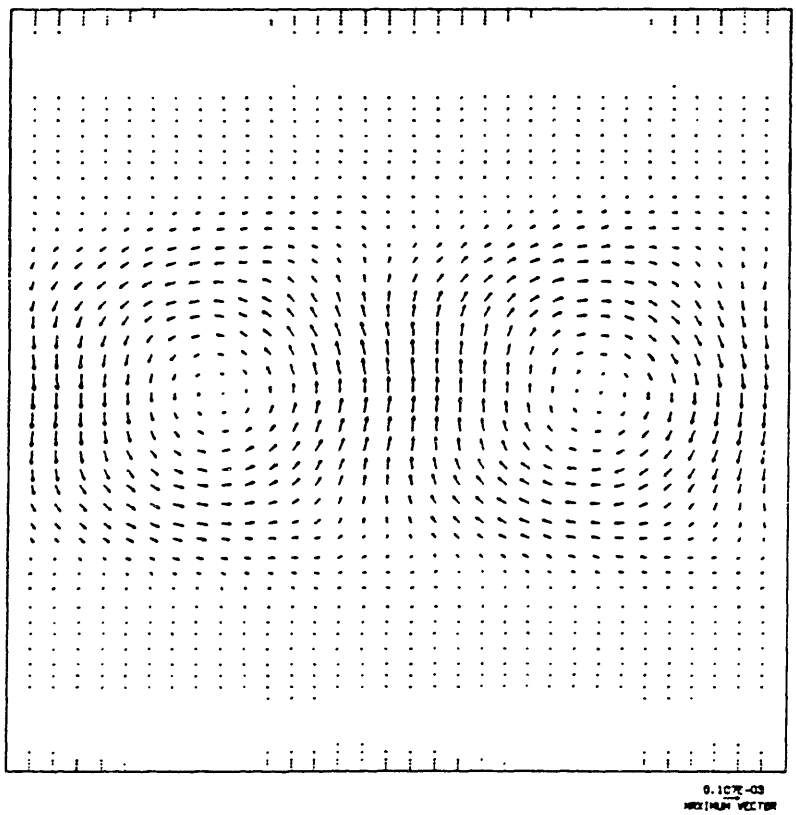

Figure 37.

$\omega t = 5\pi$

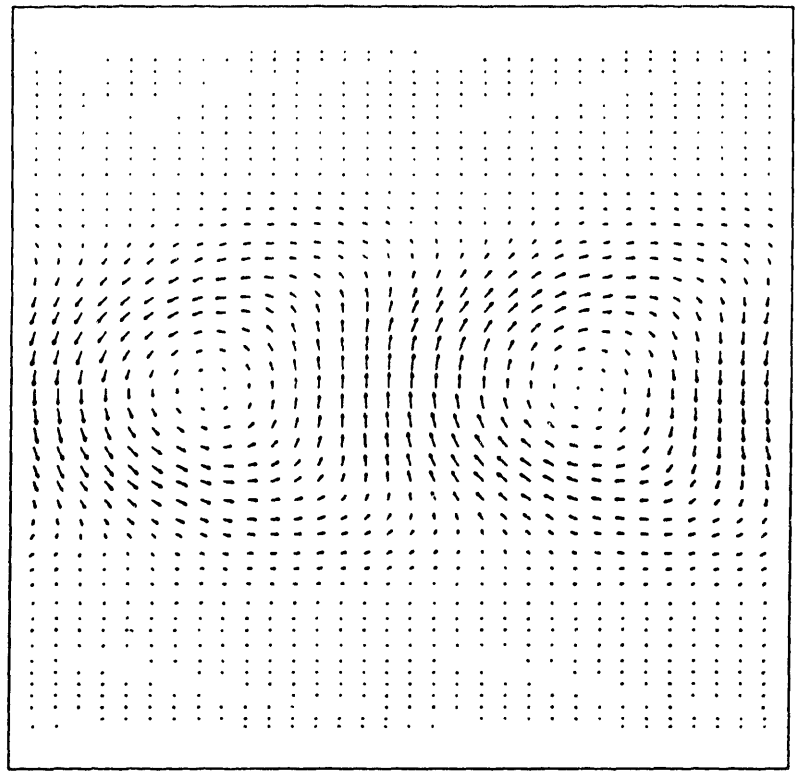

0.720E-04
MAXIMUM VECTOR

$\omega t = 11\pi/2$

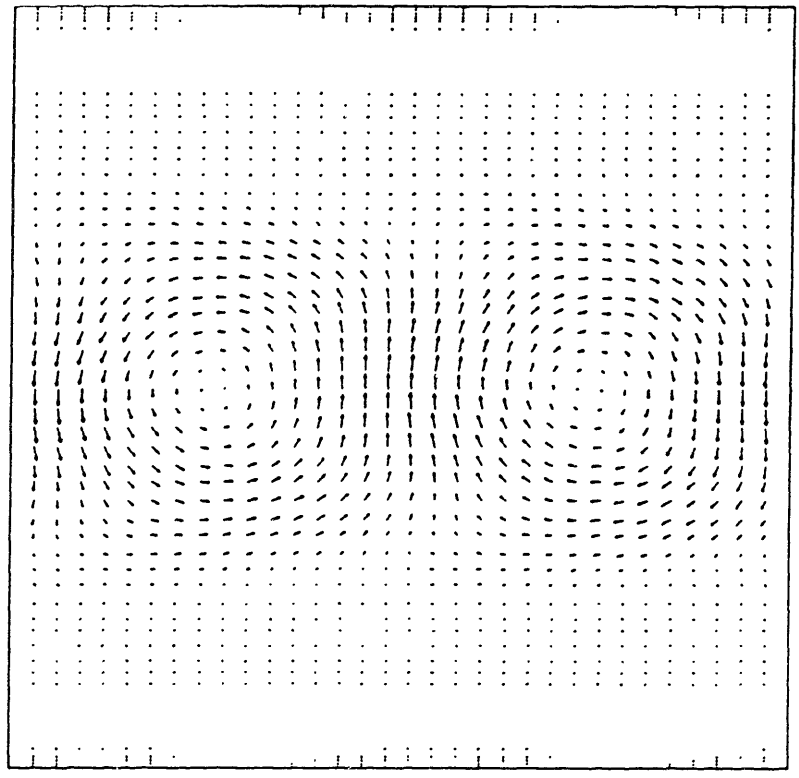

0.498E-04
MAXIMUM VECTOR

Figure 37.

$\omega t = 6\pi$

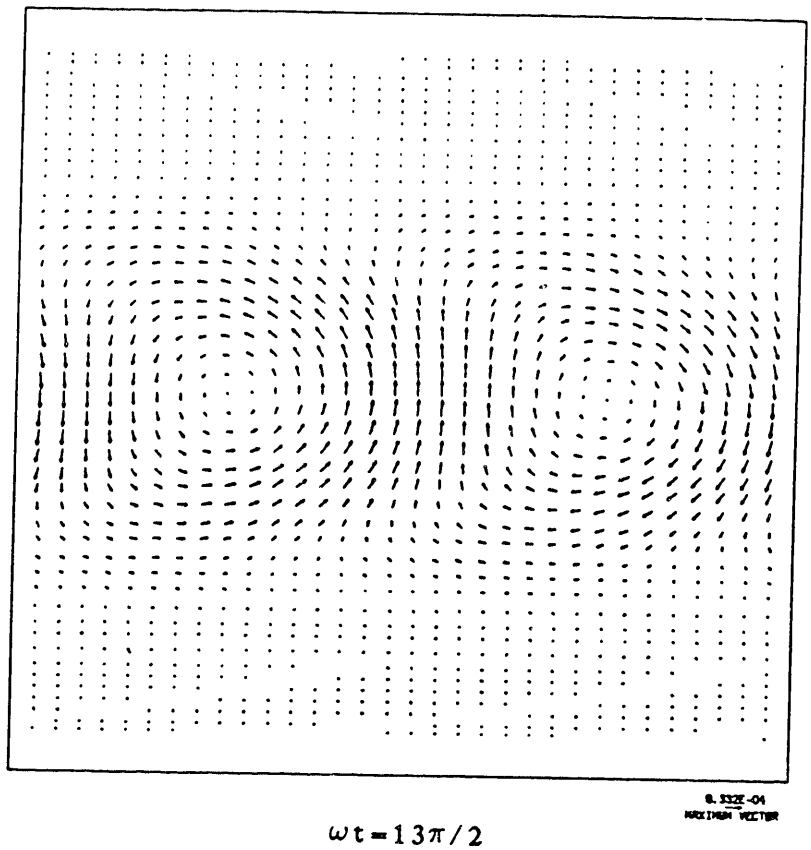

$\omega t = 13\pi/2$

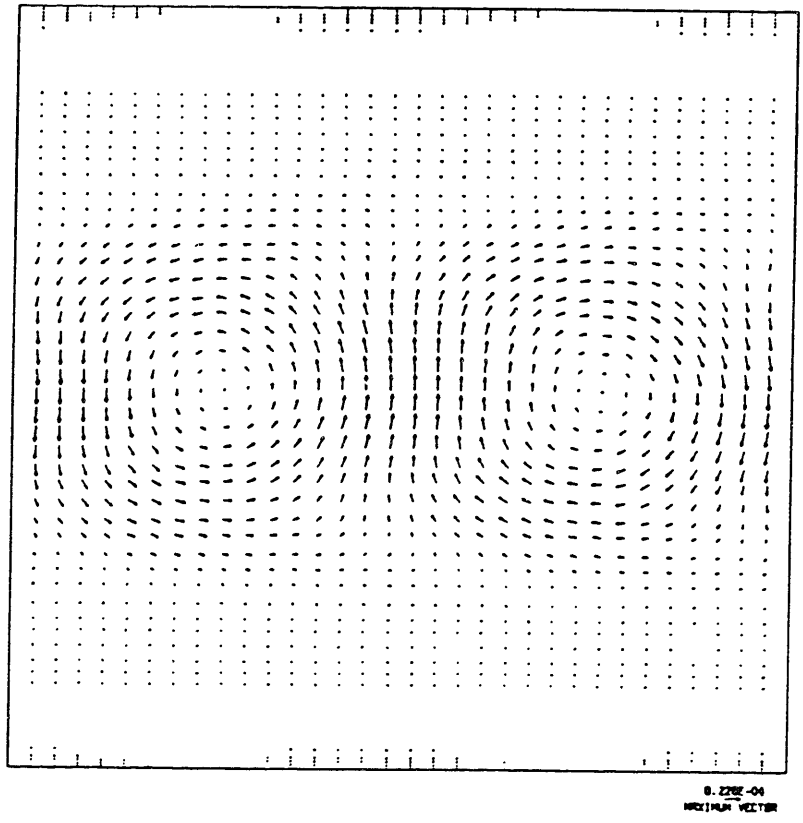

Figure 37. The disturbance field at Re^{δ}=1000.0, α=0.5 as seen in a frame of reference moving with the centerline velocity.

consist of pairs of simultaneous disturbance waves $\psi e^{\lambda t+i\alpha x}$ and $\psi^* e^{\lambda t+i\alpha x}$ which propagate in opposite directions, or else it should be of the form of a standing wave $\psi(z,t)e^{\lambda t+i\alpha x}$, where λ is real. Furthermore, the numerical simulations show that in the steady state, the phase speed of the disturbance is the same as the instantaneous axial velocity in the core. In other words the disturbances merely get convected back and forth with the mean flow. This point is shown in Figure 37, where the disturbance field in a frame of reference moving with the centerline velocity is shown.

The results for various other combinations of Reynolds number and streamwise wavenumber are shown in Figures 38 and 39. In each case the evolution of the disturbance is very similar to the case discussed above; the disturbance starts off in the boundary layer and reaches a steady-state solution with eigenmodes near the center of the channel. The resulting Floquet exponents are plotted in Figure 40. The general trends in the behavior of λ as a function of Re^{δ} and α, are identical to those obtained by von Kerczek and Davis, but the absolute magnitudes of λ are smaller. This is to be expected, since as we have seen, the disturbances are not localized within the boundary layers but migrate away until they settle into a steady-state that is compatible with the boundary conditions. For a channel flow, this steady-state consists of eigenmodes that are clustered about the center

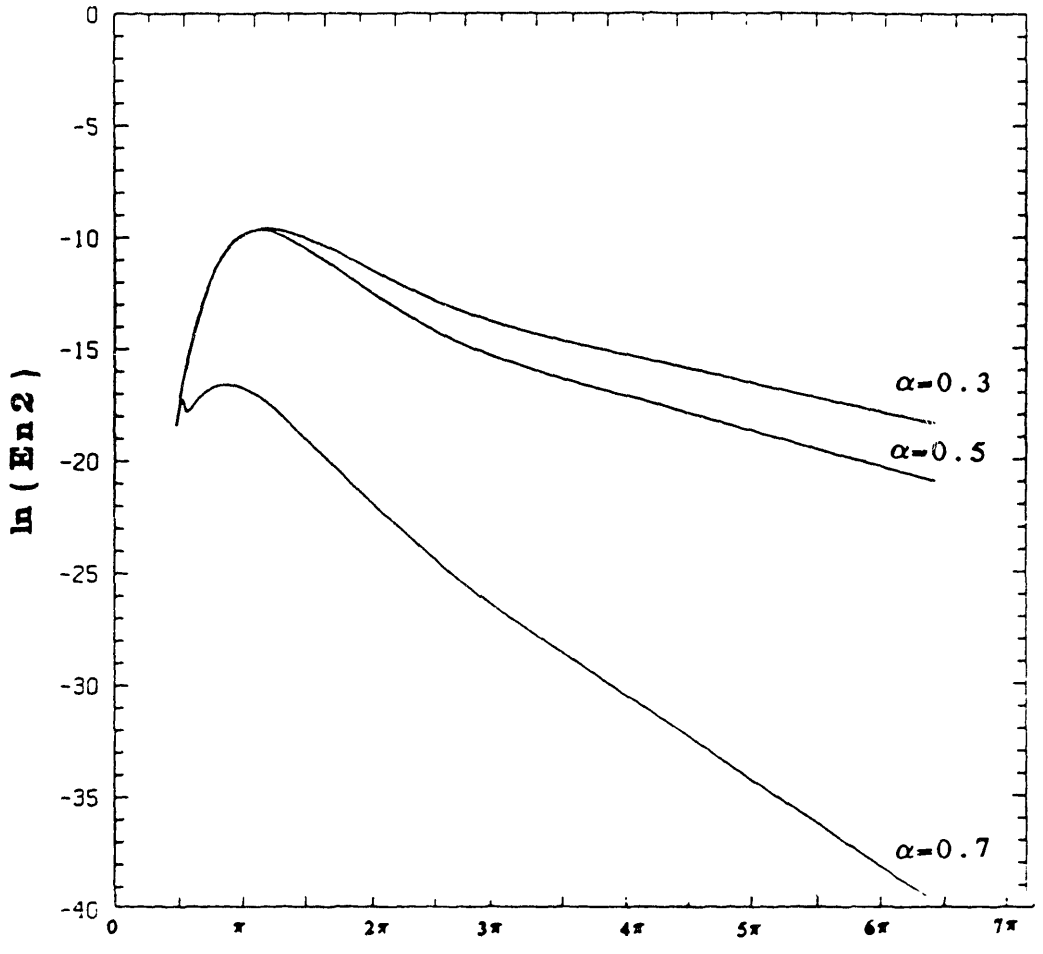

Figure 38. Evolution of two-dimensional disturbances with streamwise wavenumber α=0.3, 0.5, 0.7 at Re^{δ}=1000.0 .

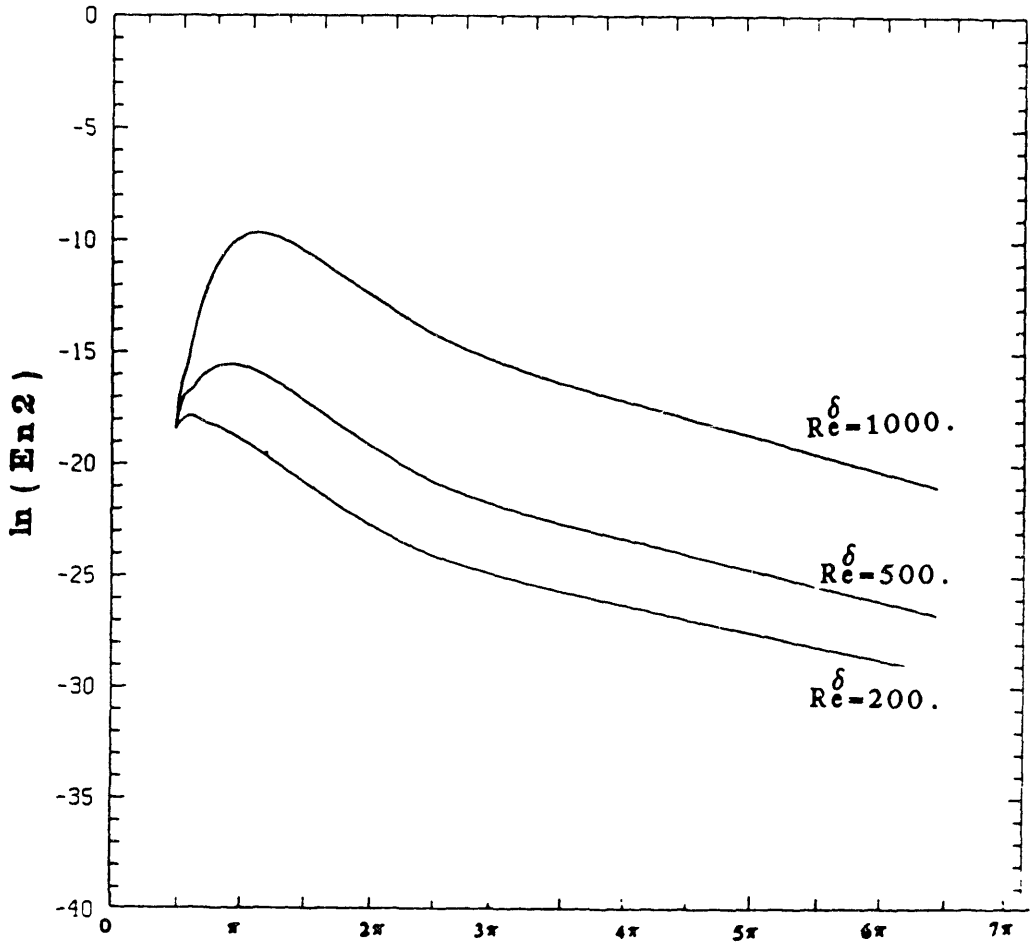

Figure 39. Evolution of two-dimensional disturbances with α=0.5 at Re^{δ} = 200.0, 500.0, 1000.0 .

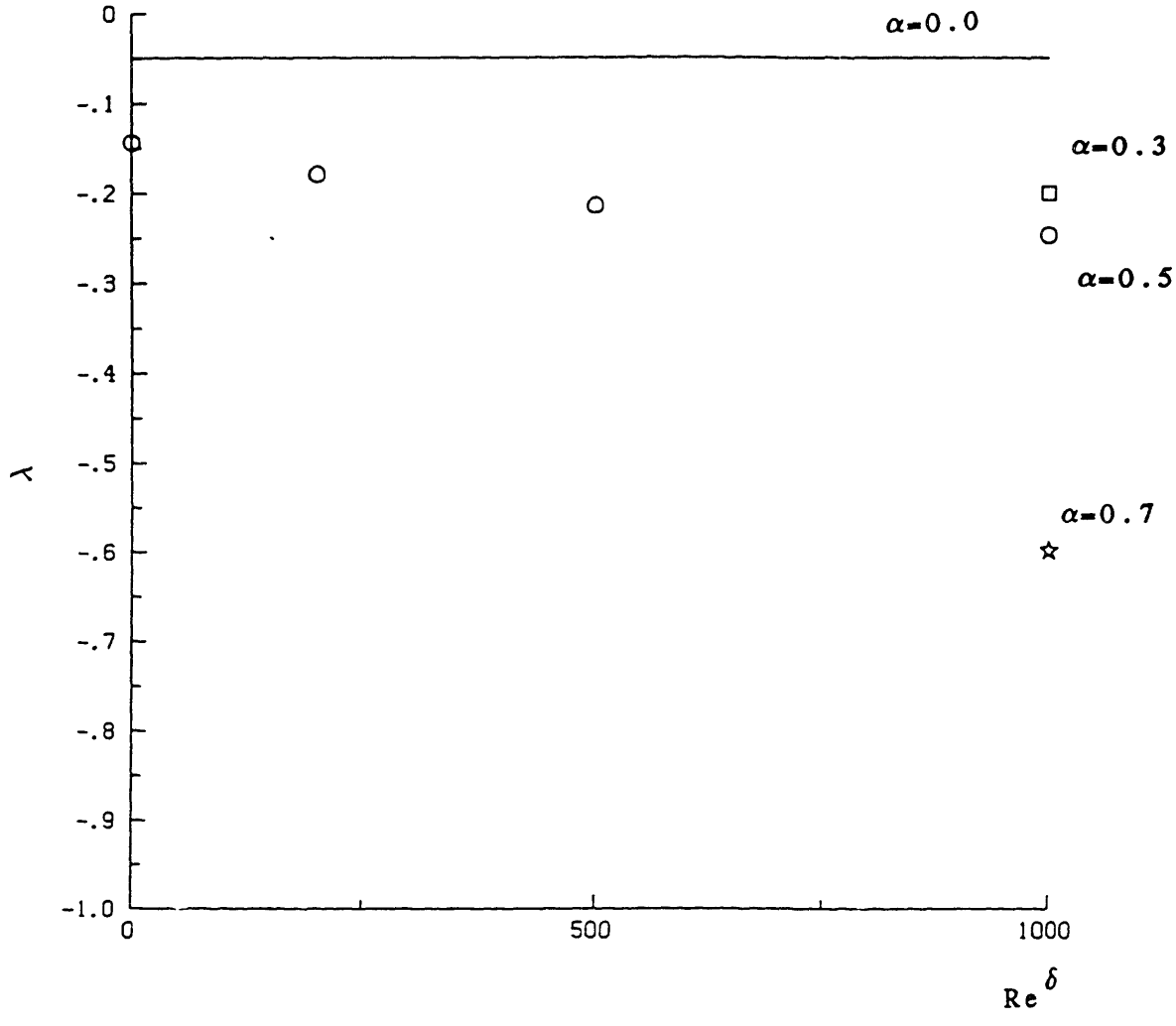

Figure 40. The principal Floquet exponent as function of Re^{δ} and α .

of the channel. For an infinite Stokes layer, the disturbances migrate away from the boundary layer and "merge" with the continuous spectrum of the infinite Stokes layer, as was shown by Hall [1978]. Von Kerczek and Davis, on the other hand, consider a bounded Stokes layer, which consists of an oscillating plate with another stationary plate a few boundary layer thicknesses away. The requirement that the disturbances go to zero on this second stationary plate, results in a problem that is distinct from either the infinite Stokes layer or the channel.

Nevertheless, our results agree with those obtained by other investigators for other examples of oscillatory Stokes layers, in that the flow is found to be stable (in the steady-state) to infinitesimal disturbances,. Not only are the principal Floquet exponents negative in all cases studied, but for a given streamwise wavenumber, the oscillatory channel flow is more stable than the motionless ($Re^{\delta}=0$) state; with the Floquet exponent a monotonic decreasing function of Re^{δ}.

Finally, one should not overlook another phenomenon revealed by the results of the direct numerical simulation; namely, that if a disturbance is present in the boundary layers near the wall, it can substantially amplify during the acceleration portion of the cycle. In an experimental setting, this result is probably more relevant than those of the Floquet analysis, since a certain level of noise is

always present throughout the flow field. In this situation, and provided the disturbances are small, they would amplify during the acceleration phase of the cycle and be damped during the deceleration phase. Indeed, Hino et al.[1978] in reporting that two classes of transitional flows are observed experimentally, describe one as consisting of "weak" disturbances that appear during the acceleration portion of the cycle.

As a result of this process,very small disturbances might be amplified to such an extent that linear theory fails. In that case, and for those disturbances that are not sufficiently small to be treated by a linearized theory, one must study the stability of the flow to finite-amplitude disturbances. This case is considered next.

3.3 Finite Amplitude Disturbances

When the perturbation is infinitesimal a linear theory results. Such a theory is very attractive in that the resulting instability is independent of the form or initial amplitude of the disturbance. However, as we have seen, linear theory cannot explain the transition phenomenon that is observed in experiments. We therefore, need to consider more general (finite-amplitude) disturbances.

We start by a consideration of two-dimensional disturbances of finite amplitude. Even though a two-dimensional theory cannot explain all the details of transition (in particular its three-dimensionality), understanding the two-dimensional behavior is important because it has been shown [Herbert and Morkovin(1980) , Orszag and Patera(1983)] that the transition process for a large class of "steady" shear flows can be explained as the instability of the intermediate state consisting of the basic laminar profile plus two-dimensional finite amplitude equilibria (or quasi-equilibria) to secondary three-dimensional disturbances.

3.3.1 Two-Dimensional Disturbances

The nonlinear theory for Stokes flow instability has not yet been developed. One problem is the lack of a critical Reynolds number according to linear theory. Nevertheless, subcritical finite-amplitude equilibria (travelling waves with constant energy) may be possible, if the nonlinear terms in the Navier-Stokes equations are destabilizing for disturbances with energies above some threshold value.

There are two routes to determining two-dimensional finite amplitude equilibria. In the first approach, the equilibrium solutions are directly obtained by eigenvalue techniques. In the second approach, evolution of specific disturbances are followed by direct numerical simulation of the Navier-Stokes equations. The eigenvalue approach is more efficient and would directly locate the equilibrium solutions within the (E,R,α) space (although it does not give the time scales of evolution to the equilibrium state). However, it requires some assumption about the specific form of the equilibrium solution. In steady flows, for example, the equilibrium solutions are of the form of a travelling wave with constant phase speed, and can be represented by

the stream function, $\psi = \sum_{n=-\infty}^{\infty} \psi_n(z)\, e^{i\alpha n(x-ct)}$. These solutions are steady in a Galilean frame moving with the (real) wavespeed c and are periodic in x. Truncation of the fourier series representing ψ would result in a set of N+1 coupled nonlinear (but time-independent) ordinary differential equations for ψ_n which can be solved to give the equilibrium solutions [Herbert(1977)].

For the Stokes problem, the basic flow is time periodic. One might therefore anticipate equilibrium solutions to be of the general form,

$$\psi = \sum_{n=-\infty}^{\infty} \psi_n(z,\tau)\, e^{i\alpha n(x-c\tau)}$$

where c is real (and possibly zero) and τ is the physical time normalized to the basic period of oscillation of the mean flow. In other words, the equilibrium solutions (if they exist) are expected to be time periodic with the same period of oscillation as the basic flow.

The above formulation would result in a nonlinear eigenvalue problem for the time periodic functions ψ_n, which can be solved in the (E,R,α) space to locate any possible equilibria.

In the present work, we adopt the second approach and follow the evolution of specific two-dimensional disturbances by direct numerical simulations of the Navier-Stokes equations. Because of the relatively large amount of

computation time involved in each simulation, we limit our search to three wavenumbers (α=0.3, 0.5 and 0.7) all at a single Reynolds number of 1000. In each case the evolution of the least stable eigenmode of the (time-independent) Orr-Sommerfeld equation for the initial (frozen) profile is followed by direct numerical simulation. The initial disturbance is normalized to have a total energy of 0.04. The simulations were obtained with a resolution P=128, 2N=32.

The results of the simulation for the case α=0.5 are shown in Figures 41 through 44. The most important question is whether the disturbances evolve to an equilibrium state, or do they decay; and if so what are the time scales of decay.

Figure 41 is a plot of the overall energy of the disturbance field as a function of time. After an initial transient period, the disturbances are seen to settle into a state of slow decay, suggesting that the initial finite-amplitude disturbance would eventually die away. The decay rates, however, are O(1) (actually, λ=-.38) on a time scale which represents the oscillation period of the basic flow. Recalling that Stokes flows result from an inherent balance between the viscous terms and temporal acceleration (and as such the period of oscillation is the same as the viscous time scale; $\delta^2/\nu \sim 1/\omega$), the decay of the two-dimensional

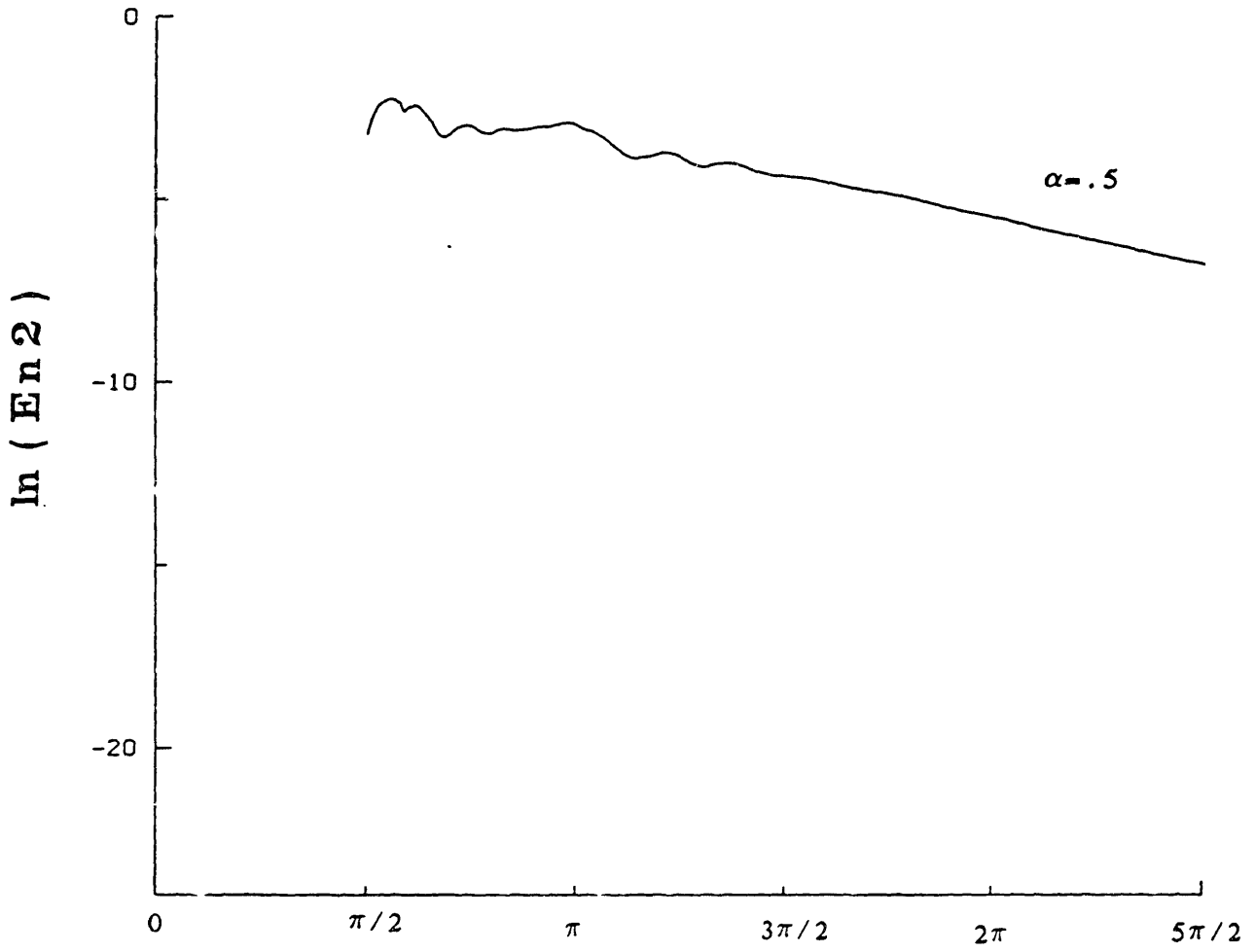

Figure 41. Evolution of two-dimensional finite-amplitude disturbances for α=0.5, Re^{δ}=1000.0 .

finite amplitude state is seen to be viscous. Transition phenomena, on the other hand, happen on convective time scales; therefore, if the mechanism that triggers transition were to involve the above two-dimensional finite amplitude state, the viscous decay of the two-dimensional disturbance field would be of little importance during the transition process. This point will be discussed further in later sections.

The development of the disturbance field from its initial "prescribed" form as the least stable eigenmode of the Orr-Sommerfeld equation, to the final quasi-equilibrium state can be seen in more detail in Figure 42 where the distribution of the energy of the disturbance across the channel is plotted at various times. The initial disturbance field is localized near the walls with a major energy peak at the (linear) critical layer and two less prominent peaks at neighboring inflection points. Within a very short period (with convective time scales) though, the disturbances migrate to the center of the channel and settle into a quasi-equilibrium state where they basically get convected back and forth with the mean flow, maintaining their energy to O(1/R).

Both the disturbance field and the magnitude of the attenuation rate λ, are not too different from the Floquet theory results of the linear theory. Nonlinear effects tend

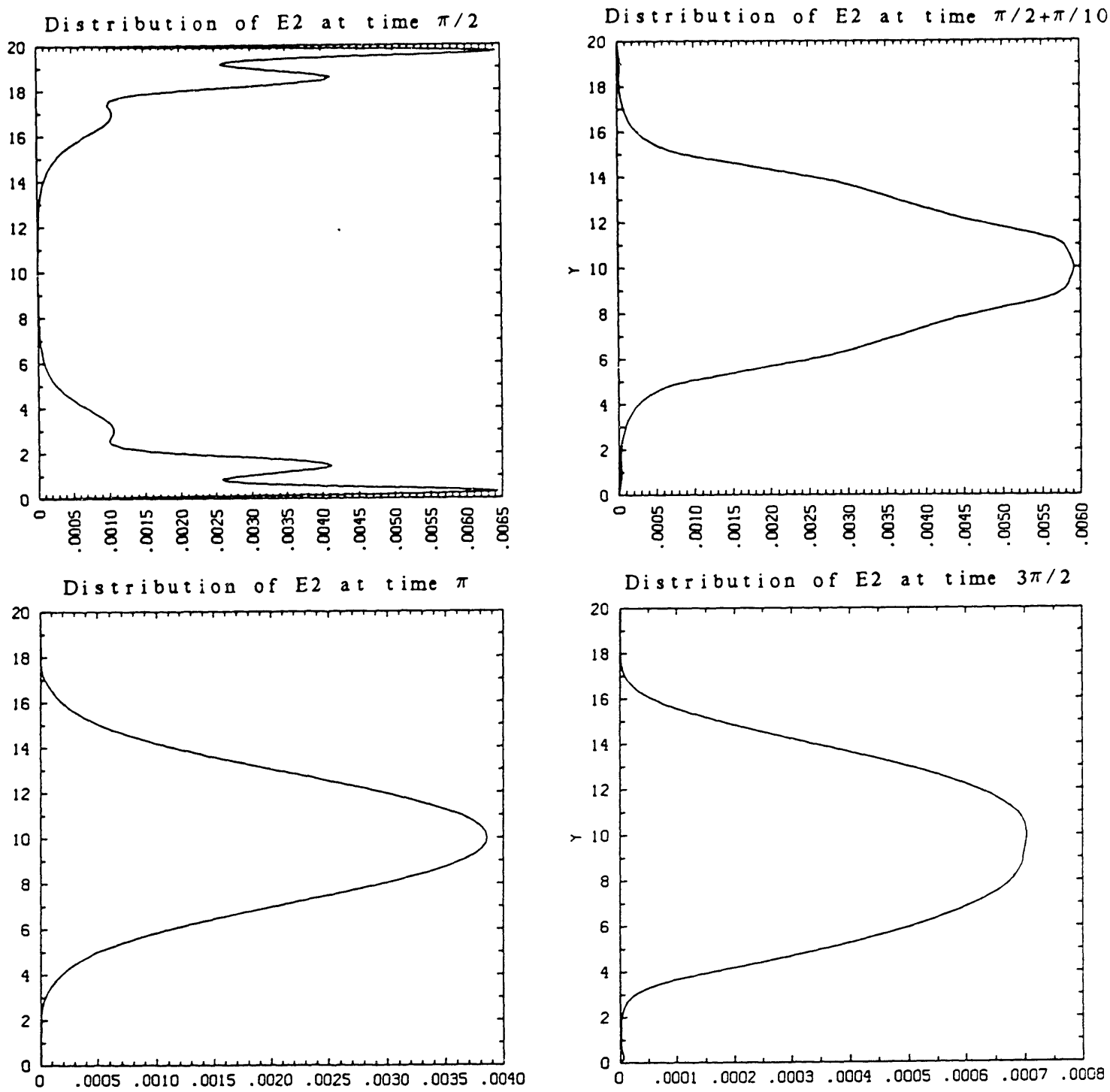
Distribution of E2 at time π/2
Distribution of E2 at time π/2+π/10
Distribution of E2 at time π
Distribution of E2 at time 3π/2
Y

figure 42.

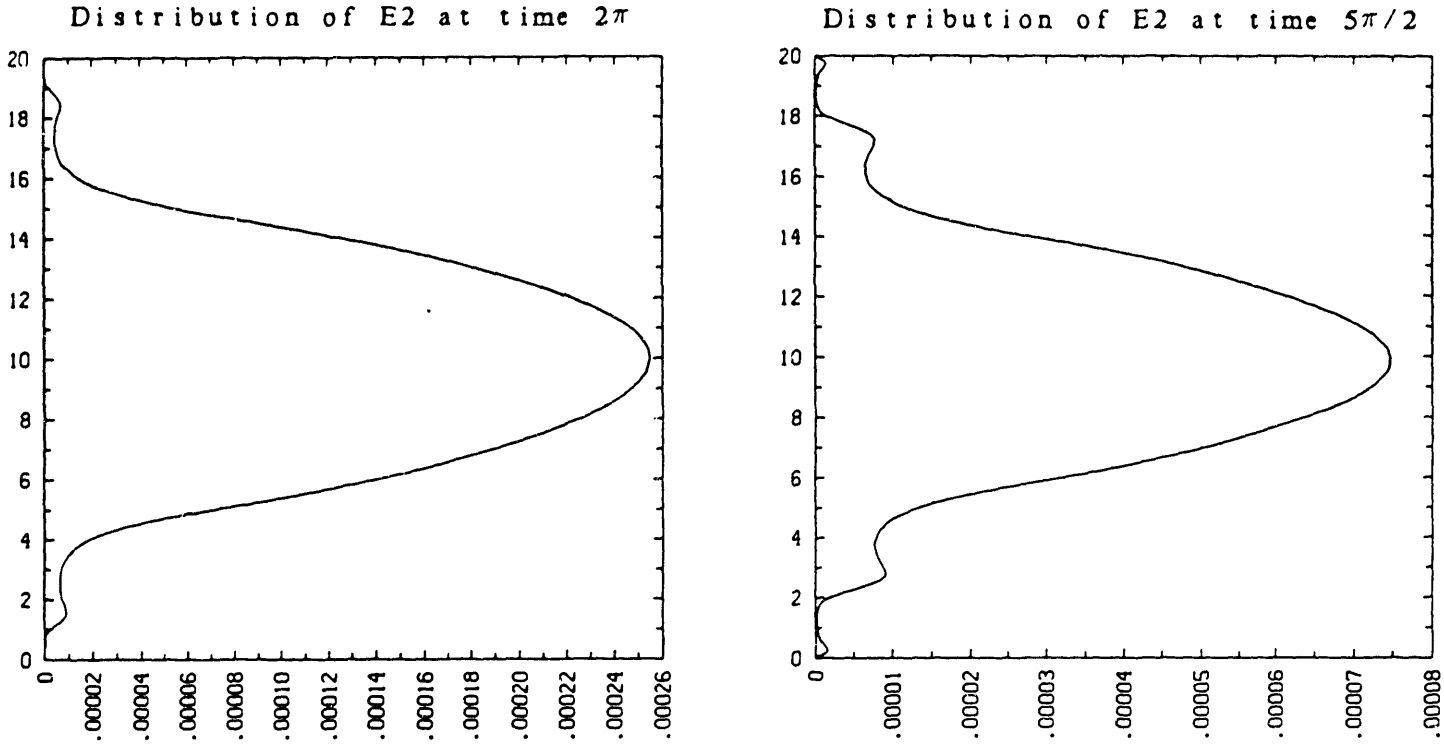

Figure 42. Evolution of two-dimensioanl finite-amplitude disturbances for α=0.5, Re^{δ}=1000.0 . The initial disturbance is the least stable eigenmode of the Orr-Sommerfeld equation for the frozen initial profile.

to spread out the perturbation over a wider section of the cross-section, and to result in slightly larger values for λ (λ=-.38 for the finite amplitude disturbance as compared to λ=-.25 for the linear case).

The effect of the nonlinear terms on the mean velocity profiles is shown in Figure 43. The biggest correction appears near the center of the channel and away from the boundary layers, as this is where the disturbances are localized.

Finally, the contribution of various streamwise Fourier modes to the overall energy of the disturbance field is shown in Figure 44. Even though 16 fourier modes (2N=32) were used in the simulation, only the first five are shown in Figure 44, as higher modes have very small amplitudes. At the time $\omega t=5\pi/2$, for example, the various modes have the following energy contents:

n	1	2	3	4
E_n	0.112E-02	0.102E-05	0.630E-7	0.858E-08

n	5	10	15
E_n	0.171E-08	0.621E-12	0.707E-16

It should be noted however, that even though the higher fourier modes become unimportant at large times, an insufficient number of streamwise fourier components would affect the initial transient behavior of the disturbances; mainly because small round off errors introduced in the boundary layers could result in new instabilities because of

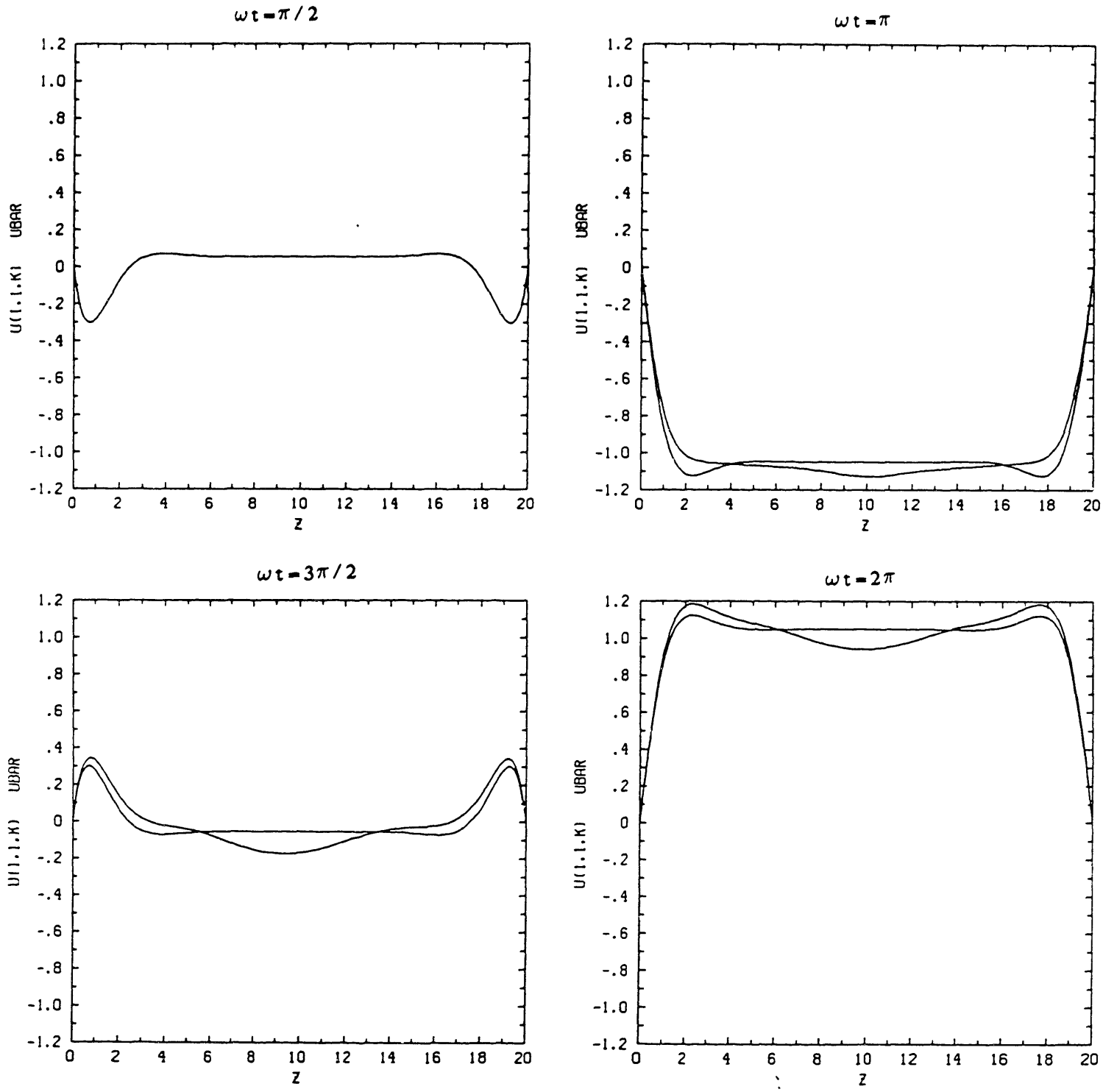
ωt=π/2
ωt=π
ωt=3π/2
ωt=2π
U(1,1,K) UBAR
Z
1.2
1.0
.8
.6
.4
.2
0
-.2
-.4
-.6
-.8
-1.0
-1.2
0 2 4 6 8 10 12 14 16 18 20

Figure 43.

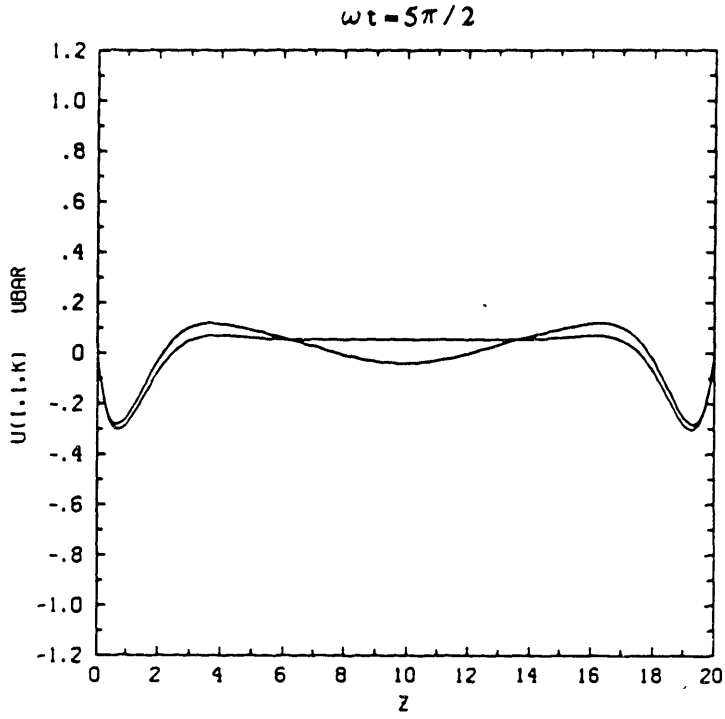

Figure 43. Average velocity profiles in the presence of two-dimensional finitite-amplitude disturbances (α=0.5, Re^{δ}=1000.0) compared to the laminar profiles.

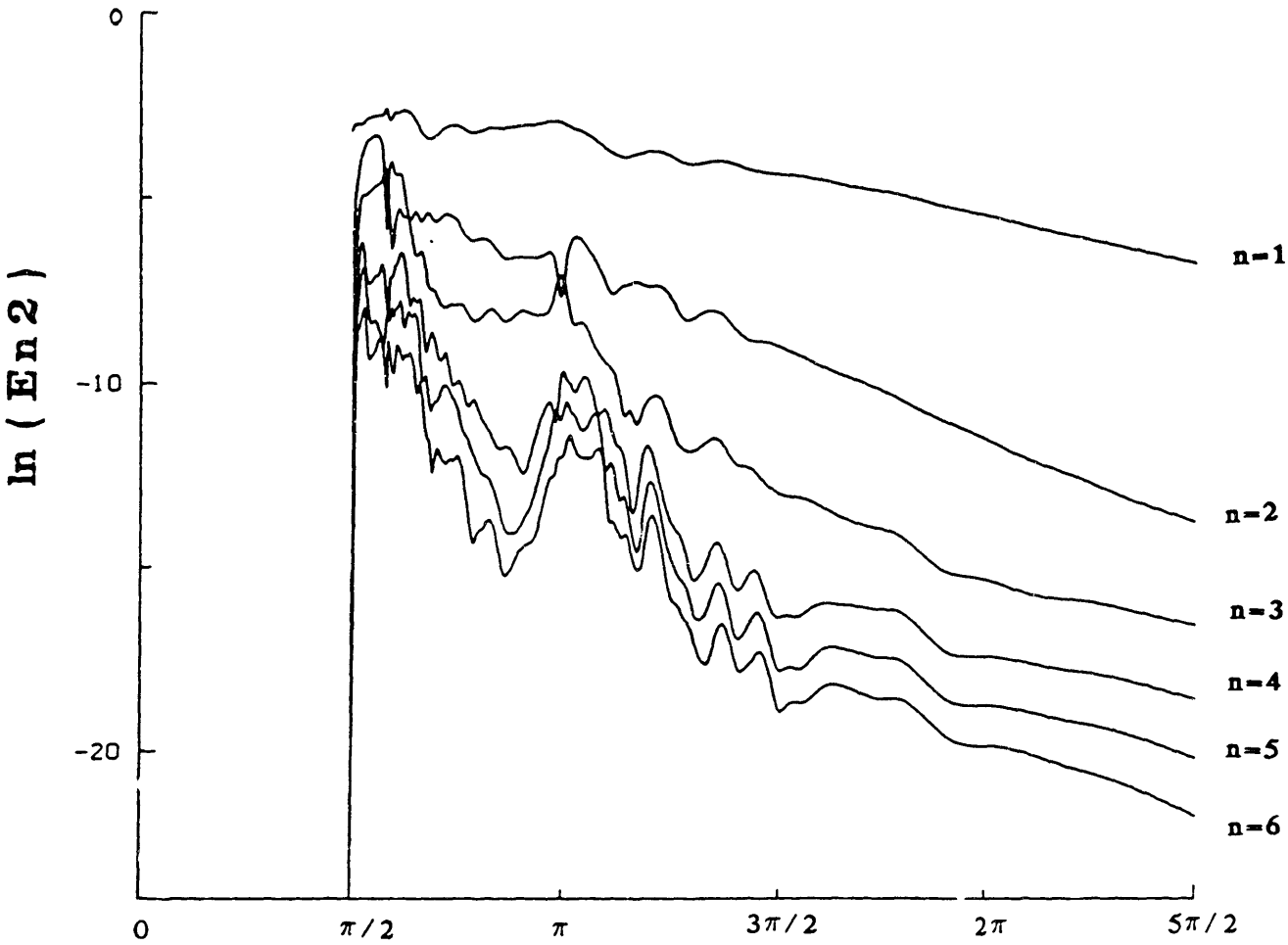

Figure 44. Development of higher order modes for an initial finite-amplitude disturbance with α=0.5, Re^{δ}=1000.0

the highly unstable nature of the boundary layers. For the above simulation convergence has been verified by repeating the simulation with 2N=16, P=65, which gave nearly identical results.

3.3.2 Three-Dimensional Instability

When only two-dimensional disturbances are allowed the flow, as we have seen, evolves to a quasi-equilibrium state of travelling waves that decay over viscous time scales. If no further interactions with other disturbances take place, this flow remains well ordered at all times and shows no sign of the chaotic small-scale structure of real turbulent flows. However, the same two-dimensional state may undergo further instabilities if subjected to infinitesimal three-dimensional disturbances [Herbert and Morkovin (1980) , Orszag & Patera (1983)].

Let A be the amplitude of the two-dimensional wave and B that of the infinitesimal three-dimensional disturbance. With $A \gg B$, the development of the two-dimensional wave is not influenced by the three-dimensional disturbance, but the amplitude of B depends on A according to [Stuart(1962)],

$$\frac{d(\ln B)}{dt} = b_o + b_1 |A|^2 + \ldots$$

With $b_o < 0$, there are two possibilities; if b_1 is negative, the presence of the two-dimensional wave causes stronger damping of the three-dimensional disturbance. However if b_1 is positive, the two-dimensional wave feeds energy into the three-dimensional disturbance; leading to an exponential growth of the three-dimensional wave. The exponential growth

of the three-dimensional disturbance does not continue indefinitely, as in a short time the amplitude of B becomes comparable to A and the problem has to be reformulated. Nevertheless, this secondary instability of two-dimensional finite amplitude states to infinitesimal three-dimensional disturbances seems to explain universally many features of the early stages of transition in a wide class of "steady" shear flows as shown by Orszag & Patera [1983]. We therefore, seem justified in investigating the stability of the two-dimensional finite-amplitude states of the oscillatory channel flow (discussed in the previous section) to secondary three-dimensional disturbances.

Once again, we employ direct numerical simulations of the full time-dependent Navier Stokes equations for our investigation. In particular we will study the time evolution of flows resulting from initial conditions,

$$\vec{v}(x,y,z,t=0) = \bar{U}\,\hat{x} + \vec{v}_{2D} + \epsilon\vec{v}_{3D}$$

Here $\bar{U}$ is the basic laminar flow, $\vec{v}_{2D}$ is the initial finite amplitude two-dimensional disturbance with wave vector $(\alpha,0)$ which is specified to be in the form of the least stable eigenmode of the Orr-Sommerfeld equation for the frozen initial profile and is normalized to have a total energy E_{2D} of 0.04; and $\vec{v}_{3D}$ is the initial infinitesimal three-dimensional disturbance which has the form of a streamwise vortex with wave vector $(0,\beta)$ and has a total energy ϵ of

10^{-8}. Only one mode is kept in the spanwise direction owing to linearity and separability. N modes (2N=32) are kept in the streamwise direction because of nonlinear effects.

As the instability depends critically on the persistence of the two-dimensional finite amplitude state down to transitional Reynolds numbers (since in the absence of the two-dimensional wave the three-dimensional disturbance has to die away according to linear theory), we will choose for α, the most stable of the three wavenumbers studied in the previous section, namely α=0.5 .

The stability of this flow to disturbances with various spanwise wavenumbers β , simulated numerically at Re^{δ}=1000, is illustrated in Figure 45. To begin with, the simulations verify that there is, indeed, a strong three-dimensional instability. The three-dimensional disturbance grows in energy by a factor of 10 in the time it takes the fluid to travel 5 channel widths at maximum bulk velocity. This corresponds to a convective (and not viscous) growth rate, and suggests that the instability mechanism is inviscid.

Secondly, the instability is most effective at β>O(1), emphasizing the three-dimensional nature of the instability. There is a weak maximum in the magnitude of the growth rate at $\beta \simeq 1$, but beyond that the preference in β is very weak.

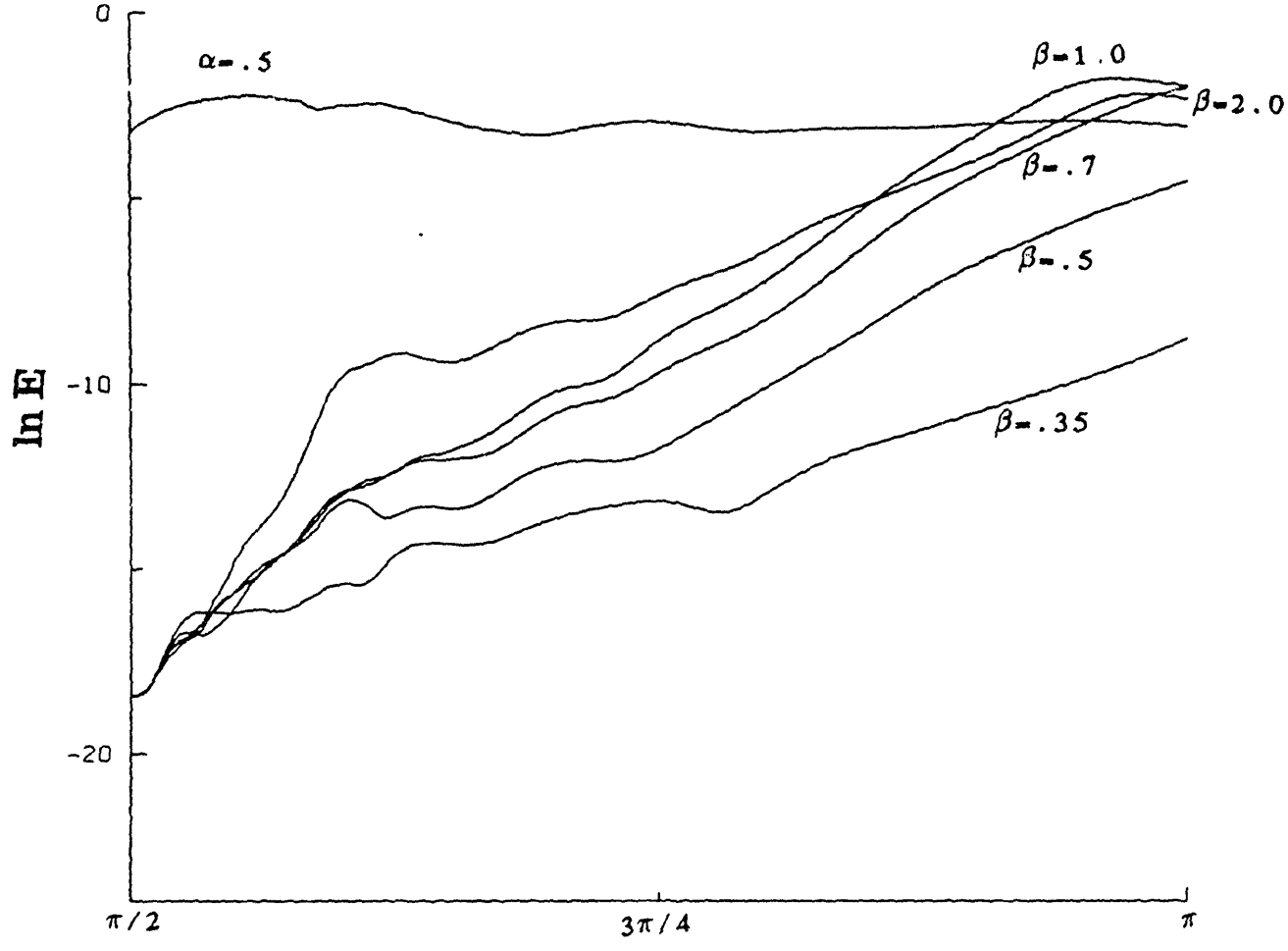

Figure 45. Spanwise wavenumber dependence of the three-dimensional growth rate at Re^{δ}=1000.0, α=0.5

We may characterize the transition process by three parameters; the transitional Reynolds number, the time scale of the instability and the spatial dimensionality of the perturbation responsible for the instability. We have so far shown the instability described above is three-dimensional and grows on convective time scales. It still remains to be shown that the instability cuts off at $Re^{\delta} \simeq 500$, which is the value observed experimentally for transition. This point is demonstrated in Figure 46 where the evolution of the two-dimensional quasi-equilibrium state and the three-dimensional perturbation are followed at Reynolds numbers of 200, 500 and 1000 for α=0.5 and β=1.0 . Note that a Reynolds number on the order of 500 is singled out as the critical Reynolds number below which three-dimensional perturbations decay. This statement may require some clarification considering the observation that the three-dimensional disturbance shows positive growth at all three Reynolds numbers. The point is, that the three-dimensional disturbance needs the two-dimensional finite-amplitude wave to continue its growth. For Reynolds numbers below 500 before the three-dimensional disturbance has grown to finite amplitudes, the level of the two-dimensional wave has dropped to such small amplitudes that it can no more maintain the instability process. As a result the three-dimensional wave never grows to finite amplitudes and the instability is turned off. This argument has been verified by continuing the simulation at Re^{δ}=200 to longer times, and

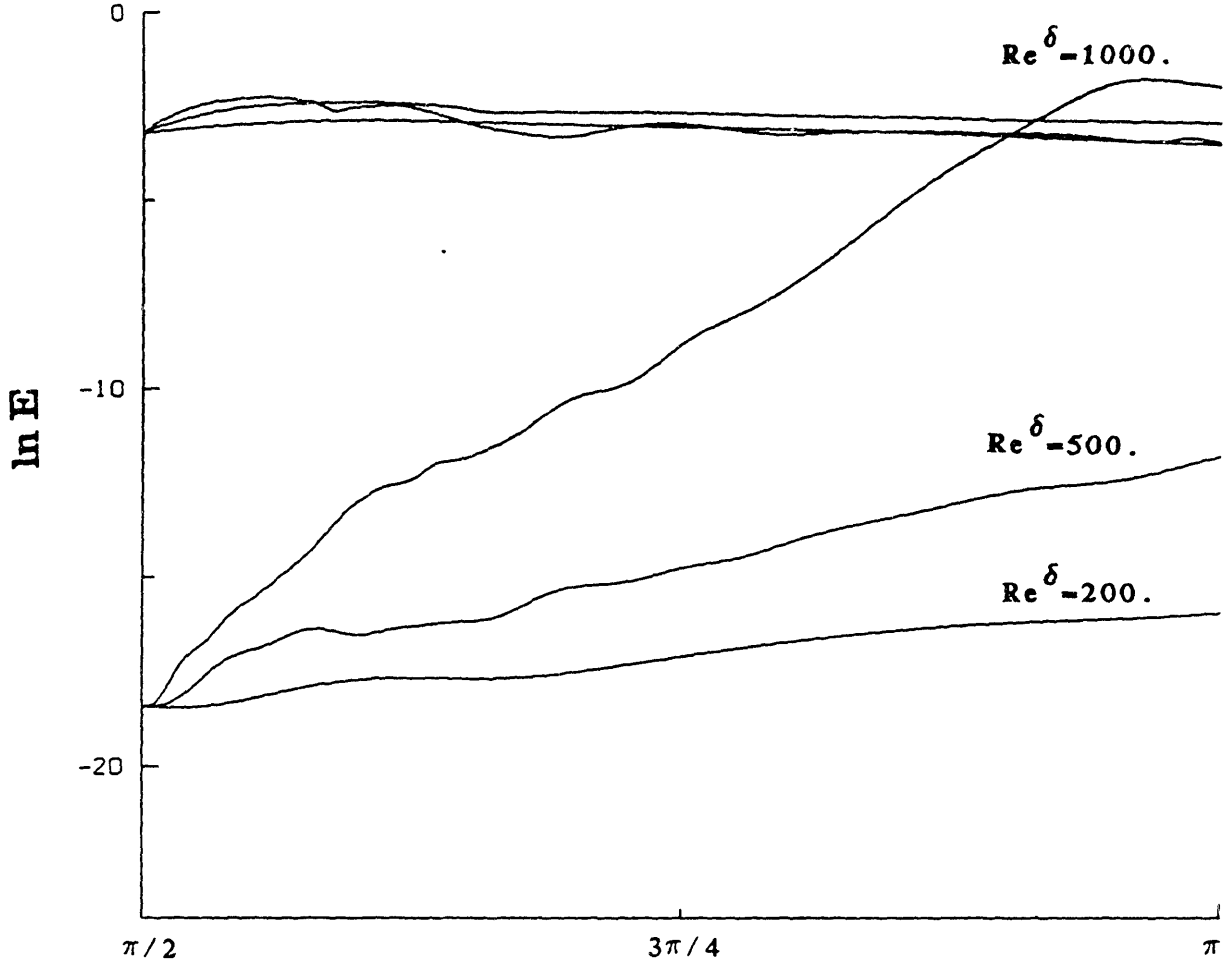

Figure 46. Reynolds-number dependence of the three-dimensional growth rate at α=0.5, β=1.0 . Observe that disturbances decay for Re^{δ}<500.

the three-dimensional disturbance is indeed seen to ultimately decay as a result of the decay of the two-dimensional wave. Note also that the the rate of decay of the two-dimensional base state is roughly the same in all three Reynolds numbers, indicating that the cutoff is due mainly to viscous damping of the three-dimensional perturbation.

3.3.3 Secondary Instability and Transition

We would like to determine to what extent the secondary instability mechanism discussed in this section relates to the transition process that has been observed in experiments.

With respect to transition, the single most important parameter is the Reynolds number. The critical Reynolds number predicted by the secondary instability has already been shown to be in good agreement with the value of 500 that is observed in experiments.

The next question is whether the secondary instability presented here saturates in an ordered state when it reaches finite amplitudes or whether it results in chaotic behavior; and in general to what degree does the resulting flow resemble turbulent flow structures that are observed in experiments. To answer this question we have carried out a large numerical simulation at a Re^{δ} of 1000. and with initial disturbances with wavenumbers α=0.5, β=1.0 .

The initial development of an infinitesimal three-dimensional disturbance (with wave vector (0,β) and initial

energy=10^{-8}) in the presence of a finite-amplitude two-dimensional wave (with wave vector (α,0) and initial energy=$4x10^{-2}$) was first simulated using a run with resolution P=128, 2N=32, 2M=2 and starting at time t=$\pi/2$. At the time t=$9\pi/10$ when the three-dimensional disturbance had grown to an energy of .015 (and with En2 still equal to .0475) the run was restarted with resolution P=128, 2M=32, 2N=16.

The results of the full simulation are shown in Figures 47 and 49. In Figure 47, the overall energy of the three-dimensional disturbance field (integrated over the channel cross-section) is plotted as a function of the phase of the cycle. For comparison the overall energy of the disturbances (integrated over the pipe cross-section) from the experimental run at Re^{δ}=1080, Λ=10.6 is also shown in Figure 48. Note the excellent agreement between the results of the simulation for $3\pi/2<\omega t<5\pi/2$ and experimental results. (The results of the simulation for $\pi/2<\omega t<3\pi/2$ are not in as good an agreement because of the effect of the artificial initial conditions). In particular the disturbances can be seen to decay during the acceleration phase ($3\pi/2<\omega t<2\pi$) and explosively reappear with the start of the deceleration ($\omega t\simeq 2\pi$) in accord with experiments. Furthermore, the plots of instantaneous average velocity from the numerical simulations show striking similarity to the experimental profiles (Figure 6), in that for the acceleration phase the

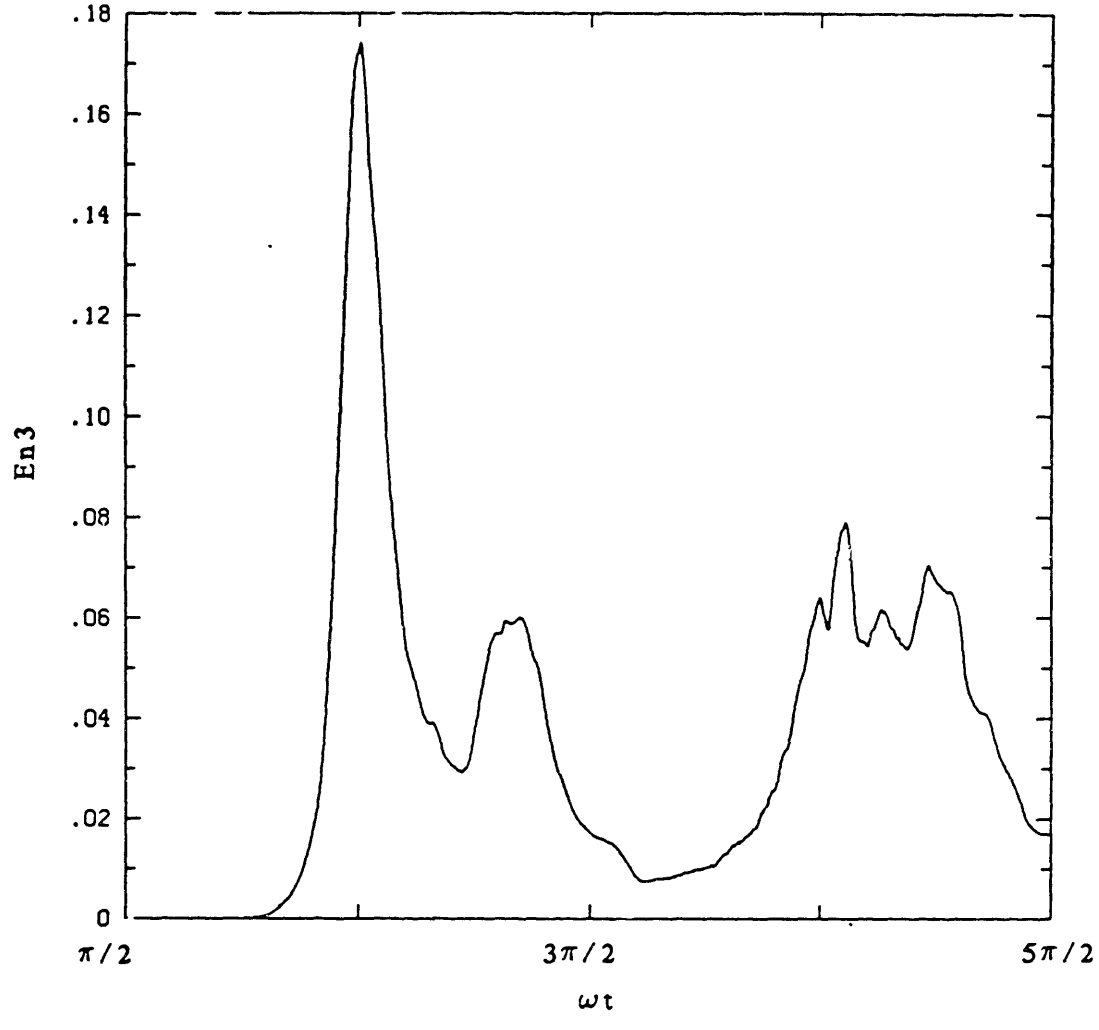

Figure 47. Phase variation of the overall energy of three-dimensional disturbances from the numerical simulation (Re^{δ}=1000. H=10.0)

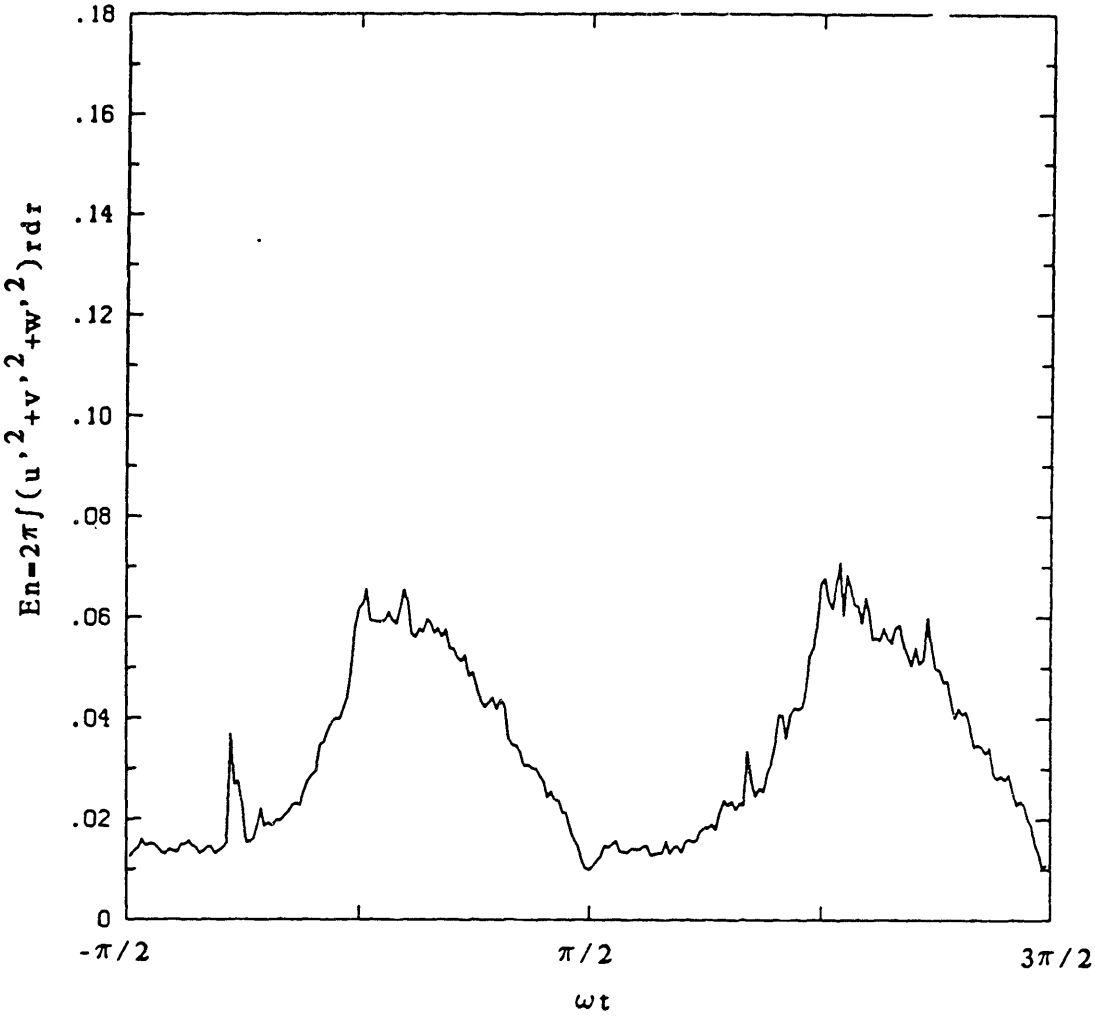

Figure 48. Phase variation of the overall energy of disturbances from experiments (Re^{δ}=1000.,Λ=10.0). Here the value of w' is estimated to be equal to v'.

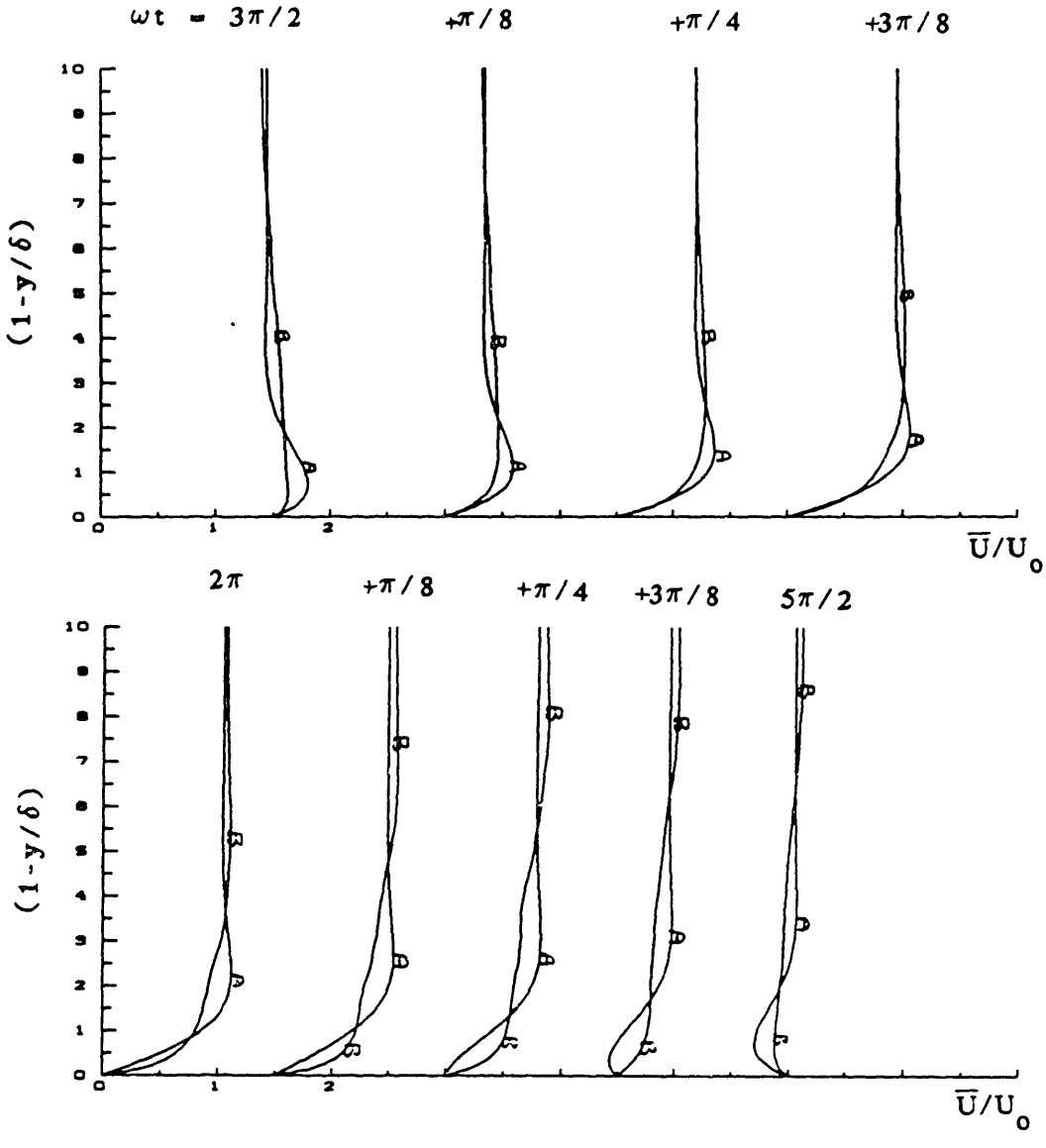

Figure 49. Average velocity profiles for various phases from the numerical simulation at Re^{δ}=1000., Λ=10.0 (curve B) compared to the laminar solution (curve A).

profiles are "full", while during the deceleration phase they are inflectional outside the boundary layer.

IV. SUMMARY AND CONCLUSIONS

In this work we have attempted to bridge some of the gaps between theory and experiment regarding transition and turbulence in bounded oscillatory Stokes flows. Earlier work on this subject consist of, on the one hand, experiments that show the flow undergoes transition at a $Re^{\delta}\sim500$; and on the other hand, theoretical studies that are either in the form of Floquet analyses of the "linearized" equations and predict all disturbances would decay, or are in the form of various quasi-steady treatments of the "linearized" equations which in turn are subjects of dispute because of the assumption of quasi-steadiness.

Our experiments for oscillatory flow in a pipe, for the range of parameters $230<Re^{\delta}<1710$, $3<\Lambda<10$, are in good agreement with earlier investigations and show the flow undergoes transition at a $Re^{\delta}\sim500$ independent of the value of Λ. The resulting turbulent flow is characterized by the sudden explosive appearance of turbulence with the start of the deceleration phase of the cycle, and reversion to "laminar" flow during the acceleration phase. Instantaneous profiles of ensemble-averaged axial velocity provide a strong 'clue' to the mechanism of instability. During the acceleration phase, these profiles are "full" and resemble

the laminar profiles that would be obtained for sinusoidal flow starting from initial conditions $u(r,0)\equiv 0$. During the deceleration phase, however, the velocity profiles are inflectional just outside the boundary layers as a result of momentum exchange between the low speed fluid near the wall and the higher speed fluid further towards the center. These profiles have a striking similarity to "instantaneous" profiles that have been observed in steady boundary layers during the ejection phase of the turbulent bursts (at "peaks"); and suggest that the fundamental process of generation of turbulence in the oscillatory flow may be in the form of bursts similar in nature to those that occur in steady boundary layers. The relaminarization of the flow during the acceleration phase can then be attributed to cessation of "bursting" because of the favorable pressure gradients that are present during this period.

The starting point for a burst in steady shear flows, is the development of streamwise vorticity as a result of nonlinear interaction of two- and three-dimensional disturbance waves. Furthermore the development of the three-dimensional waves can be traced back to instability of infinitesimal three-dimensional perturbations in the presence of finite-amplitude two-dimensional equilibria or quasi-equilibria. Both the nonlinear interaction and the development of infinitesimal three-dimensional disturbances, are independent of the shape of the mean

profiles; and are the result of interaction of two- and three-dimensional waves in a general shear flow. It therefore, seems reasonable to expect the same mechanism to prevail for oscillatory flows, provided the two- and three-dimensional waves can develop. The time variation of the flow, in this case, would be unimportant as long as the ratio Re^{δ}/Λ, representing the ratio of time scale of oscillation to the (convective) time scale of the instability, is large.

To substantiate these ideas, we have studied the stability of the oscillatory flow in a channel (for Λ=10) to various classes of infinitesimal and finite-amplitude two- and three-dimensional disturbances. The results of this study can be summarized as follows,

- For infinitesimal disturbances, Squires' theorem can be extended to the oscillatory flow problem, with the conclusion that only two-dimensional infinitesimal disturbances need to be considered. The development of a two-dimensional disturbance which initially is in the form of the least stable eigenmode of the Orr-Sommerfeld equation for the "frozen" initial profile is followed by direction simulations of the Navier-Stokes equations. The results of the simulation immediately explain the discrepancies between quasi-steady theories and Floquet theory treatments of the linearized equations. For the first cycle the disturbance is

seen to develop in ways not too different from quasi-steady predictions. During this period the disturbance follows the inflection points or critical layers of the instantaneous profiles. Because of the intrinsic nature of the profiles, at the end of the cycle the disturbance ends up in a radial location too far away from the wall to be able to perturb the same modes that were excited earlier. Instead it excites modes that are located further away from the wall. This mode hopping continues until the disturbance has moved all the way to the center of the channel, at which point it settles into a periodic steady-state and decays as predicted by Floquet theory. It should be noted that while the disturbance is still localized near the boundary layers, it does amplify with inviscid growth rates. This inviscid growth, however, can not explain the transition phenomenon that is observed in experiments; because maximum growth for this type of instability is observed around flow reversal (i.e, at the start of acceleration) which is opposite in phase to where turbulence is observed in experiments. These disturbances, however, may explain the "weakly turbulent" flow regime that was observed in Hino's experiments during the acceleration phase of the cycle.

- No finite-amplitude two-dimensional equilibria were found, however quasi-equilibria (with viscous decay rates) were observed for two-dimensional finite-amplitude disturbance at transitional Reynolds numbers.

-The secondary instability of the above quasi-equilibrium states to infinitesimal three-dimensional disturbances can successfully explain the transitional Re^{δ} of 500 that is observed in experiments. The infinitesimal three-dimensional disturbance is seen to grow explosively (on convective time scales) to finite amplitudes. The mechanism of instability is the result of interaction of the two-and three-dimensional waves and is independent of the shape (and inflectional nature) of the profiles. Here, again the time variation of the basic flow is not of much consequence as long as the ratio $Re^{\delta}/\Lambda >> 1$.

- Nonlinear interaction of the two- and three-dimensional disturbance waves, shows structures that are in very good agreement with experiments. Disturbances are seen to decay during the acceleration phase of the cycle, and explosively grow with the start of deceleration. The instantaneous average velocity profiles are inflectional during the deceleration phase and are full during the acceleration.

References

BENNEY,D.J. & LIN,C.C. (1960) On the secondary motions induced by oscillations in a shear flow. Phys. Fluids 3:656.

BUCHAVE,P., GEORGE,W.K. & LUMLEY,J.L. (1979) The measurement of turbulence with the laser-Doppler anemometer. Ann. Rev. Fluid Mech. 63:209-224.

CODDINGTON,E.A. & LEVINSON,N. (1955) Theory of Ordinary Differential Equations.

COLLINS, J.I. (1963) Inception of turbulence at the bed under periodic gravity waves. J. Geophysical Res. 18:6007-6014.

COWLEY, S.J. (1985) High frequency Rayleigh instability of Stokes layers. Stability of Time Dependent and Spatially Varying Flows, ed. D.L. Dwoyer and M.Y. Hussaini. Springer-Verlag

DRAZIN,P.G. & REID,W.H. (1981) Hydrodynamic Stability. Cambridge University Press.

ELLINGSON,T. & PALM,E. (1975) Stability of linear flow. Phys. Fluids 18:487-488.

HALL,P. (1978) The linear stability of flat Stokes layers. Proc. Roy. Soc. Lond. A 359:151-166.

HERBERT,Th. (1977) Finite amplitude stability of parallel flows by higher-order amplitude expansions. AIAA Journal 18:243.

HERBERT,Th. & MORKOVIN,M.V. (1980) Dialouge on bridging some gaps in stability and transition research. In Laminar Turbulent Transition, IUTAM Conf. Proc. (ed. R. Eppler and H. Fasel), p.47.

HINO,M., SAWAMOTO,M. & HARA,T. (1976) Experiments on transition to turbulence in an oscillatory pipe flow. J. Fluid Mech. 75:193-207.

HINO,M., KASHIWAYANAGI,M., NAKAYAMA,A. & HARA,T. (1983) Experiments on the turbulence statistics and the structure of a reciprocating oscillatory flow. J. Fluid Mech. 131:363-400.

KERCZEK,C. von & DAVIS,S.H. (1974) Linear stability theory of oscillatory Stokes layers. J. Fluid Mech. 62:753-773.

KLINE,S.J., REYNOLDS,W.C., SCHRAUB,F.A. and RUNSTADLER,P.W. (1967) The structure of turbulent boundary layers. J. Fluid Mech. 30:741-773.

KOVASZNAY,L.S., KOMODA,H., and VASUEDVA,B.R. (1962) Detailed flow field in transition. Proc. Heat Transfer and Fluid Mech. Inst., p.1. Stanford University Press.

LI,H. (1954) Stability of oscillatory laminar flow along wall. Beach Erosion Bd. Corps Engrs., U.S.A., Tech. Memo no. 47.

MERKLI,P. & THOMANN,H. (1975) Transition to turbulence in oscillatory pipe flow. J. Fluid Mech. 68:567-575.

MONKEWITZ,P.A. & BUNSTER,A. (1985) The stability of the Stokes layer: visual observations and some theoretical considerations. Stability of Time Dependent and Spatially Varying Flows, ed. D.L. Dwoyer and M.Y. Hussaini. Springer-Verlag

OHMI,M., IGUCHI,M., KAKEHASHI,K. & MASUDA,T. (1982) Transition to turbulence and velocity distribution in an oscillating pipe flow. Bull. JSME 25:365-371.

ORSZAG,S.A. (1971) Numerical simulation of incompressible flows within simple boundaries. I.Galerkin (spectral) representations. Stud. Appl. Math. 50: 293.

ORSZAG,S.A. & KELLS,L.C. (1980) Transition to turbulence in plane Poiseulle and plane Couette flow. J. Fluid Mech. 96:159-205.

ORSZAG,S.A. & PATERA,A.T. (1983) Secondary instability of wall-bounded shear flows. J. Fluid Mech. 128:347-385.

SERGEEV,S.I. (1966) Fluid oscillations in pipes at moderate Reynolds numbers. Fluid Dyn. 1:21-22.

STOKES,G.G. (1851) On the effect of the internal friction of fluids on the motion of pendulums. Cambr. Phil. Trans. IX, 8.

STUART,J.T. (1962) On three-dimensional nonlinear effects in the stability of parallel flows. Adv. Aero. Sci. 3:121-142.

TENNEKES H. and LUMLEY,J.L. (1972) A First Course in Turbulence. MIT Press.

UCHIDA,S. (1956) The pulsating viscous flow superposed on the steady laminar motion of incompressible fluids in a circular pipe. ZAMP 7:403-422.

VINCENT, G.E. (1957) Contribution to the study of sediment transport on a horizontal bed due to wave action. Proc. 6th Conf. on Coastal Engng(Florida),pp.326-335.

WOMERSLEY,J.R. (1955) Method for the calculation of velocity, rate of flow and viscous drag in arteries when the pressure gradient is known. J.Physiol. 127:553-563.

YIH,C.S. (1968) Instability of unsteady flows or configurations. Part 1. Instability of a horizontal liquid layer on an oscillating plane. J. Fluid Mech. 31:737-751.